GeoForschungsZentrum Potsdam
Sektion 2.5: Geodynamische Modellierung

Real-time GNSS for Fast Seismic Source Inversion and Tsunami Early Warning

Dissertation
zur Erlangung des akademischen Grades
"doctor rerum naturalium"
(Dr. rer. nat.)
in der Wissenschaftsdisziplin "Geophysik"

eingereicht an der
Mathematisch-Naturwissenschaftlichen Fakultät
der Universität Potsdam

von
Kejie Chen

Potsdam, den 01, 02, 2016

Published online at the
Institutional Repository of the University of Potsdam:
URN urn:nbn:de:kobv:517-opus4-93174
http://nbn-resolving.de/urn:nbn:de:kobv:517-opus4-93174

Abstract

Over the past decades, rapid and constant advances have motivated GNSS technology to approach the ability to monitor transient ground motions with mm to cm accuracy in real-time. As a result, the potential of using real-time GNSS for natural hazards prediction and early warning has been exploited intensively in recent years, e.g., landslides and volcanic eruptions monitoring. Of particular note, compared with traditional seismic instruments, GNSS does not saturate or tilt in terms of co-seismic displacement retrieving, which makes it especially valuable for earthquake and earthquake induced tsunami early warning. In this thesis, we focus on the application of real-time GNSS to fast seismic source inversion and tsunami early warning.

Firstly, we present a new approach to get precise co-seismic displacements using cost effective single-frequency receivers. As is well known, with regard to high precision positioning, the main obstacle for single-frequency GPS receiver is ionospheric delay. Considering that over a few minutes, the change of ionospheric delay is almost linear, we constructed a linear model for each satellite to predict ionospheric delay. The effectiveness of this method has been validated by an out-door experiment and 2011 Tohoku event, which confirms feasibility of using dense GPS networks for geo-hazard early warning at an affordable cost.

Secondly, we extended temporal point positioning from GPS-only to GPS/GLONASS and assessed the potential benefits of multi-GNSS for co-seismic displacement determination. Out-door experiments reveal that when observations are conducted in an adversary environment, adding a couple of GLONASS satellites could provide more reliable results. The case study of 2015 Illapel Mw 8.3 earthquake shows that the biases between co-seismic displacements derived from GPS-only and GPS/GLONASS vary from station to station, and could be up to 2 cm in horizontal direction and almost 3 cm in vertical direction. Furthermore, slips inverted from GPS/GLONASS co-seismic displacements using a layered crust structure on a curved plane are shallower and larger for the Illapel event.

Thirdly, we tested different inversion tools and discussed the uncertainties of using real-time GNSS for tsunami early warning. To be exact, centroid moment tensor inversion, uniform slip inversion using a single Okada fault and distributed slip inversion in layered crust on a curved plane were conducted using co-seismic displacements recorded during 2014 Pisagua earthquake. While the inversion results give similar magnitude and the rupture center, there are significant differences in depth, strike, dip and rake angles, which lead to different tsunami propagation scenarios. Even though, resulting tsunami forecasting along the Chilean coast is close to each other for all three models.

Finally, based on the fact that the positioning performance of BDS is now equivalent to GPS in Asia-Pacific area and Manila subduction zone has been identified as a zone of potential tsunami hazard, we suggested a conceptual BDS/GPS network for tsunami early warning in South China Sea. Numerical simulations with two earthquakes (Mw 8.0 and Mw 7.5) and induced tsunamis demonstrate the viability of this network. In addition, the advantage of BDS/GPS over a single GNSS system by source inversion grows with decreasing earthquake magnitudes.

Zusammenfassung

In den letzten Jahrzehnten haben schnelle und ständige Fortschritte die GNSS Technologie motiviert, die Fähigkeit zu erreichen, vorübergehende Bodenbewegungen mit einer Genauigkeit von mm bis cm in Echtzeit zu überwachen. Als Ergebnis wurde das Potential der Benutzung von Echtzeit GNSS zur Vorhersage von Naturgefährdungen und Frühwarnungen in den letzten Jahren intensiv ausgenutzt, zum Beispiel beim Beobachten von Hangrutschungen und vulkanischen Eruptionen. Besonders im Vergleich mit traditionellen seismischen Instrumenten tritt bei GNSS bei seismischen Verschiebungen keine Sättigung oder Neigung auf, was es für Erdbeben und durch Erdbeben induzierte Tsunamis besonders wertvoll macht. In dieser Arbeit richtet sich der Fokus auf die Anwendung von Echtzeit GNSS auf schnelle seismische Quelleninversion und Tsunami Frühwarnung.

Zuerst präsentieren wir einen neuen Ansatz, um präzise seismische Verschiebungen durch kosteneffiziente Einzelfrequenz-Empfänger zu erhalten. Wie in Bezug auf Hochpräzisions-Positionierung bekannt ist, ist das hauptsächliche Hindernis für Einzelfrequenz-GPS die Verzögerung durch die Ionosphäre. Unter Berücksichtigung der Tatsache, dass die Änderung in der ionosphärischen Verzögerung über mehrere Minuten hinweg linear ist, haben wir ein lineares Modell für jeden Satelliten konstruiert, um die ionosphärische Verzögerung vorherzusagen. Die Effizienz dieser Methode wurde bei einem Freiluft-Experiment und bei dem Tohoku Ereignis 2011 validiert, was die Verwendbarkeit eines dichten GPS Netzwerks für Frühwarnung vor Geo-Gefahren bei vertretbaren Kosten bestätigt.

Als Zweites haben wir die zeitliche Punkt-Positionierung von GPS-only zu GPS/GLONASS erweitert und den potentiellen Nutzen von Multi-GPNSS für die Bestimmung seismischer Verschiebungen bewertet. Freiluft-Experimente zeigen, dass zusätzliche GLONASS Satelliten in feindlicher Umgebung verlässlichere Ergebnisse liefern könnten. Die Fallstudie vom 2015 Illapel Erdbeben mit 8,3 Mw zeigt, dass die mit GPS-only und GPS/GLONASS abgeleiteten seismischen Verschiebungen von Station zu Station variieren und bis zu 2 cm in horizontaler Richtung und beinahe 3 cm in vertikaler Richtung betragen könnten. Zudem sind Verwerfungen, die durch GPS/GLONASS seismische Verschiebungen umgekehrt sind und eine geschichtete Krustenstruktur benutzen, auf einer gekrümmten Ebene flacher und größer für das Illapel Ereignis.

Als Drittes haben wir verschiedene Inversionstools getestet und die Unsicherheiten der Benutzung von Echtzeit GNSS zur Tsunami Frühwarnung diskutiert. Um genau zu sein, wurden eine Schwerpunkts Momenten-Tensoren-Inversion, eine gleichmäßige Verwerfungsinversion bei Benutzung einer einzelnen Okada Verwerfung und eine verteilte Verwerfungs-Inversion in geschichteter Kruste auf einer gekrümmten Ebene durchgeführt. Dafür wurden seismische Verschiebungen genutzt, die beim Pisagua Erdbeben 2014 aufgezeichnet wurden. Während die Inversionsergebnisse ähnliche Magnituden und Bruchstellen liefern, gibt es signifikante Unterschiede bei Tiefe, Streichen, Einfalls- und Spanwinkel, was zu verschiedenen Tsunami Ausbreitungs-Szenarien führt. Trotzdem ist die resultierende Tsunami Vorhersage entlang der chilenischen Küste allen drei Modellen ähnlich.

Schlussendlich und basierend auf der Tatsache, dass die Positionierungsleistung von BDS nun äquivalent zu GPS im Asia-Pazifischen Raum ist und die Manila Subduktionszone als potentielle Tsunami Gefährdungszone identifiziert wurde, schlagen wir ein Konzept für ein BDS/GPS Netzwerk für die Tsunami Frühwarnung im Südchinesischen Meer vor. Numerische Simulationen mit zwei Erdbeben (Mw 8.0 und Mw 7.5) und induzierten Tsunamis demonstrieren die Realisierbarkeit dieses Netzwerks. Zusätzlich wächst der Vorteil von BDS/GPS gegenüber einem einzelnen GNSS Sytem bei steigender Quelleninversion mit abnehmender Erdbebenmagnitude.

Acknowledgements

First and foremost, I want to thank my advisors Dr. Andrey Babeyko, Dr. Maorong Ge and Prof. Stephan Sobolev. I appreciate all their contributions of time, patience, ideas and funding, without which the accomplishment of my PhD study could not have been possible. They gave me a lot of encouragements to fulfill me with hope, took me out of tough times in my PhD pursuit. They also have set excellent examples as being enthusiastic scientists which will benefit my future academic career greatly. I am overwhelmed with gratitude for their help during the past three and half years.

The members of the real-time GNSS precise positioning group (from section 1.1), seismic source inversion group (from section 2.1) and tsunami early warning group (from section 2.5) have contributed immensely to my personal and interdisciplinary professional time at GFZ. The groups have been not only a source of productive collaborations and constructive advices but also sincere friendships. Discussions with Dr. Zhiguo Deng, Dr. Xingxing Li, Dr. Rui Tu, Dr. Kaifei He, Dr. Hua Chen, Xiaolei Dai, Yang Liu, Yumiao Tian, Cuixian Lv, and Zhouzheng Gao have provided me deeper insight and understanding of the basic principle of precise GNSS positioning, satellite orbit and clock determination. Dr. Rongjiang Wang, Dr. Yong Zhang, Dr. Faqi Diao and Dr. Andreas Hoechner showed me the world of seismology and shared codes for fast rupture inversion based on geodetic co-seismic displacements. Dr. Patrizio Petricca, Dr. Natalia Zamora worked together with me to exploit tsunami scenarios. Dr. Elvira Mulyukova, Dr. Rene Gassmoeller, Iskanda Muldashev, Anthony Osei Tutu, Juliane Dannberg, Eva Bredow, the wine seminars we had together make my research life joyful.

Special thanks should go to Prof. Qin Zhang, Prof. Chaoying Zhao, associate Prof. Guanwen Huang, Dr. Shuangcheng Zhang, Le Wang from Chang‘an University. During the past years, you have helped me selflessly both in academic progress and daily life, especially in last year when my father was badly ill, for which I am forever grateful. Prof. Chuang Shi, associate Profs. Min Li and Rongxin Fang from Wuhan University continued to care about my development after my graduation from GNSS Research Center, Wuhan University. Dr. Huizhong Zhu from Liaoning Technical University communicated with me intensively and updated my knowledge about recent academic advances in China, and he generously offered finical support to me for scientific conference.

Happy swimming and beer time with Rong Wang, Weishi Wang, Shaoyang Li has expelled the loneliness and depression in a foreign land. I believe these experiences will be one of the most previous memories for us.

Lastly, I am indebted a lot to my family for all their love and encouragement. My parents raised me with strong character and tenacity, and they supported me in all my pursuits. As Chinese parents, they never put pressure on me to find a girlfriend get married during my PhD study, which is especially commendable for being parents of an older single youth. My younger brother Chuangju Chen has devoted much to taking care of my father and I could focus more on my research. Thank you.

Kejie Chen
Potsdam, 01.02.2016

Table of Content

List of Figures

Acronyms and abbreviations

BDS	BeiDou Navigation Satellite System
CMT	Centroid Moment Tensor
CSC	China Scholarship Council
DART	Deap-ocean Assessment and Reporting of Tsunamis
GEBCO	General Bathymetric Chart of the Oceans
GFZ	GeoForschungsZentrum
GITWS	German-Indonesian Tsunami Early Warning System
GLONASS	GLObal Navigation Satellite System
GNSS	Global Navigation Satellite System
GPS	Global Positioning System
IGS	International GNSS Service
INATEWS	Indonesian Tsunami Early Warning System
IPOC	Integrated Plate boundary Observatory Chile
JMA	Japan Meteorological Agency
MGEX	Multi-GNSS Experiment
NOAA	National Oceanic and Atmospheric Administration
OMC	Observed Minus Computed
PBO	Plate Boundary Observation
PDOP	position dilution of precision
PPP	Precise Point Positioning
PTWC	Pacific Tsunami Warning Center
RMS	Root Mean Square
RTK	Real Time Kinematic
RTS	Real-Time Service
SCS	South China Sea
SDM	Steepest Descent Method
SNR	signal-to-noise ratio
TEWS	Tsunami Early Warning System
TPP	Temporal Point Positioning
USGS	United States Geological Survey
VADASE	Variometric Approach for Displacements Analysis Stand-alone Engine

Chapter 1 Introduction

1.1 Background

Tsunamis are a series of very long waves in a water body, while they can be caused by landslides, volcanic eruptions or even meteorite strikes, mostly, they are generated by powerful undersea thrust earthquakes [*NGDC/WDS*, n.d.]. In this thesis, we specify our research in the earthquake-induced tsunamis. Considering the huge amount of energy that is carried in tsunami generation, propagation and run-up, coastal communities will suffer from devastating results once tsunamis break out. Meanwhile, recent decades have seen a rapidly increasing number of people and infrastructure located in coastal areas where earthquakes and tsunamis are active. To minimize loss of life and property damage, a tsunami early warning system (TEWS) which could precisely predict tsunami wave height in advance and issue warnings is a must. As a matter of fact, several TEWSs have been running operationally over the past years, e.g., the Pacific Tsunami Warning Center (PTWC) and West Coast and Alaska Tsunami Warning Center (WCATWC) operated by National Oceanic and Atmospheric Administration (NOAA), Japanese earthquake and tsunami early warning system run by Japan Meteorological Agency (JMA) [*An*, 2015].

With respect to the two TEWSs operated by the NOAA, they rely on ocean bottom pressure observations from deployed DART (Deap-ocean Assessment and Reporting of Tsunamis) buoys and teleseismic measurements, that‘s to say, they are only far field warning systems and no reliable near field warning could be issued. By comparison, TEWS of JMA was designed for near field warnings. Various tsunami scenarios are computed in advance based on different seismic sources, and as soon as an undersea earthquake strikes, JMA will invert its hypocenter and magnitude based on seismic data on-the-fly to carry out a database query of precomputed scenarios, the warning information is then broadcast to the public.

Despite the fact that these traditional techniques have proved their reliability for most historical cases over the last decades, unfortunately, as the most deadly tsunami ever recorded in history, the 26th December 2004 Sumatra tsunami shocked the international community and addressed the imperfection of existing TEWSs in an extremely hash way. Viewed from the standpoint of methodology, it has been realized that this tragedy was blamed partially on the severe underestimation of the earthquake magnitude [*Kerr*, 2005; *Menke and Levin*, 2005] in the first hours after the origin. Once again, during the 2011 Mw=9.0 Great Tohoku event, the true magnitude was significantly underestimated in the first fifty minutes after the earthquake [*Japan Meteorological Agency (JMA)*, 2013], and the aftermath killer waves urged us to build a more robust TEWS.

The causes related to magnitude underestimation during the first several minutes after huge earthquakes can be classified into physical and instrumental aspects. As is well known, various types of earthquake magnitudes are derived based on seismic waveforms recorded by seismographs with different periods, e.g., surface wave (period20 ± 2 s) magnitude M_s and body wave (period $0.5\sim12$ s) magnitude M_b. Theoretically, as the magnitude increases, there will be more long period (low frequency) seismic energy radiation [*Haskell*, 1964], which indicates that

M_s and M_b would saturate [*Kanamori*, 1983]. To get a better representation of the energy released for tsunami early warning, moment magnitude *Mw* which is related to the physical process of an earthquake is favorable, and the definition of the moment magnitude *Mw* is as follow:

$$M_w = \frac{2}{3} log M_0 - 6.07 \quad (1)$$

where M_0 is the seismic moment, equal to the product of shear modulus, area of the rupture and average displacement [*Hanks and Kanamori*, 1979]. As clearly illustrated in Fig. 1.1, even having the same M_s and M_b, the actual energy of two earthquakes can be different and the potential tsunami dangers would be under estimated by M_s.

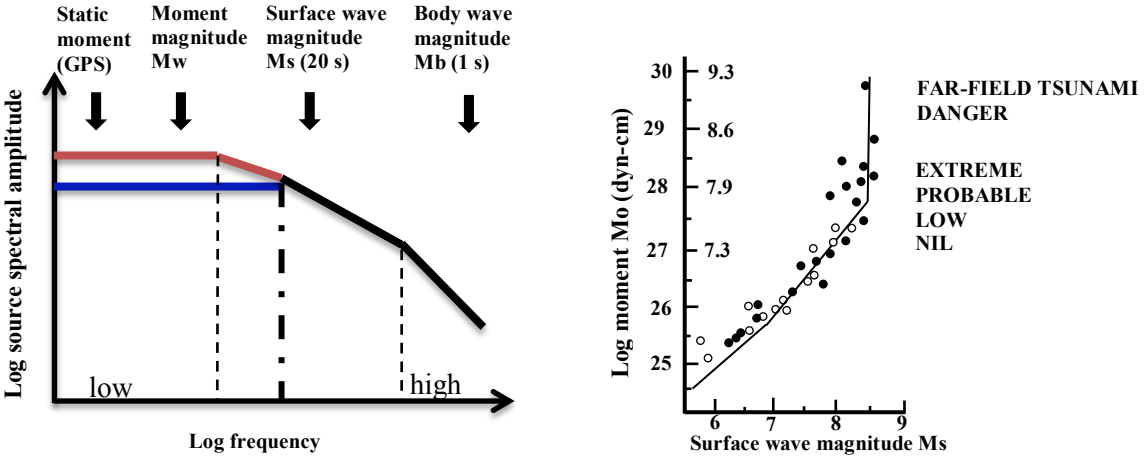

Figure 1. 1 Illustration of magnitude saturation. (Left) Earthquakes that have the same body wave magnitudes and surface magnitudes may have different moment magnitudes, the earthquake with spectrum shown in red has moment magnitude larger than the one shown in blue. GPS can sample static offsets thus has the lowest frequency part of the spectrum. (Right) Due to surface wave magnitude saturation, earthquakes with the same magnitudes could trigger different danger levels of tsunamis. Figure source: *Blewitt et al.* [2009].

Since seismographs saturate in case of strong shaking, to stay on scale, strong motion sensors which have low gains are adopted [*Melgar*, 2014]. While strong motions do not saturate in terms of amplitude and can be employed close to the source, the usual band-pass filtering of waveforms aimed to avoid processing unambiguity caused by co-seismic tilting [*Boore and Bommer*, 2005] effectively leads to magnitude saturation due to removal of long periods which are essential for huge earthquakes [*Melgar et al.*, 2013a]. See, for example, *Hirose et al.* [2011] and *Japan Meteorological Agency (JMA)* [2013] regarding the analysis of the strong-motion magnitude saturation during the Great Tohoku earthquake.

Recent advances in real-time GNSS technology makes monitoring instantaneous ground motion with millimeters to centimeters accuracy possible. Most importantly, compared with seismograph and strong motion sensors, GNSS approach provides arbitrary displacements directly without saturations or tilts, and has motivated pioneering scientists to exploit its potential application for tsunami early warning. Specially, *Blewitt et al.* [2006] first demonstrated the important role that GPS could play for TEWS, pointed out that the true danger of the 2004 Sumatra tsunami could have been fully realized within minutes if near-real-time GPS data connections existed during the shaking time. Later, the prototype of the operational system was depicted in *Blewitt et al.* [2009]. Almost simultaneously, *Sobolev et al.* [2007] presented the concept of "GPS-Shield" and other

tsunami-genic active regions in the world. As a result, German Indonesia Tsunami Early Warning System (GITEWS) implemented real-time GPS as part of its sensors [*Babeyko et al.*, 2010]. Different from the idea of magnitude based TEWS, *Song* [2007] used co-seismic displacements from near-field GPS stations to infer continental slope displacements and tilts and further detected seafloor displacements and tsunami scales. *Ohta et al.* [2012] showed that even a simple slip inversion based on co-seismic displacements retrieved from GPS could provide reliable tsunami early warning information for 2011 Tohoku event. In addition, *Hoechner et al.* [2013] replayed the Tohoku 2011 event from raw GPS data processing to tsunami propagation, which again confirmed the feasibility of GPS for tsunami early warning. Now using real-time GPS for earthquake and tsunami early warnings is an active area of research.

Generally speaking, there are two categories of open questions when applied real-time GNSS to TEWSs, i.e., algorithms to obtain co-seismic displacements from GNSS observations and methodologies to invert seismic sources for tsunami initialization based on the derived co-seismic displacements. The former can be labeled as ―upstream" and the latter is then ―downstream". This thesis focuses on both ―upstream" and ―downstream" issues and the purpose is twofold: (1) developing and analyzing new GNSS algorithms (2) comparing source inversion techniques and testing the uncertainties in the scenario of tsunami early warning.

1.2 Real-time GPS precise positioning for co-seismic displacements determination

As suggested by *Sobolev et al.* [2007], the precision of the order of few cm is required to ensure a reliable GPS-based TEWS. This requirement of high precision suggests dual-frequency GNSS receivers as first candidates for retrieving co-seismic displacements. In fact, a numerous methods that have been proposed [*Bock et al.*, 2000; *Colosimo et al.*, 2011; *Ohta et al.*, 2012; *Li et al.*, 2013b, 2013c] are based on dual-frequency GNSS observations. However, it should be pointed out that in addition to accuracy of individual displacements, inversion for source parameters requires, also dense and geographically broad distributed GPS-network which may comprise several hundreds of individual stations (e.g., GEONET GPS-network in Japan). Employment of a large number of expensive dual-frequency receivers makes dense GPS networks difficult to afford, especially for hazard-prone developing countries. Compared with dual-frequency receivers, single-frequency ones are not only cost-efficient, but also require lower power consumption. The later one is also very crucial for stations without regular electricity supply. Nonetheless, because of the ionospheric delays, single-frequency receivers could not provide cm level positioning precision.

To date, in most cases, geo-hazard monitoring (TEWS included) with GNSS is restricted to GPS-only system, e.g., GEONET in Japan, Plate Boundary Observation (PBO) in U.S., the receivers only track GPS constellation. This is understandable considering that GPS is the most mature system and related error models and products, e.g., satellite antenna phase center offset, satellite orbit and clock biases, are the most precise. As a matter of fact, GPS is just one member of the GNSS family. Nowadays, GLObal Navigation System (GLONASS) built by Russia is undergoing modernization, Galileo built by European Union and BeiDou System (BDS) built by China have been on pilot run or providing regional service, the multi-GNSS era is coming.

Accordingly, Multi-GNSS Experiment (MGEX) have been initialed by International GNSS Service (IGS) to pave the way for provision accurate products for all constellations [*Montenbruck et al.*, 2014]. Compared with a single GPS system, multi-GNSS can significantly improve the satellite visibility, optimize the spatial geometry, reduce dilution of precision (PDOP) and will be of great benefits to both scientific applications and engineering services[*Li et al.*, 2015]. While previous studies concentrated on GPS-only system, it is quite meaningful to exploit the performance of multi-GNSS in TEWS.

1.3 Fast seismic source inversion for tsunami early warning

From the perspective of GNSS-based TEWS center, immediately after the full co-seismic displacements are determined, seismic sources shall be inverted to predict tsunami scenarios. Currently, several inversion tools are available and can be implemented to a TEWS.

Employing local and real-time GNSS co-seismic displacements only, fastCMT introduced by *Melgar et al.* [2012] can rapidly determine centroid moment tensor for large earthquakes without any prior knowledge about fault characteristics in just 2-3 minutes. The reliable strike and dip information provided fastCMT is very valuable to decide the earthquake type (e.g., thrust, normal) and whether it will trigger tsunami or not. Since fastCMT takes the source as a point and does not take the finiteness into account, its results are not trustworthy when the earthquake is extremely large, for example, the Mw=9.0 Tohoku earthquake. For revision, the concept line fastCMT was put forward [*Melgar et al.*, 2013b].

As a matter of fact, a detailed slip distribution rather than a point source is more favorable in terms of TEWS. Working in a simulated real-time mode, by using Green‘s functions derived from Okada‘s formulation, *Crowell et al.*[2012] inverted for finite fault slip in a homogeneous elastic half-space. Two approaches were tested and compared in their case studies, the first inversion started with a catalog of predefined faults, while the second was based on a rapid centroid moment tensor solution (e.g., from fastCMT). Promisingly, in both cases, the finite fault slip and moment magnitudes could be determined in less than two minutes, which reduces the latency by an order of magnitude compared with traditional seismic methods.

Steepest descent method (SDM) coded by *Wang et al.*, [2009] has also been extensively utilized for slip distribution inversion. Features and special advantages of SDM are as follows [*Wang et al.*, 2013]:

1) Because of closed-form Green functions, inversion of geodetic data for fault rupture is mostly based on a uniform half-space earth model. By contrast, SDM uses a layered structure, and the inversion results could be greatly affected by the layered structure of the crust.
2) For simplicity, rupture inversion is usually conducted on a rectangular fault or a so called ―curved fault" which actually consists of several connected rectangular segments. However, with respect to most mega thrust earthquakes, both dip and strike angles are variable, SDM has taken this into consideration. Otherwise, it will lead to an artificial loss of the slip resolution and data fit.

Please note, a priori knowledge about the curved geometry of the fault is necessary when using SDM, and this can be obtained in advance, for example, from SLAB 1.0 [*Hayes et al.*, 2012] in

subduction zone. However, in areas of complex faulting, the determination of a good approximation of proper fault geometry is not easy [*Crowell et al.*, 2012]. In addition, some earthquakes may happen out of the plate interface.

We also suggested a novel method that inverts uniform slip distribution on a single Okada fault in a homogeneous elastic half-space directly. The only constraint is the scaling law for rupture length and width and through a combination of brute-force and Monte-Carlo search, the one which has the best fit of the observation data is set as the final inversion result.

Not surprisingly, different inversion methods yield different results even with the same co-seismic displacements, and in this context, the differences are labeled as uncertainties. Since our main concern is tsunami early warning, it is important to assess the impact of uncertainties for the final tsunami forecasting.

1.4 Organization of thesis

This thesis is initialized by an introductory chapter (Chapter 1) which describes the scientific background and the objectives. In the following, four individual first-author manuscripts (Chapters 2–5) detail our contributions towards to ~~"re~~al-time GNSS for fast rupture inversion and tsunami early warning". Two of the manuscripts have been published in peer reviewed journals and the rest are currently under review.

Chapter 2: Retrieving real-time precise co-seismic displacements with a standalone single-frequency GPS receiver

This chapter has been published in entirety in **Advances in Space Research**. By using observations prior to an earthquake, a precise ionospheric delay prediction model is established for each tracked satellite, thus it enables to get co-seismic displacements using a standalone low cost single single-frequency receiver and makes a dense GPS monitoring network affordable.

Chapter 3: Retrieving real-time co-seismic displacements using GPS/GLONASS: a preliminary report from September 2015 Mw8.3 Chile Illapel earthquake

This chapter has been submitted to **Geophysical Journal International**. Whereas the multi-GNSS era is coming, so far, only GPS and GLONASS offer global coverage. Through out-door experiments and the 2015 Mw8.3 Chile Illaple earthquake, this chapter ponderingly assesses the performance of GPS/GLONASS and compares it with GPS-only in co-seismic displacement determination and further for tsunami early warning.

Chapter 4: Comparing source inversion techniques for GNSS-based tsunami early warning: a case study 2014 Pisagua M8.1 earthquake, northern Chile

This chapter has been submitted to **Geophysical Research Letters**. Three different source inversion techniques: fastCMT (centroid moment tensor), distributed slip along pre-defined plate interface and unconstrained inversion into a single Okada fault were compared in the 2014 Mw 8.1 Pisagua earthquake. The three methods provide significantly different far-field tsunami forecast but show surprisingly similar tsunami predictions in the near-field.

Chapter 5: Precise Positioning of BDS, BDS/GPS: Implications for Tsunami Early Warning in South China Sea

This chapter has been published in **Remote Sensing**. Toward the end of 2012, BDS has been providing regional positioning service. At the same time, South China Sea is identified as a tsunami potential zone. Thus a conceptual BDS/GPS based TEWS is suggested.

The main results and conclusions of this work are summarized in chapter 6.

1.5 Reference

Allen, R. M., and A. Ziv (2011), Application of real-time GPS to earthquake early warning, *Geophys. Res. Lett.*, *38*(16), 1–7, doi:10.1029/2011GL047947.

An, C. (2015), Inversion of tsunami waveforms and tsunami warning.

Babeyko, A. Y., A. Hoechner, and S. V Sobolev (2010), Source modeling and inversion with near real-time GPS: a GITEWS perspective for Indonesia, *Nat. Hazards Earth Syst. Sci.*, *10*, 1617–1627, doi:10.5194/nhess-10-1617-2010.

Banerjee, P., F. Pollitz, B. Nagarajan, and R. Bürgmann (2007), Coseismic Slip Distributions of the 26 December 2004 Sumatra–Andaman and 28 March 2005 Nias Earthquakes from gps Static Offsets, *Bull. Seismol. Soc. Am.* , *97* (1A), S86–S102, doi:10.1785/0120050609.

Blaser, L., F. Kruger, M. Ohrnberger, and F. Scherbaum (2010), Scaling Relations of Earthquake Source Parameter Estimates with Special Focus on Subduction Environment, *Bull. Seismol. Soc. Am.*, *100*(6), 2914–2926, doi:10.1785/0120100111.

Blewitt, G., C. Kreemer, W. C. Hammond, H.-P. Plag, S. Stein, and E. Okal (2006), Rapid determination of earthquake magnitude using GPS for tsunami warning systems, *Geophys. Res. Lett.*, *33*(11), L11309–L11309, doi:10.1029/2006GL026145.

Blewitt, G., W. C. Hammond, C. Kreemer, H. P. Plag, S. Stein, and E. Okal (2009), GPS for real-time earthquake source determination and tsunami warning systems, *J. Geod.*, *83*, 335–343, doi:10.1007/s00190-008-0262-5.

Bock, Y., R. M. Nikolaidis, P. J. Jonge, and M. Bevis (2000), Instantaneous geodetic positioning at medium distances with the Global Positioning System, *J. Geophys. Res. Solid Earth*, *105*(B12), 28223–28253.

Bock, Y., L. Prawirodirdjo, and T. I. Melbourne (2004), Detection of arbitrarily large dynamic ground motions with a dense high‐rate GPS network, *Geophys. Res. Lett.*, *31*(6).

Bock, Y., D. Melgar, and B. W. Crowell (2011), Real-time strong-motion broadband displacements from collocated GPS and accelerometers, *Bull. Seismol. Soc. Am.*, *101*(6), 2904–2925, doi:10.1785/0120110007.

Boore, D. M., and J. J. Bommer (2005), Processing of strong-motion accelerograms: needs, options and consequences, *Soil Dyn. Earthq. Eng.*, *25*(2), 93–115.

Chen, K., N. Zamora, A. Y. Babeyko, X. Li, and M. Ge (2015a), Precise Positioning of BDS, BDS/GPS: Implications for Tsunami Early Warning in South China Sea, *Remote Sens.*, *7*(12), 15955–15968.

Chen, K., M. Ge, X. Li, A. Babeyko, M. Ramatschi, and M. Bradke (2015b), Retrieving real-time precise co-seismic displacements with a standalone single-frequency GPS receiver, *Adv. Sp. Res.*

Colosimo, G., M. Crespi, and A. Mazzoni (2011), Real-time GPS seismology with a stand-alone receiver: A preliminary feasibility demonstration, *J. Geophys. Res. Solid Earth*, *116*(B11).

Crowell, B. W., Y. Bock, and D. Melgar (2012), Real‐time inversion of GPS data for finite fault modeling and rapid hazard assessment, *Geophys. Res. Lett.*, *39*(9).

Diao, F., X. Xiong, S. Ni, Y. Zheng, and C. Ge (2011), Slip model for the 2011 M w 9.0 Sendai (Japan) earthquake and its M w 7.9 aftershock derived from GPS data, *Chinese Sci. Bull.*, *56*(27), 2941–2947.

Fang, R., C. Shi, W. Song, G. Wang, and J. Liu (2013), Determination of earthquake magnitude using GPS displacement waveforms from real-time precise point positioning, *Geophys. J. Int.* , doi:10.1093/gji/ggt378.

Ge, L. (1999), GPS seismometer and its signal extraction, in *Proc. 12th Int. Tech. Meeting of the Satellite Division of the US Inst. of Navigation GPS ION'99*.

Ge, L., S. Han, C. Rizos, Y. Ishikawa, M. Hoshiba, Y. Yoshida, M. Izawa, N. Hashimoto, and S. Himori (2000), GPS seismometers with up to 20 Hz sampling rate, *Earth, planets Sp.*, *52*(10), 881–884.

Geist, E. L. (2001), Effect of depth-dependent shear modulus on tsunami generation along subduction zones shallow depths in comparison to standard earth, , *28*(7), 1315–1318.

Geng, J., and Y. Bock (2015), GLONASS fractional-cycle bias estimation across inhomogeneous receivers for PPP ambiguity resolution, *J. Geod.*, 1–18.

Geng, T., X. Xie, R. Fang, X. Su, Q. Zhao, G. Liu, H. Li, C. Shi, and J. Liu (2015), Real‐time capture of seismic waves using high‐rate multi‐GNSS observations: Application to the 2015 Mw 7.8 Nepal earthquake, *Geophys. Res. Lett.*

Hanks, T. C., and H. Kanamori (1979), A Moment Magnitude Scale, *J. Geophys. Res.*, *84*(B5), 2348–2350.

Haskell, N. A. (1964), Total energy and energy spectral density of elastic wave radiation from propagating faults, *Bull. Seismol. Soc. Am.*, *54*(6A), 1811–1841.

Hayes, G. P., D. J. Wald, and R. L. Johnson (2012), Slab1.0: A three-dimensional model of global subduction zone geometries, *J. Geophys. Res.*, *117*(B1), B01302–B01302, doi:10.1029/2011JB008524.

Hirahara, K., T. Nakano, Y. Hoso, S. Matsuo, and K. Obana (1994), An experiment for GPS strain seismometer, in *Japanese symposium on GPS*, pp. 67–75.

Hirose, F., K. Miyaoka, N. Hayashimoto, T. Yamazaki, and M. Nakamura (2011), Outline of the 2011 off the Pacific coast of Tohoku Earthquake (M w 9.0)—Seismicity: foreshocks, mainshock, aftershocks, and induced activity—, *Earth, planets Sp.*, *63*(7), 513–518.

Hoechner, A., A. Y. Babeyko, and S. V Sobolev (2008), Enhanced GPS inversion technique applied to the 2004 Sumatra earthquake and tsunami, *Geophys. Res. Lett.*, *35*(8), L08310–L08310, doi:10.1029/2007GL033133.

Hoechner, A., M. Ge, a. Y. Babeyko, and S. V Sobolev (2013), Instant tsunami early warning based on real-time GPS – Tohoku 2011 case study, *Nat. Hazards Earth Syst. Sci.*, *13*(5), 1285–1292, doi:10.5194/nhess-13-1285-2013.

Hofmann-Wellenhof, B., H. Lichtenegger, and E. Wasle (2007), *GNSS–global navigation satellite systems: GPS, GLONASS, Galileo, and more*, Springer Science & Business Media.

Japan Meteorological Agency (JMA) (2013), Lessons learned from the tsunami disaster caused by the 2011 Great East Japan Earthquake and improvements in JMA ' s tsunami warning system October 2013 Japan Meteorological Agency, , (October), 1–13.

Jing-nan, L., and G. Mao-rong (2003), PANDA software and its preliminary result of positioning and orbit determination, *Wuhan Univ. J. Nat. Sci.*, *8*(2), 603–609.

Kanamori, H. (1983), Magnitude scale and quantification of earthquakes, *Tectonophysics*, *93*(3), 185–199.

Kanamori, H., and L. Rivera (2008), Source inversion of W phase: speeding up seismic tsunami warning, *Geophys. J. Int.* , *175* (1), 222–238, doi:10.1111/j.1365-246X.2008.03887.x.

Kennett, B. L. N., E. R. Engdahl, and R. Buland (1995), Constraints on seismic velocities in the Earth from traveltimes, *Geophys. J. Int.*, *122*(1), 108–124.

Kerr, R. A. (2005), Failure to Gauge the Quake Crippled the Warning Effort, *Sci.* , *307* (5707), 201, doi:10.1126/science.307.5707.201.

Larson, K. M. (2009), GPS seismology, *J. Geod.*, *83*(3-4), 227–233.

Larson, K. M., P. Bodin, and J. Gomberg (2003), Using 1-Hz GPS data to measure deformations caused by the Denali fault earthquake, *Science (80-.).*, *300*(5624), 1421–1424.

Li, X., M. Ge, Y. Zhang, R. Wang, B. Guo, J. Klotz, J. Wickert, and H. Schuh (2013a), High-rate coseismic displacements from tightly integrated processing of raw GPS and accelerometer data, *Geophys. J. Int.*, doi:10.1093/gji/ggt249.

Li, X., M. Ge, X. Zhang, Y. Zhang, B. Guo, R. Wang, J. Klotz, and J. Wickert (2013b), Real-time high-rate co-seismic displacement from ambiguity-fixed precise point positioning: Application to earthquake early warning, *Geophys. Res. Lett.*, *40*(2), 295–300, doi:10.1002/grl.50138.

Li, X., M. Ge, B. Guo, J. Wickert, and H. Schuh (2013c), Temporal point positioning approach for real-time GNSS seismology using a single receiver, *Geophys. Res. Lett.*, *40*(21), 5677–5682, doi:10.1002/2013GL057818.

Li, X., M. Ge, X. Dai, X. Ren, M. Fritsche, J. Wickert, and H. Schuh (2015), Accuracy and reliability of multi-GNSS real-time precise positioning: GPS, GLONASS, BeiDou, and Galileo, *J. Geod.*, *89*(6), 607–635, doi:10.1007/s00190-015-0802-8.

Liu, Y., M. Ge, C. Shi, Y. Lou, J. Wickert, and H. Schuh (2015), Improving GLONASS Precise Orbit Determination through Data Connection, *Sensors*, *15*(12), 30104–30114.

Melgar, D. (2014), Seismogeodesy and Rapid Earthquake and Tsunami Source Assessment, 247 pp., University of California San Diego,

Melgar, D., Y. Bock, and B. W. Crowell (2012), Real-time centroid moment tensor determination for large earthquakes from local and regional displacement records, *Geophys. J. Int.*, *188*(2), 703–718, doi:10.1111/j.1365-246X.2011.05297.x.

Melgar, D., Y. Bock, D. Sanchez, and B. W. Crowell (2013a), On robust and reliable automated baseline corrections for strong motion seismology, *J. Geophys. Res. Solid Earth*, *118*(3), 1177–1187.

Melgar, D., B. W. Crowell, Y. Bock, and J. S. Haase (2013b), Rapid modeling of the 2011 Mw 9.0 Tohoku-oki earthquake with seismogeodesy, *Geophys. Res. Lett.*, *40*(12), 2963–2968, doi:10.1002/grl.50590.

Menke, W., and V. Levin (2005), A strategy to rapidly determine the magnitude of great earthquakes, *Eos, Trans. Am. Geophys. Union*, *86*(19), 185–188.

Montenbruck, O., P. Steigenberger, R. Khachikyan, G. Weber, R. B. Langley, L. Mervart, and U. Hugentobler (2014), IGS-MGEX: preparing the ground for multi-constellation GNSS science, *Insid. GNSS*, *9*(1), 42–49.

Mooney, W. D., G. Laske, and T. G. Masters (1998), CRUST 5.1: A global crustal model at 5× 5, *J. Geophys. Res. Solid Earth*, *103*(B1), 727–747.

NGDC/WDS (n.d.), National Geophysical Data Center / World Data Service (NGDC/WDS): Global Historical Tsunami Database. National Geophysical Data Center, NOAA, *Access on 15.01.2015*, doi:10.7289/V5PN93H7. Available from: http://www.ngdc.noaa.gov/hazard/tsu_db.shtml

O'Toole, T. B., A. P. Valentine, and J. H. Woodhouse (2012), Centroid–moment tensor inversions using high-rate GPS waveforms, *Geophys. J. Int.*, *191*(1), 257–270.

O'Toole, T. B., A. P. Valentine, and J. H. Woodhouse (2013), Earthquake source parameters from GPS‐measured static displacements with potential for real‐time application, *Geophys. Res. Lett.*, *40*(1), 60–65.

Ohta, Y. et al. (2012), Quasi real-time fault model estimation for near-field tsunami forecasting based on RTK-GPS analysis: Application to the 2011 Tohoku-Oki earthquake (M w 9.0), *J. Geophys. Res. Solid Earth*, *117*, doi:10.1029/2011JB008750.

Okada, Y. (1985), Surface deformation due to shear and tensile faults in a half-space, *Bull. Seismol. Soc. Am.*, *75*(4), 1135–1154.

Saastamoinen, J. (1972), Atmospheric correction for the troposphere and stratosphere in radio ranging satellites, *use Artif. Satell. Geod.*, 247–251.

Schüler, T. (2014), The TropGrid2 standard tropospheric correction model, *GPS Solut.*, *18*(1), 123–131.

Shi, C., Y. Lou, H. Zhang, Q. Zhao, J. Geng, R. Wang, R. Fang, and J. Liu (2010), Seismic deformation of the M w 8.0 Wenchuan earthquake from high-rate GPS observations, *Adv. Sp. Res.*, *46*(2), 228–235.

Simons, M., Y. Fialko, and L. Rivera (2002), Coseismic Deformation from the 1999 Mw 7.1 Hector Mine, California, Earthquake as Inferred from InSAR and GPS Observations, *Bull. Seismol. Soc. Am.* , *92* (4), 1390–1402, doi:10.1785/0120000933.

Sobolev, S. V, A. Y. Babeyko, R. Wang, R. Galas, M. Rothacher, D. SEIN, J. Schröter, J. Lauterjung, and C. Subarya (2006), Towards real-time tsunami amplitude prediction, *Eos (Washington. DC).*, *87*(37).

Sobolev, S. V, A. Y. Babeyko, R. Wang, A. Hoechner, R. Galas, M. Rothacher, D. V Sein, J. Schröter, J. Lauterjung, and C. Subarya (2007), Tsunami early warning using GPS-Shield arrays, *J. Geophys. Res. Solid Earth*, *112*(B8), B08415–B08415, doi:10.1029/2006JB004640.

Song, Y. T. (2007), Detecting tsunami genesis and scales directly from coastal GPS stations, *Geophys. Res. Lett.*, *34*(19).

Tian, Y., M. Ge, and F. Neitzel (2015), Particle filter-based estimation of inter-frequency phase bias for real-time GLONASS integer ambiguity resolution, *J. Geod.*, *89*(11), 1145–1158.

Tsuji, H., Y. Hatanaka, T. Sagiya, and M. Hashimoto (1995), Coseismic crustal deformation from the 1994 Hokkaido‐Toho‐Oki earthquake monitored by a nationwide continuous GPS array in Japan, *Geophys. Res. Lett.*, *22*.

Tu, R., and K. Chen (2014), Tightly Integrated Processing of High-Rate GPS and Accelerometer Observations by Real-Time Estimation of Transient Baseline Shifts, *J. Navig.*, *67*(05), 869–880.

Vigny, C., W. J. Simons, S. Abu, R. Bamphenyu, C. Satirapod, N. Choosakul, and B. A. C. Ambrosius (2005), Insight into the 2004 Sumatra–Andaman earthquake from GPS measurements in southeast Asia, *Nature*, *436*, 201–206.

Wang, L., R. Wang, F. Roth, B. Enescu, S. Hainzl, and S. Ergintav (2009), Afterslip and viscoelastic relaxation following the 1999 M 7.4 İzmit earthquake from GPS measurements, *Geophys. J. Int.*, *178*(3), 1220–1237, doi:10.1111/j.1365-246X.2009.04228.x.

Wang, R., F. L. Mart n, and F. Roth (2003), Computation of deformation induced by earthquakes in a multi-layered elastic crust—FORTRAN programs EDGRN/EDCMP, *Comput. Geosci.*, *29*(2), 195–207.

Wang, R., F. Diao, and A. Hoechner (2013), SDM-A geodetic inversion code incorporating with layered crust structure and curved fault geometry, in *EGU General Assembly Conference Abstracts*, vol. 15, p. 2411.

Yang, Y., J. Li, A. Wang, J. Xu, H. He, H. Guo, J. Shen, and X. Dai (2014), Preliminary assessment of the navigation and positioning performance of BeiDou regional navigation satellite system, *Sci. China Earth Sci.*, *57*(1), 144–152.

Chapter 2 Retrieving real-time precise co-seismic displacements with a standalone single-frequency GPS receiver

Kejie Chen, Maorong Ge, Xingxing Li, Andrey Babeyko, Markus Ramatschi, Markus Bradke
German Research Centre for Geosciences(GFZ), Telegrafenberg, 14473 Potsdam, Germany; email: kejie@gfz-potsdam.de

ABSTRACT: Nowadays, Global Positioning System (GPS) plays an increasingly important role in retrieving real-time precise co-seismic displacements for geo-hazard monitoring and early warning. Several real-time positioning approaches have been demonstrated for such purpose, such as real-time kinematic relative positioning, precise point positioning, etc., where dual-frequency geodetic receivers are applied for the removal of ionosphere delays by inter-frequency combination. At the same time, it would be also useful to develop efficient algorithms for estimating precise displacements with low-cost GPS receivers since they can make a denser network or multi-sensors combination without putting too much financial burden. In this contribution, we present a new method to retrieve precise co-seismic displacements in real-time using a standalone single-frequency receiver. In the new method, observations prior to an earthquake are utilized to establish a precise ionospheric delay prediction model, so that precise co-seismic displacements can be obtained without any convergence process. Our method was validated with an outdoor experiment as well as by re-processing of 1-Hz GPS data collected by the GEONET network during the 2011 Tohoku Mw 9.0 earthquake. For the latter, RMS against dual-frequency receivers constituted 2 cm for horizontal components and 3 cm for the vertical component.

We specially address the observation biases and their impact on the accuracy of single frequency positioning. Our approach makes real-time GPS displacement monitoring with dense network much more affordable in terms of financial costs.

Key words: GPS• single-frequency receiver• ionospheric delay correction •co-seismic displacements

2.1 Introduction

Besides monitoring secular deformation, like plate motion (see, e.g., Wang et al., 2001; Prawirodirdjo and Bock 2004; Lifton et al., 2013), GPS is also applied to detect instantaneous ground shaking in real-time for geohazard monitoring and early warning, for example, earthquake and tsunami early warning (see, e.g., Blewitt et al., 2006; Sobolev et al., 2007; Li et al.,2013a; Geng et al., 2013). Several positioning approaches have been proposed to capture ground displacements, such as Real Time Kinematic (RTK) relative positioning (see, e.g., Ren et al., 2010; Ohta et al., 2012; Sudhakar et al., 2013), Precise Point Positioning (PPP) (see, e.g., Larson et al., 2003; Shi et al., 2010; Li et al., 2013a). Since by relative positioning reference stations may be subjected to the earthquake shaking as well, reliability of the derived co-seismic displacements may become degraded (Ohta et al., 2012). In PPP, precise positioning is achieved based on precise orbit and clock corrections estimated from a global reference network. As no or only few stations are displaced by the earthquake, orbits and clocks are hardly contaminated and so is the estimated displacement. More important is that the Real-Time Service (RTS) (http://rts.igs.org/products) of the International GNSS Services (IGS) has been providing precise

orbits and clocks operationally since last year, which enables real-time PPP for such applications. However, real-time PPP needs a long period (about 30 min, Geng et al., 2011) to resolve integer phase ambiguities to achieve centimeter-level accuracy. If an earthquake happens during PPP's (re) convergence period or there are data interruptions caused by an earthquake, reliability of PPP-based displacements would be significantly reduced.

In fact, a major role of GPS in applications like tsunami early warning is providing co-seismic ground displacements for subsequent tsunami source inversion. Thus, most important in this context are not absolute positions of GPS stations but their co-seismic displacements caused by an earthquake, i.e., station displacements with respect to their positions before an earthquake (Li et al., 2013b). Under this circumstance , the "variometric" approach (Colosimo et al., 2011) and temporal point positioning (TPP) (Li et al., 2013b) were proposed to avoid the long convergence of PPP solution. Furthermore, it has been proved that these methods can be equivalent if all error components are carefully considered (Li et al., 2014b).

Sobolev et al. (2007) numerically analyzed the performance of a hypothetical GPS-network on Sumatra, Indonesia, and concluded that real-time GPS-precision on the order of few centimeters is required to assure reliable GPS-based tsunami early warning. This requirement of high precision suggests dual-frequency GPS-receivers as first candidates for retrieving co-seismic displacements. On the other hand, inversion for source parameters requires, in addition to accuracy of individual displacements, a dense and geographically broadly distributed GPS-network which may comprise several hundreds of individual stations (e.g., GEONET GPS-network in Japan). The employment of a large number of expensive dual-frequency receivers makes dense GPS networks difficult to afford, especially for hazard-prone developing countries. Compared with dual-frequency receivers, single-frequency ones are not only cost-efficient, but also require lower power consumption. The later one is also very crucial for stations without regular electricity supply.

Certainly, single-frequency receivers cannot compete in accuracy of absolute positioning with dual-frequency devices. The main idea behind the current study is to employ single-frequency receivers to retrieve accurate co-seismic displacements during a very limited time interval: just 3-5 minutes after an earthquake. In other words, we are interested in a cost-efficient technique that can precisely derive short-term station displacements. These time considerations come from the fact that duration of local slip, that establishes significant co-seismic offset at near-field GPS stations, typically, does not exceed two to three minutes in case of tsunamigenic earthquakes. Even in the case of extremely long Giant December 2004 Sumatra-Andaman Mw>9.1 earthquake which lasted for more than 10 minutes, local fast-slip rise time was under 5 min (Lay et al., 2005). Moreover, it is clear that giant (Mw>9) subduction zone earthquakes possess enormous tsunamigenic potential and, without any doubt, must trigger tsunami warning. Our primary goal is detection and evaluation of tsunamigenic potential of earthquakes with smaller magnitudes which do not necessarily trigger tsunamis (Mw 7.5 - 8.5).

In order to get accurate co-seismic displacements directly from single-frequency observation, the ionospheric delay must be precisely modeled, because it cannot be eliminated by forming the ionosphere-free inter frequency combination as for dual-frequency data. Most of the approaches developed so far to tackle ionospheric correction regularly adopt a correction model (see, e.g., Klobuchar et al.,1987; Schaer, 1996). Unfortunately, due to the lack of well distributed data and simplified mathematical representations, published models can only reach an accuracy suitable for sub-meter positioning (Van Bree and Tiberius, 2012), which is definitely not enough for co-seismic displacement monitoring.

Considering that atmospheric delays and remaining orbit and clock biases could be eliminated or mostly reduced over very short intervals such as 1 s or even shorter by epoch-to-epoch differences, the "variometric" approach proposed by G. Colosimo et al. (Colosimo et al., 2011) could be extended to single-frequency as well (Benedetti et al., 2014; Li et al., 2014a). Promisingly, even by using the broadcast ephemeris, final velocity estimation can reach millimeter per second precision. However, one important limitation for earthquake source inversion must be noted: integration of velocities into co-seismic displacements, required for the inversion, introduces inevitable bias (Tu et al., 2013).

As it was mentioned before, we are interested in displacements which take place in just a few minutes. At the same time, ionospheric delays for each satellite are normally strongly correlated during such a short period. This fact also implies that the delays can be feasibly represented by a low-order time-dependent polynomial and, furthermore, can be predicted with an accuracy of few centimeters (Geng et al., 2010; Zhang and Li, 2012). In this study, we develop a new algorithm for retrieving real-time precise co-seismic displacements with a standalone single-frequency GPS receiver by estimating ionospheric corrections based on data before earthquake and predicting the corrections for observations afterwards.

In the following, in section 2 and section 3 we present technological details of the new algorithm, in section 4 some specific issues related to the new algorithm are further discussed. In section 5 we validate it by an outdoor experiment and then it is applied to process GPS dataset recorded during the Great March 11, 2011 Tohoku Mw 9.0 earthquake.

2.2 Basic observation equations

Following the approach and notation of Li et al. (2014b), GPS measurements on a single frequency can be expressed as follows

$$l_r^s = -u_r^s \cdot x - o^s - \tau^s + \tau_r + B_r^s - I_r^s + T_r^s + \varepsilon_r^s \tag{1}$$

$$P_r^s = -u_r^s \cdot x - o^s - \tau^s + \tau_r + I_r^s + T_r^s + \varepsilon_r^s \tag{2}$$

where the superscript s denotes the satellite, subscript r-means receiver; l_r^s and P_r^s are the "Observed Minus Computed" (OMC) phase and range values; u_r^s denotes the unit vector from receiver r to satellite s; x denotes the vector of receiver position increments relative to a priori position x_0, which is used for linearization; o^s, τ^s and τ_r stand for satellite orbit error, clock error, receiver clock error, correspondingly; B_r^s is the phase ambiguity; I_r^s and T_r^s are the ionosphere and troposphere delays and ε_r^s is measurement noise. For precise positioning, other effects, like relativistic effects, phase center variations, phase wind up, tidal loading, should be also taken into account carefully. As range observations are much noisier than phases, they are mainly used for getting receiver clock biases instead of displacement.

Since the station position is usually precisely known for any epoch t_n before an earthquake, i.e., $x(t_n)$ in Eq. 1 is zero, thus it can be rewritten as:

$$l(t_n) = -o^s(t_n) - \tau^s(t_n) + \tau_r(t_n) + B(t_n) - I(t_n) + T(t_n) + \varepsilon(t_n) \tag{3}$$

For any epoch t_m after the starting time of an earthquake, we have

$$l(t_m) = -u(t_m) \cdot x(t_m) - o^s(t_m) - \tau^s(t_m) + \tau_r(t_m) + B(t_m) - I(t_m) + T(t_m) + \varepsilon(t_m) \quad (4)$$

Similar to the "variometric" (Colosimo et al., 2011) and TPP (Li et al., 2013b) approaches, differenced observations between epochs m and n are utilized to remove or to reduce the biases.

Normally, for GPS stations designed for co-seismic displacement monitoring the occasional loss lock of signal is extremely rare. As a result, the ambiguity is usually unchanged over the time of interest. Otherwise, the epoch-differenced obseravtions could not contribute to the estimation (Colosimo et al., 2011, Li et al., 2014a). Subtracting (3) from (4), an epoch-differenced measurement can be formed as:

$$l(t_{m,n}) = -u(t_m) \cdot x(t_m) - o^s(t_{m,n}) + \tau_r(t_{m,n}) - \tau^s(t_{m,n}) - I(t_{m,n}) + T(t_{m,n}) + \varepsilon(t_{m,n}) \quad (5)$$

Here $t_{m,n}$ indicates the difference between epoch m and epoch n, $x(t_m)$ is the co-seismic displacements to be estimated, and $\tau_r(t_{m,n})$ the receiver clock as unknown as well.

Thanks to the contribution from RTS, accuracies of real time orbits and clocks have been improved to about a few centimeters, their remaining biases $o^s(t_{m,n})$ and $\tau^s(t_{m,n})$ in Eq.5 are further reduced by forming the epoch-difference and, thus, can be safely neglected.

The total slant tropospheric delay is corrected by the following empirical model (Urquhart et al., 2014)

$$T = T_{zhd} \cdot M^h + T_{zwd} \cdot M^w \quad (6)$$

where T_{zhd} and T_{zhw} are dry and wet part of zenith delay calculated from a mathematical model (e.g., Saastamoinen 1972), and M^h and M^w are corresponding mapping functions dependent on elevation angle (e.g., Boehm et al., 2006), respectively. Promisingly, these models can reach accuracy of several centimeters (Schueler, 2014). If meteorological condition does not change abruptly, the tropospheric delay will change slowly against time. As a result, the accuracy of epoch-differenced tropospheric delay $T(t_{m,n})$ can be further improved. For the residual tropospheric delays, they can be precisely treated as part of ionospheric delays, because they are rather small and elevation-angle dependent. Hence, Eq.5 can be simplified as

$$l(t_{m,n}) = \tau_r(t_{m,n}) - u(t_m) \cdot x(t_m) - I(t_{m,n}) + \varepsilon(t_{m,n}) \quad (7)$$

Finally, the biggest obstacle for retrieving accurate co-seismic displacements with single-frequency data is quantification of ionospheric variations.

2.3 Precise modeling of ionospheric delays

Similar to Eq.7, and assuming that the loss lock do not occur before the earthquake, epoch-difference between epoch l and n is formed before an earthquake can be expressed as:

$$l(t_{l,n}) = \tau_r(t_{l,n}) - I(t_{l,n}) + \varepsilon(t_{l,n}) \tag{8}$$

Within a short time period of few minutes the ionospheric delay can be represented by a low-order polynomial. However, the receiver clock bias can change rapidly, especially when using low-cost receivers. Hence, an inter-satellite difference is formed to cancel the effect of the unstable receiver clock. After applying the difference between satellite s and a reference satellite j, we can write:

$$l^j(t_{l,n}) - l^s(t_{l,n}) = -I^j(t_{l,n}) + I^s(t_{l,n}) + \varepsilon^j(t_{l,n}) - \varepsilon^s(t_{l,n}) \tag{9}$$

For each satellite, we assume that its ionospheric delay is depicted by a linear model in time t:

$$I = a \cdot t + b \tag{10}$$

Then Eq.9 can be then rewritten as:

$$l^j(t_{l,n}) - l^s(t_{l,n}) = (a_s - a_j) \cdot t + b_s - b_j + \varepsilon^j(t_{l,n}) - \varepsilon^s(t_{l,n}) \tag{11}$$

Here, the multipath effect is the dominate part of the unmodeled error sources ε. For a permanent station, over a short time span, its surrounding environment remain almost the same and after epoch differencing ε can be greatly canceled. With a continuous dataset, a set of observation equations of type Eq.11 can be formed to solve for the polynomial coefficients. Due to the functional correlation between a_s and a_j, b_s and b_j, the resulting matrix is linearly-dependent and, instead of solving for all the four parameters, one can just estimate their differences $a_s - a_j$ and $b_s - b_j$. It is easy to prove that this does not affect the final positioning result.

First of all, for generic satellite s, Eq.7 can be re-written as:

$$l^s(t_{m,n}) = -u^s(t_m) \cdot x(t_m) + \tau_r(t_{m,n}) - I^j(t_{m,n}) - (I^s(t_{m,n}) - I^j(t_{m,n})) + \varepsilon^s(t_{m,n}) \tag{12}$$

Substituting in Eq.12 ionospheric delay difference between satellite s and j with their polynomial representations (Eq.10), we obtain for all satellites but the reference satellite j:

$$l^s(t_{m,n}) = -u^s(t_m) \cdot x(t_m) + \tau_r(t_{m,n}) - I^j(t_{m,n}) - \left((a_s - a_j)t + b_s - b_j\right) + \varepsilon^s(t_{m,n}) \tag{13}$$

Similarly, for the reference satellite j itself, Eq.13 is :

$$l^j(t_{m,n}) = -u^j(t_m) \cdot x(t_m) + \tau_r(t_{m,n}) - I^j(t_{m,n}) + \varepsilon(t_{m,n}) \tag{14}$$

In Eq.13 and Eq.14, one can see that for all of satellite observations, they have the common parameter $\tau_r(t_{m,n}) - I^j(t_{m,n})$, which indicates that ionospheric delays of reference satellite j can be absorbed by receiver clock parameter, so that we do not need to solve for a_s, b_s, a_j, b_j individually.

It was confirmed that the accuracy of predicted ionospheric delay changes is highly related to the time latency $t_{m,n}$ and the satellite elevation angle (Geng et al., 2010; Zhang and Li 2012). Observations corrected by the predicted ionospheric delay changes should be properly weighted. For example, in present study, following weighting strategy is employed:

$$P = \begin{cases} 1.0 & t \le 30s \\ 2\sin(E) & 30s \le t \le 300s \;\&\; E \le 30^\circ \\ 1.0 & 30s \le t \le 300s \;\&\; E > 30^\circ \end{cases} \tag{15}$$

In general, predictions over a shorter time and at higher elevations are more reliable and, hence, deserve larger weight.

2.4 Implementation remarks

From the above description, the key point for retrieving real-time co-seismic displacement is precise prediction of ionospheric delay changes which can be well handled with the proposed linear fitting model. However, there are still several other aspects which may affect final solution and, hence, deserve special consideration.

The first issue is the length of the data window prior to an earthquake used to derive coefficients of the polynomial, *a* and *b* (see Eq. 10). On one hand, with a long arc of data, the prediction accuracy could be degraded due to possible variations of ionospheric delays that do not follow a polynomial form. On the other hand, too few epochs may not be enough to represent the correct trend of ionospheric delay changes. Since there is no rule of thumb for selection of an optimal time window, after a number of experimental tests we decided to use two minutes prior to earthquake. Concerning the length of the prediction window: as was explained in the introduction, the ground shaking of tsunamigenic earthquakes typically is limited to 2-3 minutes. Having this in mind, we confine our prediction time window to five minutes.

Secondly, although ionospheric delays of a reference satellite could be absorbed by the receiver clock parameters (see Eq.13-14), precise linear fitting and prediction of inter-satellite ionospheric delay require that the reference satellite should not have any large nonlinear temporal variations. Otherwise, it will introduce bias to other satellites. Hence, optimization of selection of reference satellite is absolutely necessary. Change of ionospheric slant delays is mainly caused by the change of the satellite elevation angle and by the change of the total electron content in space and time. As the latter is usually rather small and gentle over several minutes, we choose the satellite with the highest elevation angle as a reference satellite to minimize the effect of the change of elevation angle.

The stability of ionospheric delay of a satellite could be further assessed by the fitting residuals of the inter-satellite differenced ionospheric delays. Satellites with poor stability should be down weighed in order to reduce their bad effect on estimates.

Nevertheless, the predicted ionospheric delay for some satellites could still have large bias, although their polynomial fitting looks well. In order to get rid of such problematic predictions, a real-time quality control procedure is definitely necessary. We employed a very simple and commonly used method by checking the estimated observation residuals. At each epoch, we carried out the estimation with all observations. Then the problematic satellites are identified by checking the observation residuals and confirmed by their residuals estimated after discarding or down-weighting the observations of the related satellites.

Lastly, it should be pointed out that the linear model may be not so effective if there is nolinear change in ionospehric delays, for example, under the equatorial ionospheric anomaly and scintillation. This is still an issue under investigation also for the method by Li et al. (2014a).

2.5 Outdoor validation and the application for 2011 Tohoku earthquake

Though assessing the performance of single-frequency GPS algorithm using L1 observations of dual-frequency receivers is a quite common practice among geodetic community (see, e.g., Van Bree and Tiberius, 2012; Tu et al., 2013; Li et al., 2014a), to demonstrate the reliability of single-frequency receiver, here the new method was evaluated first with a real single-frequency data of a dedicated experiment and then it was applied to the L1 observations of dual-frequency receviers collected during the 2011 Tohoku earthquake.

2.5.1 Outdoor validation using a real single-frequency receiver

We first conducted an experiment using a real single-frequency NOVATEL (NOVATEL SmartAntenna in the OEM4 family) receiver. In addition, a dual-frequency JAVAD (JAVARD Delts- with an TRE-3 board and a Javad GrAnt G5T Antenna) receiver was also placed within one foot to the single-frequency receiver and they were fixed together by a piece of steel plate, the whole device for the test is shown in Figure 2.1. By such a platform, the ionospheric delay of both receivers should be the same and their movements can be guaranteed to be strictly coherent .

Figure 2.1 Experimental platform for single-frequency receiver validation

Sampling rates of both receivers are 1 Hz, in order to obtain converged carrier phase ambiguities and precise receiver positions, we processed as long as 10 hours JAVAD dual-frequency data using static PPP. After its position was determined, then position of NOVATEL was calculated in relative positioning mode with respect to the dual-frequency receiver. At last, the two receivers were pushed forward and backward for several times along the fixed track from 12, March,

2015,13:06 GPS time. Movements retrieved by dual-frequency TPP and our suggested method using single-frequency data are shown in Figure 2.2. As clearly depicted, on horizontal direction, the performance of single-frequency is almost as good as dual-frequency, the RMS between them is at the level of 1.7 cm. For vertical component, it is slightly worse, the largest bias is almost 5 cm while the overall fit is limited to 3 cm in terms of RMS. To conclude, it is trustworthy to use the new method when it comes to single-frequency receiver.

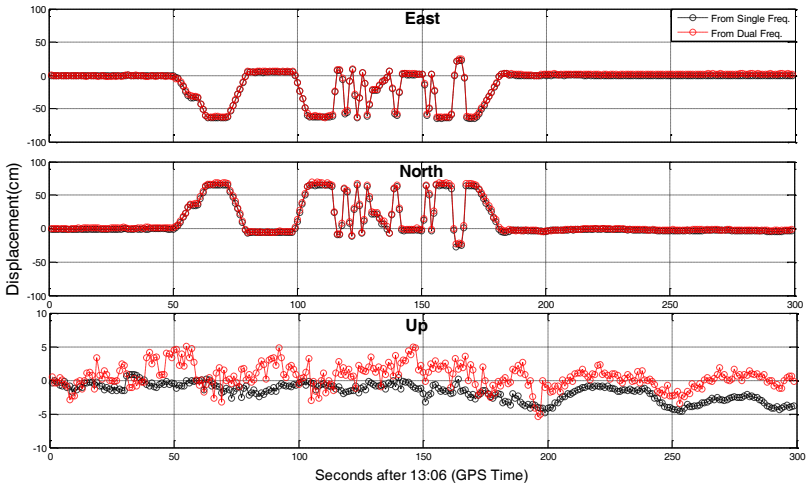

Figure 2.2 Displacements retrieved from single-frequency and dual-frequency receiver

2.5.2 Application for 2011 Tohoku earthquake

To validate the new method more broadly, we reprocessed 1 Hz GPS data collected by GEONET stations during the Great Mw 9.0 Tohoku earthquake (11 March, 2011, 05:46 UTC, GPS Time-UTC=15s). Because original GPS data were actually collected in a dual-frequency mode, for their replay in a single-frequency scenario we used only C/A code and L1 phase. 75 stations across Japan were selected for data processing. Co-seismic displacements from dual-frequency TPP method was used for benchmark of the new method.

2.5.2.1 Accuracy of predicted ionospheric change

As known, the geometry-free combination of dual-frequency data gives the ionospheric delay information according to:

$$LG = \lambda_1 \cdot L_1 - \lambda_2 \cdot L_2 = I \cdot c \cdot \frac{f_1^2 - f_2^2}{f_1^2 f_2^2} + (\lambda_1 \cdot N_1 - \lambda_2 \cdot N_2) \tag{16}$$

I is the slant ionospheric delay, c , f_i , λ_i , N_i are the speed of light, frequency, wavelength and phase ambiguity of the related signals, respectively.

Assuming that there is no cycle slip from epoch m to epoch n , the change of the delay on $L1$ can be expressed as:

$$I_{m,\mathrm{n}} = LG_{m,n} \cdot \frac{f_2^2}{f_1^2 - f_2^2} \tag{17}$$

Since all the stations in the GEONET GPS-network are equipped with dual frequency receivers, such ionospheric delay changes could be derived as "ground truth" for evaluating the predicted ones.

In order to assess the accuracy of the predicted ionospheric delays and their impact on the estimated displacements, we selected observation window of about seven minutes length starting from the GPS-time 05:26, which is just 20 minutes prior to the main Tohoku 2011 shock. During this time window, GEONET stations experienced no notable displacements and their positions were well known.

First we computed the $L1$ residuals using Eq.7 with known station coordinates for the whole period. Please note, since between-satellites single difference was adopted to remove the effect of receiver clock bias, residuals were then related to a reference satellite, so that they included mainly ionospheric delay changes and remaining errors in satellite orbits and clocks as well as residual tropospheric delays. The true ionospheric delay changes were also calculated with Eq.17 using dual-frequency phase observations for comparison.

For illustration purpose, the residuals with respect to G27 and the true ionospheric changes at the station 0219 are shown in Figure 2.3 together with satellite elevation angles.

One can see that ionospheric delay change is strongly correlated with both the absolute value and variations of the satellite elevation angle. For example, satellites G15 and G21 have very small change in elevation, as a result, their ionospheric delay changes do not exceed 10 cm. In contrast, ionospheric delay change of G18 reaches up to 65 cm. Note, despite G27 rises faster than G18, its ionospheric delay change is smaller because of the significantly higher elevation. As expected, G27'sionospheric delay change smoothly and nearly linearly supporting the feasibility of linear fitting.

Ionospheric delay changes from dual-frequency data were first converted to relative delay changes with respect to the same reference satellite G27 and then the differences between the two relative delay changes were calculated and shown in Figure 2.4. They agree with each other better than 1 to 2 cm in RMS. This comparison verifies once again that the new algorithm can represent relative ionospheric variations with enough degree of reliability.

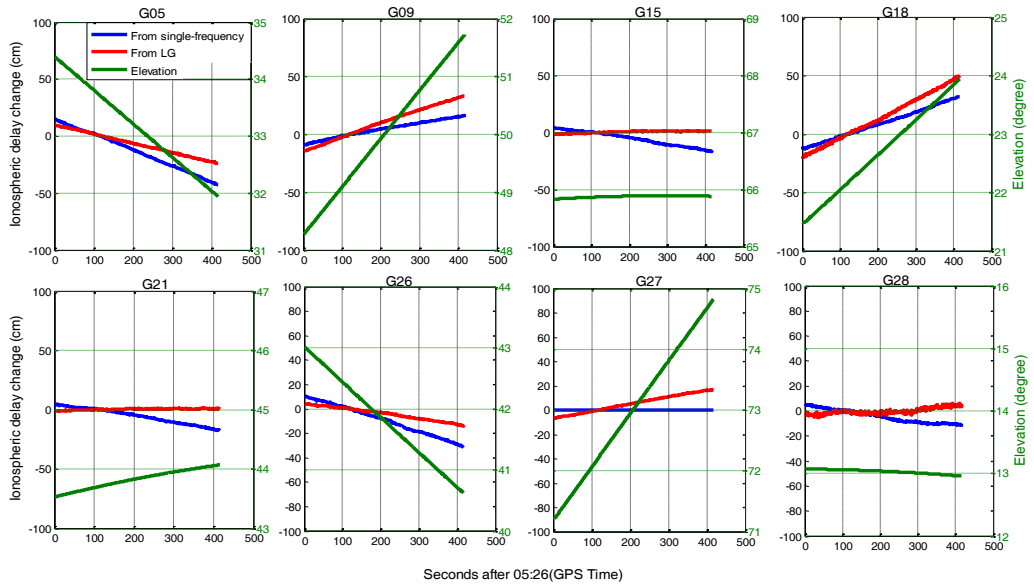

Figure 2.3 Ionospheric delay changes on L1 frequency at station 0219: blue-derived with the proposed single-frequency method and using G27 as reference satellite; red-derived from dual-frequency observations. Elevation angles are also plotted (green).

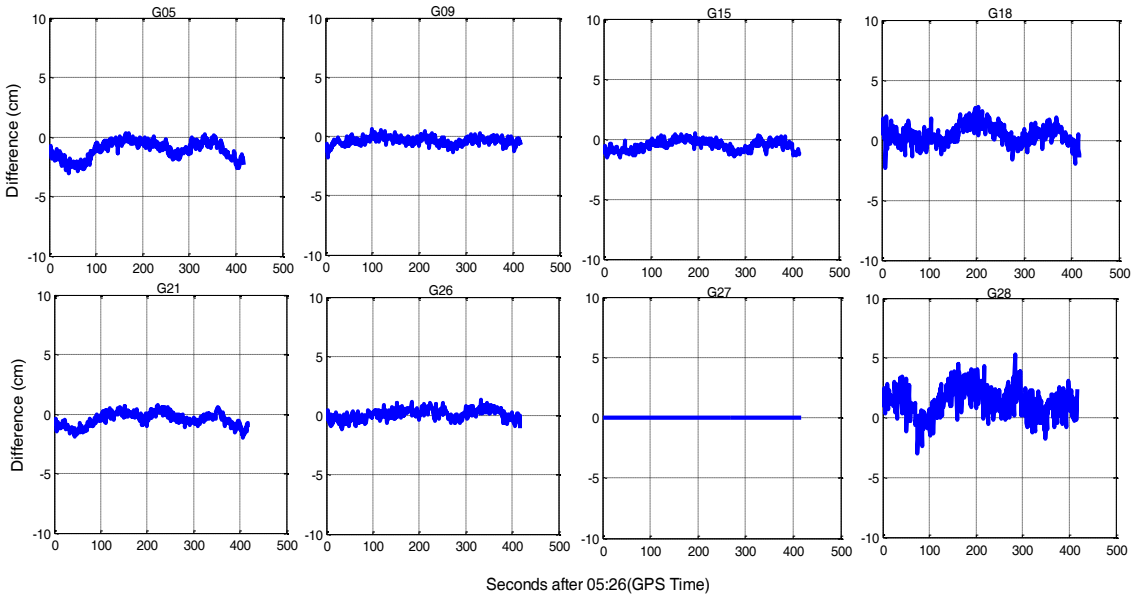

Figure 2.4 Differences between relative ionospheric delay changes on L1 from single-frequency and from geometry-free combination of dual-frequency observations, here G27 is the reference satellite.

Relative ionospheric delay changes during the first two minutes were used to establish a linear model for the ionospheric delay change of each satellite. With this estimated linear model, ionospheric delay changes for all epochs over next five minutes were calculated and applied to the observation equations. Pre-fit residuals shown in Figure 2.5 can be considered as a quality index for the performance of the linear model. The red dashed line divides data into two parts: (1) two minutes before the dashed line for fitting and (2) five minutes for displacement estimation with predicted ionospheric corrections. Residuals of the first part can be also treated as residuals of the polynomial fitting. For all satellites, the residuals are smaller than 1 cm RMS. This experiment convincingly demonstrates that within short time intervals, ionospheric delay changes

can be fitted strictly linearly. Not surprisingly, error grows with time. However, on the whole, accuracy remains better than 2 cm.

Applying the corrections to the single-frequency data processing, we got the five-minute time series of displacements shown in Figure 2.6. Variations in both horizontal and vertical components are limited to 2cm and 3 cm, respectively.

For comparison, positioning was also performed using uncorrected L1 directly. As expected, the results (Figure 2.7) show an obvious linear trend. Mostly, a linear fit model is suggested to remove this effect. Here we used the first two minutes time series to obtain the corresponding linear parameters. For east-west component, the model is quite encouraging. However, with respect to north-south and vertical components, the linear model causes tens of centimeters misfit, which implies linear fit cannot guarantee reliable accuracy.

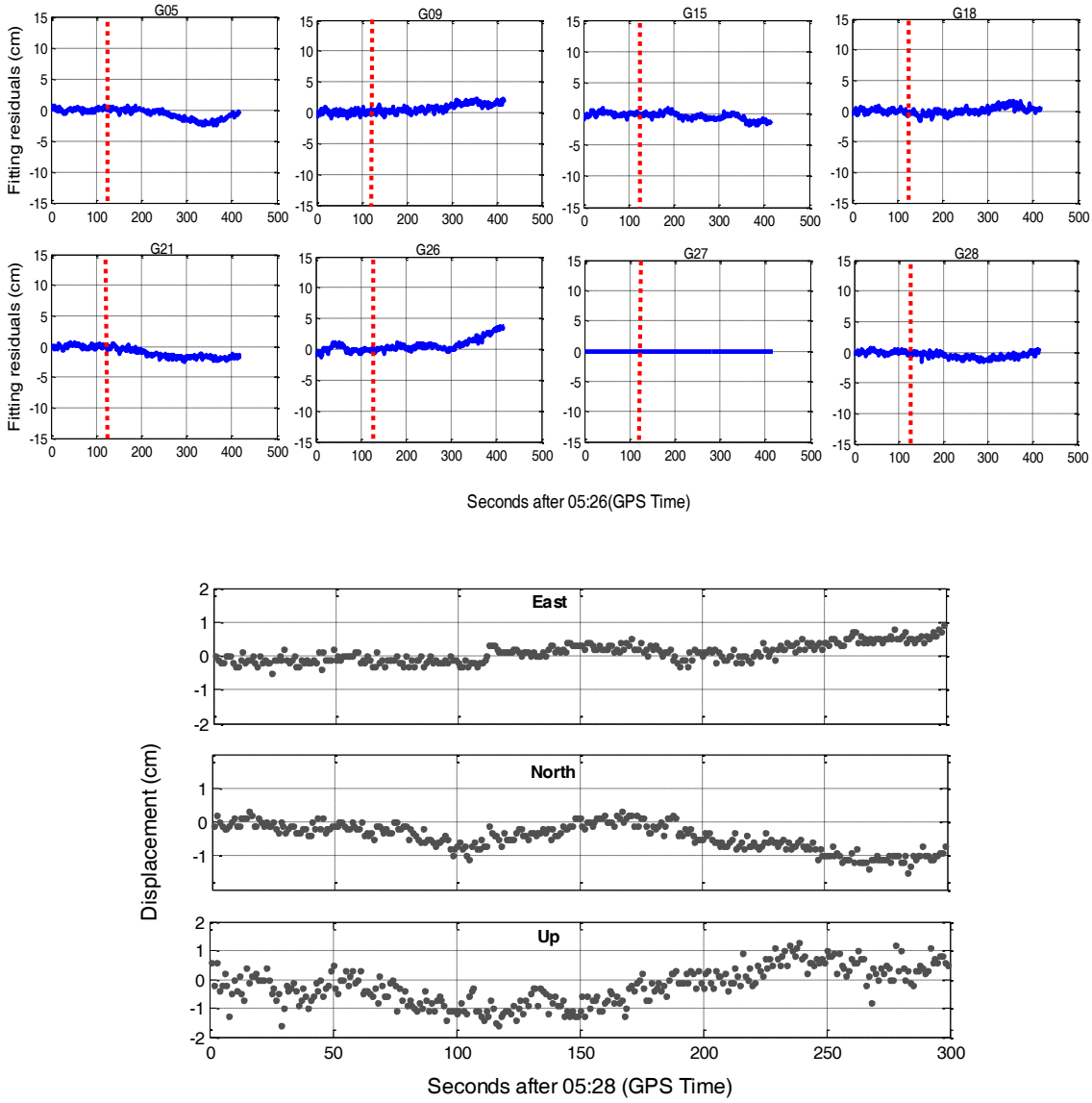

Figure 2.6 Displacements of station 0219 using L1 phase observations, which were corrected by the predicted ionospheric delay changes.

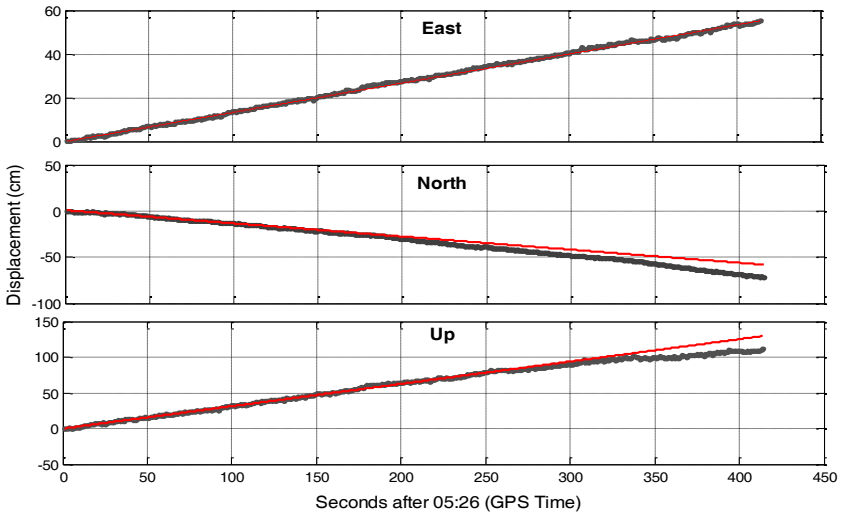

Figure 2.7 Displacements of station 0219 using L1 phase observations without ionospheric delay correction, the black dots denote displacements while the red line means linear fit.

2.5.2.2 Quality control of the predicted ionospheric delays

As mentioned above, there could be satellites with biased ionospheric delay predictions. This may result in contaminated displacement. Figure 2.8 shows the displacement time series of station 0008 with an obvious drift of about 10 cm in vertical component. As there was not any tectonic movement during the time period, the drift is most likely caused by a significantly wrong prediction of relative ionospheric delays. That is supported by the plot of ionospheric delays in Figure 2.9. For satellite G28, the trend of ionospheric changes is very different for the time before and after the dashed line. In such a case, linear fitting produces a bias trend for the prediction interval. Note the large prediction error of about 13 cm for G28 in comparison with an error of a few centimeters for all other satellites (Figure 2.10). Fortunately, bad predictions can be automatically detected by the proposed ~~"q~~uality control" procedure, so that displacements of high accuracy as shown in Figure 2.11 could still be achieved. It should be pointed out, that there is a slight ~~"j~~ump" in the displacement time series after the problematic satellite is first detected and discarded. However, the typical ~~"j~~ump" is rather small (1 to 2 cm) and can be completely avoided by re-processing the original data without any detected problematic satellites.

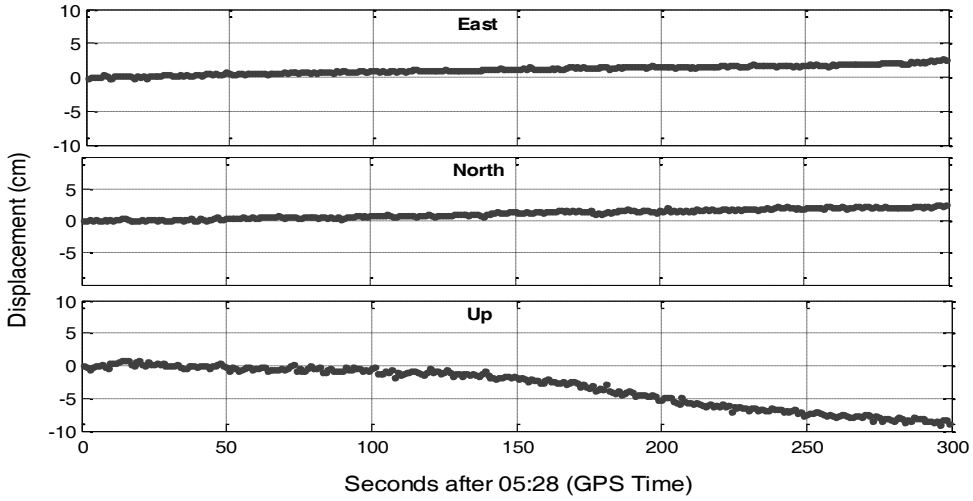

Figure 2.8 Displacements of station 0008 (before quality control correction): an obvious drift exists in vertical component.

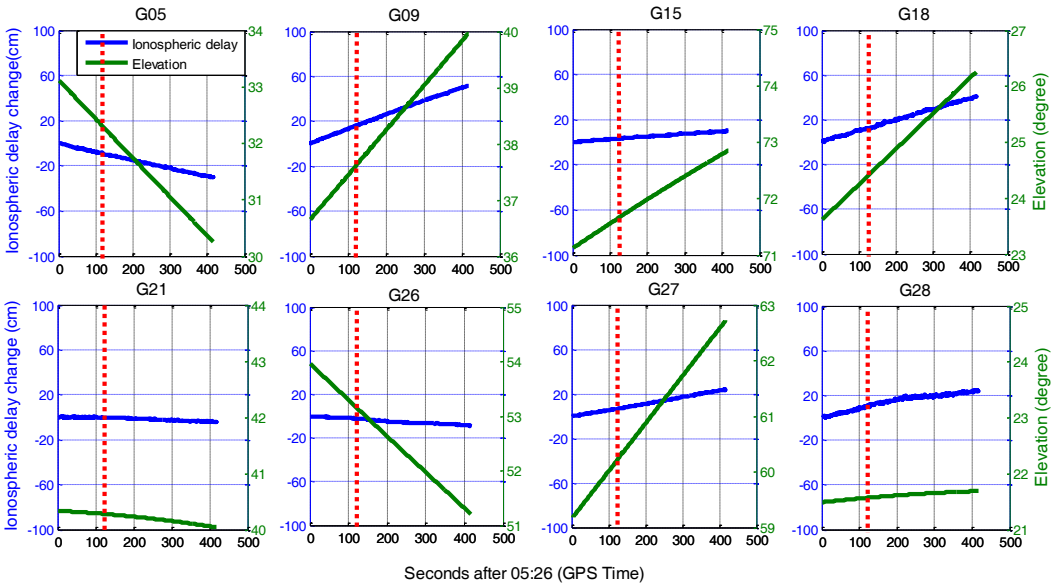

Figure 2.9 Time evolution of the ionospheric delay (blue) and elevation angle change on L1 (green) at station 0008 starting from GPS Time 05:26. Time window from beginning to the red dash line is used to derive parameters for linear fitting.

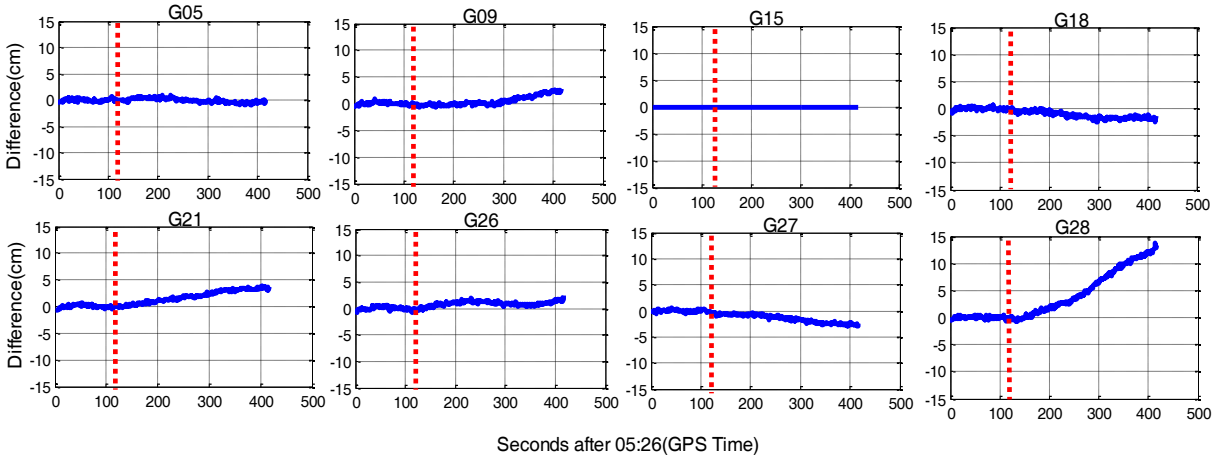

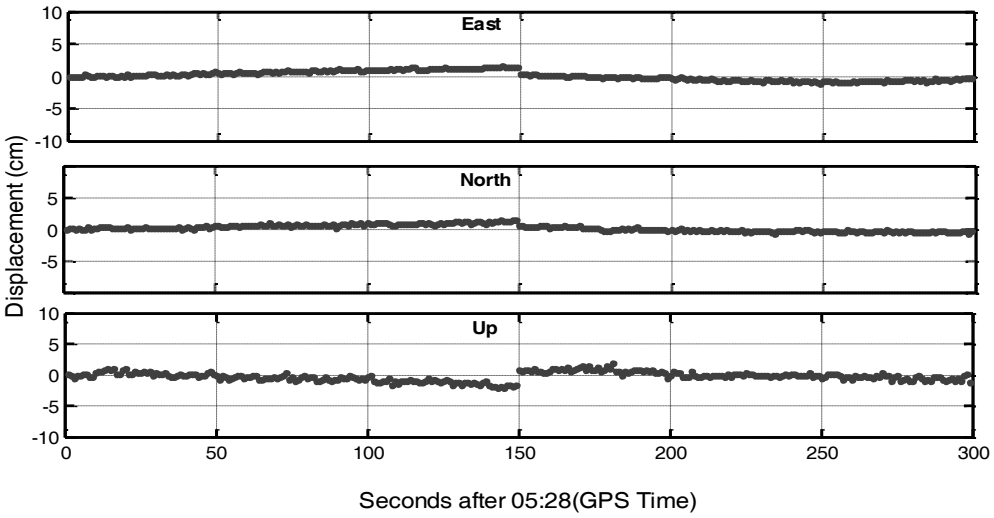

Figure 2.11 Displacements at station 0008 after applying proposed quality control procedure. The jump shows the epoch from which the problematic predictions were detected and rejected.

2.5.2.3 Performance of single-frequency co-seismic displacements retrieving

To guarantee that the approach used here was good during the moment of earthquake ,we should first make sure that ionospheric delay at this time also changed linearly. Take station 0035 as an example, actual ionospheric delay derived from the dual-frequency data during shaking is then shown in Figure 2.12, in which one can see ionospheric delay keeps linear. For data processing of each station, seven minutes of data stream were analyzed: first two minutes for polynomial fitting and the following five minutes for estimation of ground displacements. Displacements estimated by the two methods were compared, and the RMS of their differences over the five „predicted" minutes was plotted on Figure 2.13. In terms of the RMS, the horizontal and the vertical agreements are better than 2 cm for the whole period.

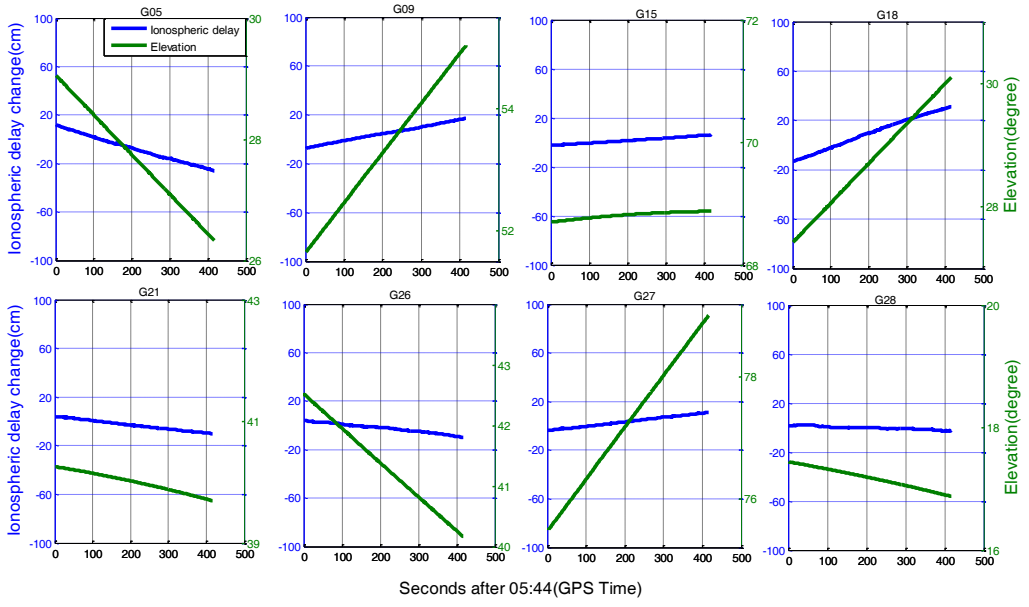

Figure 2.12 Ionospheric delay change at station 0035 during earthquake time

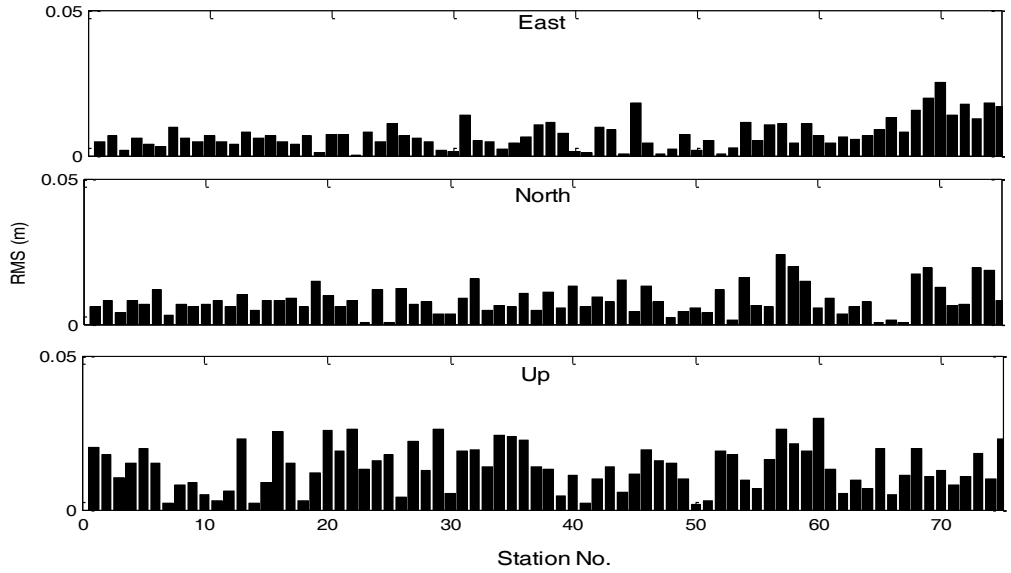

Figure 2.13 RMS of the differences between co-seismic displacement waveforms derived by the new method and the traditional dual-frequency TPP method.

Figure 2.14 shows co-seismic displacement waveforms at three selected GEONET stations derived with our new method for single-frequency data (blue line) and using the TPP method for dual-frequency data (red line). The three stations are located at different epicentral distances: station 0035 at 250 km; station 0046 at 560 km; and station 0066 at 850 km. Their co-seismic permanent displacements vary from about 2 meters to a few centimeters. Nevertheless, single-frequency displacement waveforms at all three stations are in very good agreement with the TPP displacement waveforms: discrepancies do not exceed a few centimeters during the whole evaluation period of 5 minutes. As can be expected, the discrepancy grows with time but remains within ± 2.0 cm for horizontal and ± 5 cm for vertical displacements, correspondingly.

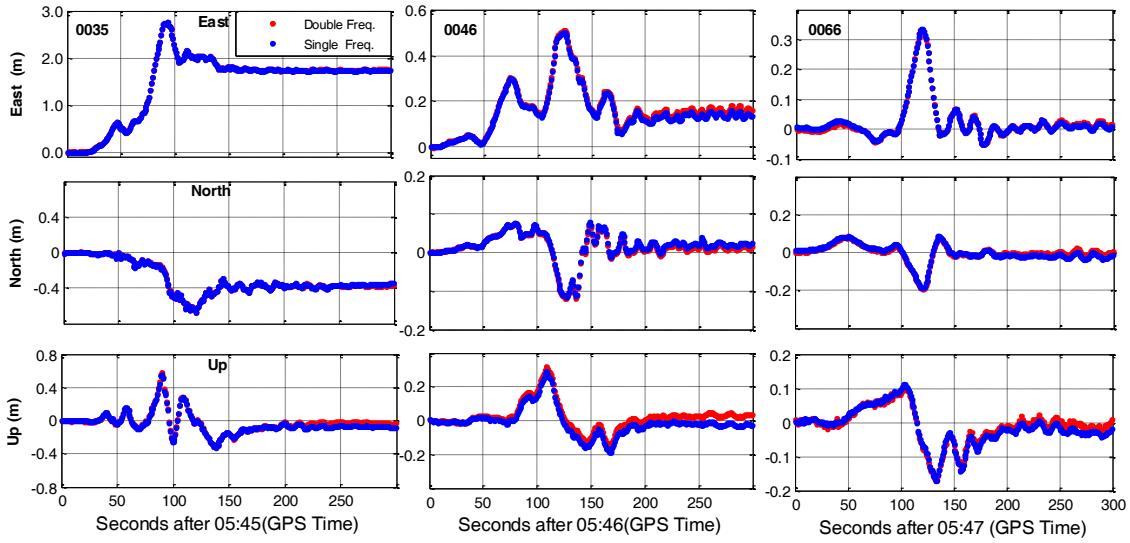

Figure 2.14 Co-seismic displacement waveforms derived using the new single-frequency method compared to the traditional dual-frequency TPP method at three different GEONET GPS-network stations.

Figure 2.15 presents in map view the final static displacements corresponding to the main Tohoku 2011 shock. Static displacements at each station were obtained by averaging displacement waveforms over the last 20 seconds of the five minutes time period (refer to Fig. 14). It is vividly demonstrated that the static displacements derived by the two methods agree with each other very well. Corresponding differences for all 75 stations are shown in Figure 2.16: RMS of the differences is 2 cm, 2 cm and 3 cm for east, north and vertical component, respectively. Furthermore, 10 hours data before and after the earthquake broke were also processed by PPP static solution strategy and then static permanent displacements were computed by differencing. For convenience, here we name them as ‗daily solution', which are also present in Figure 15.This result clearly demonstrates that single-frequency data can be certainly employed for estimating co-seismic displacement for geohazard monitoring and early warning.

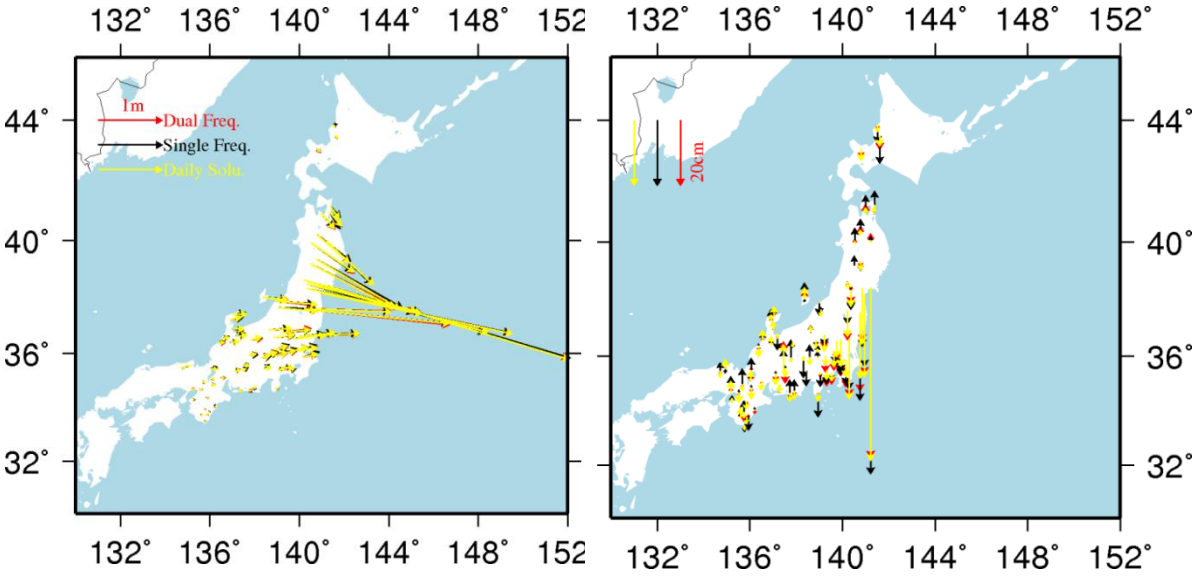

Figure 2.15 Co-seismic static displacements due to Tohoku 2011 main shock derived by the new method using single-frequency data (black) and TPP using dual-frequency data (red). Left plot shows horizontal displacement, right-vertical displacement.

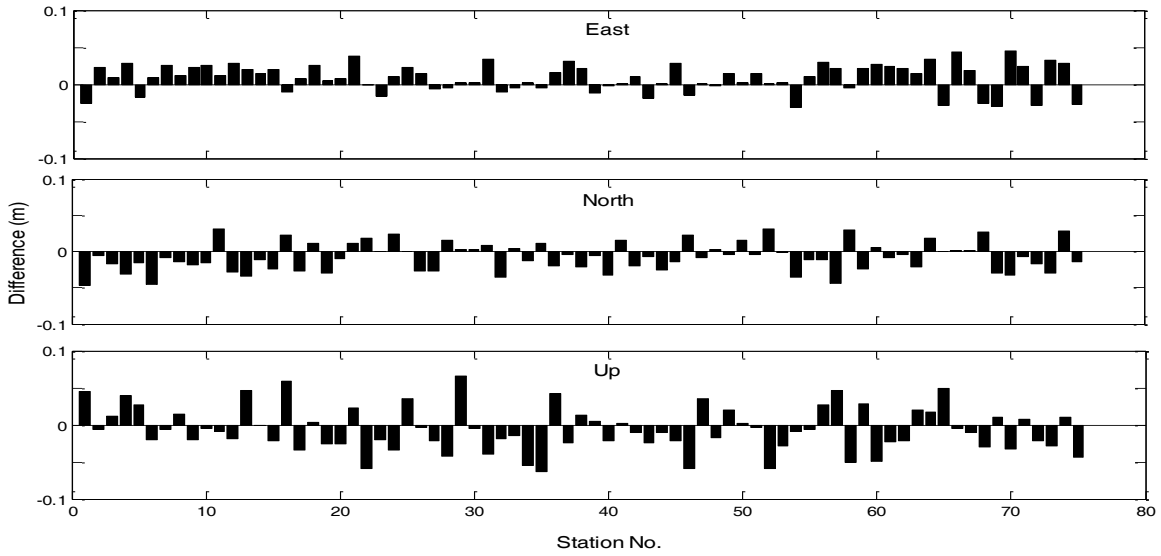

Figure 2. 16 Differences between co-seismic static displacements retrieved by the two methods at 75 GEONET stations (see description of Fig. 14).

2.6 Conclusions and perspective

In this study, we have demonstrated the potential of using single-frequency GPS for retrieving co-seismic displacements in real-time. Use of inexpensive single-frequency GPS receivers may be economically favorable for the broad and dense geodetic networks required for earthquake and tsunami early warning. A new algorithm was developed based on the precise prediction of ionospheric delay changes over a short time window around the earthquake. A linear prediction model was selected to produce reliable results. We also suggest an automatic quality control procedure for detection and removal of problematic ionospheric corrections.

Accuracy of the new method was first tested by an outdoor experiment with simultaneous implication of single- and dual-frequency receivers. Average RMS constituted 1.7 cm for horizontal and 3 cm for the vertical component. We have also successfully validated our method by re-processing 1-Hz GPS data from the GEONET network during the 2011 Tohoku M9.0 earthquake. Kinematic and permanent co-seismic displacements obtained from the proposed method using single-frequency data was compared with that of the TPP method with dual-frequency data. Results evaluated at 75 GEONET stations show good agreement in terms of RMS: 2 cm, 2cm, and 3cm for east, north and vertical components, respectively. This work suggests that using single-frequency GPS receivers for monitoring and early warning of earthquake and related geohazards, e.g., tsunamis is feasible.

Considering the rapid development of multi-constellation-Global Navigation Satellite Systems (GNSSs) and more and more widely used multi-GNSSs receivers, the benefit of multi-GNSS (Li et al., 2015a, 2015b) for geohazard applications will be investigated in the near future.

2.7 Acknowledgments

Mr. Kejie Chen is financially supported by China Scholarship Council (CSC) for his PhD study at GFZ. 1 Hz GEONET GPS-network data were provided by the Geospatial Information Authority of Japan. This work are also supported by National Natural Science Foundation of China (No. 41231174 and No. 41474020). Three anonymous reviewers are acknowledged for their valuable comments which have improved this paper considerably.

2.8 References

Blewitt, G., Kreemer, C., Hammond, W. C., Plag, H. P., Stein, S., & Okal, E. (2006). Rapid determination of earthquake magnitude using GPS for tsunami warning systems. Geophysical Research Letters, 33(11).

Boehm, J., Niell, A., Tregoning, P., &Schuh, H. (2006). Global Mapping Function (GMF): A new empirical mapping function based on numerical weather model data. Geophysical Research Letters, 33(7).

Benedetti, E., Branzanti, M., Biagi, L., Colosimo, G., Mazzoni, A., & Crespi, M. (2014). Global Navigation Satellite Systems Seismology for the 2012 Mw 6.1 Emilia Earthquake: Exploiting the VADASE Algorithm. Seismological Research Letters, 85(3), 649-656.

Colosimo, G., Crespi, M., &Mazzoni, A. (2011). Real-time GPS seismology with a stand-alone receiver: A preliminary feasibility demonstration. Journal of Geophysical Research: Solid Earth (1978–2012), 116(B11).

Geng, J., Meng, X., Dodson, A. H., Ge, M., & Teferle, F. N. (2010). Rapid re-convergences to ambiguity-fixed solutions in precise point positioning. Journal of Geodesy, 84(12), 705-714.

Geng, J., Teferle, F. N., Meng, X., & Dodson, A. H. (2011). Towards PPP-RTK: Ambiguity resolution in real-time precise point positioning. Advances in space research, 47(10), 1664-1673.

Geng, J., Bock, Y., Melgar, D., Crowell, B. W., &Haase, J. S. (2013). A new seismogeodetic approach applied to GPS and accelerometer observations of the 2012 Brawley seismic swarm: Implications for earthquake early warning.Geochemistry, Geophysics, Geosystems, 14(7), 2124-2142.

Klobuchar, J. A. (1987). Ionospheric time-delay algorithm for single-frequency GPS users. Aerospace and Electronic Systems, IEEE Transactions on, (3), 325-331.

Larson, K. M., Bodin, P., &Gomberg, J. (2003). Using 1-Hz GPS data to measure deformations caused by the Denali fault earthquake. Science,300(5624), 1421-1424.

Lay, T., Kanamori, H., Ammon, C.J., Nettles, M, Ward, S. N., Aster, R. C., Beck, S. L., Bilek, S. L., Brudzinski, M. R., Butler, R., DeShon, H. R., Ekstrom, G., Satake, K., and Sipkin, S. (2005). The Great Sumatra-Andaman Earthquake of 26 December 2004. Science 308, 1127-1133.

Li, M., Li, W., Fang, R., Shi, C., & Zhao, Q. (2014a). Real-time high-precision earthquake monitoring using single-frequency GPS receivers. GPS Solutions,19(1), 27-35.

Li, X., Ge, M., Zhang, X., Zhang, Y., Guo, B., Wang, R., &Wickert, J. (2013a). Real‐time high‐rate co‐seismic displacement from ambiguity‐fixed precise point positioning: Application to earthquake early warning. Geophysical Research Letters, 40(2), 295-300.

Li, X., Ge, M., Guo, B., Wickert, J., &Schuh, H. (2013b). Temporal point positioning approach for real‐time GNSS seismology using a single receiver.Geophysical Research Letters, 40(21), 5677-5682.

Li, X., Guo, B., Lu, C., Ge, M., Wickert, J., &Schuh, H. (2014b). Real-time GNSS seismology using a single receiver. Geophysical Journal International, ggu113.

Li, X., X. Zhang, X. Ren, M. Fritsche, J. Wickert, and H. Schuh (2015a), Precise positioning with current multi-constellation Global Navigation Satellite Systems: GPS, GLONASS, Galileo and BeiDou. Sci Rep., 5, 8328.

Li, X., M Ge, X Dai, X Ren, M Fritsche, J Wickert, and H. Schuh (2015b), Accuracy and reliability of multi-GNSS real-time precise positioning: GPS, GLONASS, BeiDou, and Galileo. Journal of Geodesy, doi: 10.1007/s00190-015-0802-8

Lifton, Z. M., Newman, A. V., Frankel, K. L., Johnson, C. W., & Dixon, T. H. (2013). Insights into distributed plate rates across the Walker Lane from GPS geodesy. Geophysical Research Letters, 40(17), 4620-4624.

Ohta, Y., Kobayashi, T., Tsushima, H., Miura, S., Hino, R., Takasu, T., &Umino, N. (2012). Quasi real‐time fault model estimation for near‐field tsunami forecasting based on RTK‐GPS analysis: Application to the 2011 Tohoku‐Oki earthquake (Mw 9.0). Journal of Geophysical Research: Solid Earth (1978–2012), 117(B2).

Prawirodirdjo, L., & Bock, Y. (2004). Instantaneous global plate motion model from 12 years of continuous GPS observations. Journal of Geophysical Research: Solid Earth (1978–2012), 109(B8).

Ren, J., Chen, G., Xu, X., Zhang, S., & Mao, C. (2010). Surface rupture of the 2008 Wenchuan, China, earthquake in the Qingpingstepover determined from geomorphologic surveying and excavation, and its tectonic implications. Bulletin of the Seismological Society of America, 100(5B), 2651-2659.

Saastamoinen, J. (1972). Atmospheric correction for the troposphere and stratosphere in radio ranging satellites. Geophysical Monograph Series, 15, 247-251.

Schaer, S., Beutler, G., Rothacher, M., & Springer, T. A. (1996, March). Daily global ionosphere maps based on GPS carrier phase data routinely produced by the CODE Analysis Center. In Proceedings of the IGS AC Workshop, Silver Spring, MD, USA (pp. 181-192).

Schueler, T. (2014). The TropGrid2 standard tropospheric correction model. GPS solutions, 18(1), 123-131.

Shi, C., Lou, Y., Zhang, H., Zhao, Q., Geng, J., Wang, R., .& Liu, J. (2010). Seismic deformation of the Mw 8.0 Wenchuan earthquake from high-rate GPS observations. Advances in Space Research,46(2), 228-235.

Sudhakar, T., Suriyakala, C. D., &Thangarasu, P. (2013, October). Case study of Tsunami warning system using RTK GPS method. In Ocean Electronics (SYMPOL), 2013 (pp. 119-126). IEEE.

Sobolev, S. V., Babeyko, A. Y., Wang, R., Hoechner, A., Galas, R., Rothacher, M., &Subarya, C. (2007). Tsunami early warning using GPS‐Shield arrays. Journal of Geophysical Research: Solid Earth (1978–2012), 112(B8)

Tu, R., Wang, R., Ge, M., Walter, T. R., Ramatschi, M., Milkereit, C., &Dahm, T. (2013). Cost-effective monitoring of ground motion related to earthquakes, landslides, or volcanic activity by joint use of a single‐frequency GPS and a MEMS accelerometer. Geophysical Research Letters, 40(15), 3825-3829.

Urquhart, L., Nievinski, F. G., & Santos, M. C. (2014). Assessment of troposphere mapping functions using three-dimensional ray-tracing. GPS solutions, 18(3), 345-354.

Van Bree,R. J., & Tiberius, C. C. (2012). Real-time single-frequency precise point positioning: accuracy assessment. GPS solutions, 16(2), 259-266.

Wang, Q., Zhang, P. Z., Freymueller, J. T., Bilham, R., Larson, K. M., Lai, X. A., ... & Chen, Q. (2001). Present-day crustal deformation in China constrained by global positioning system measurements. Science, 294(5542), 574-577.

Zhang,X., & Li, X. (2012). Instantaneous Re-initialization in Real-time Kinematic PPP with Cycle-slips Fixing. GPS solutions,16(3)315-327

Chapter 3 Retrieving real-time co-seismic displacements using GPS/GLONASS: a preliminary report from September 2015 Mw8.3 Chile Illapel earthquake

Kejie Chen[1,*], Maorong Ge[1], Andrey Babeyko[1], Xingxing Li[1], Faqi Diao[2]
GFZ German Research Center for Geosciences, 14473 Potsdam, Germany
State Key Laboratory of Geodesy and Earth's Dynamics, Institute of Geodesy and Geophysics, Chinese Academy of Sciences, Wuhan 430077, China
kejie@gfz-potsdam.de

Abstract: Compared with a single GPS system, GPS/GLONASS can improve the satellite visibility, optimize the spatial geometry and benefit the precise positioning performance. Whereas having the advantage over GPS-only in terms of positioning is clear, GPS/GLONASS's potential contribution to co-seismic displacement determination and the following seismic source inversion still requires extensive studies and validations. In this paper, we first extended temporal point positioning model from GPS-only to GPS/GLONASS. Using this new model, the performances of GPS/GLONASS for obtaining co-seismic displacements were then validated by eight out-door experiments on a shaking table. Our result reveals that GPS/GLONASS provides more accurate and robust co-seismic displacements than GPS-only in an adversary observation environment. Furthermore, as a case study, observation data recorded during September 2015 Mw8.3 Chile Illapel earthquake was re-processed. At some stations, obvious biases were found between co-seismic displacements derived from GPS-only and GPS/GLONASS. In addition to that, slip distribution inversions were conducted based on different co-seismic displacements.

Key words: GPS/GLONASS; co-seismic displacements retrieving; slip distribution inversion.

3.1 Introduction

The potential of using GPS to retrieve co-seismic displacements was discussed as early as more than decades ago (see, e.g., Hirahara et al. 1994; Tsuji et al. 1995; Ge 1999; Ge et al. 2000), which first experimentally demonstrated that GPS was able to capture transient co-seismic deformation. Following these pioneering studies, GPS has been widely exploited in monitoring seismic waveforms and extracting co-seismic offset (see, e.g., Simons et al. 2002; Larson et al. 2003; Bock et al. 2004; Vigny et al. 2005; Banerjee et al. 2007). Consequently, an interdisciplinary subject of study, namely GPS seismology, was put forward [*Larson*, 2009]. Based on the near real-time co-seismic displacements derived from GPS, seismic characteristics (e.g., magnitude, centroid location, slip distribution) can be inverted and then contribute to earthquake early warning and tsunami early warning, which is currently a research hotspot (see, e.g., Blewitt et al. 2006; Sobolev et al. 2007; Allen and Ziv 2011; Melgar et al. 2013; Li et al. 2013). Compared with traditional seismograph approach, the GPS sensor does not saturate or tilt and provides ground displacements without limits, thus it is especially valuable for near field tsunami early warning [*Blewitt et al.*, 2009].

As a matter of fact, GPS is just one member of the Global Navigation Satellite Systems (GNSSs). To date, with respect to determination of co-seismic displacements, however, in most cases, only GPS is utilized. This is understandable considering that only GPS and GLObal NAvigation Satellite System (GLONASS) built by Russia can now offer global coverage. Besides, GPS is the oldest and the most mature one, and the related error models and products, e.g., satellite antenna phase center offset, satellite orbit and clock biases, are the most precise. As a result, for many

GNSS-based networks (e.g., GEONET in Japan, PBO in U.S.), most of the receivers only ereceive and record GPS signals over the past years.

Nowadays, both GPS and GLONASS are undergoing modernization, other Navigation Satellite Systems, e.g., Galileo built by European Union, BeiDou built by China have also been on pilot run or providing regional service (see, e.g., Hofmann-Wellenhof et al. 2007; Yang et al. 2014). Totally, there will be over 100 navigation satellites available which improves observation redundancy significantly. Compared with a single system, multi-GNSS can significantly improve the satellite visibility, optimize the spatial geometry, reduce dilution of precision and will be of great benefits to both scientific applications and engineering services [*Li et al.*, 2015]. Accordingly, Multi-GNSS Experiment (MGEX) have been initialed by International GNSS Service (IGS) to pave the way for provision accurate products for all constellations [*Montenbruck et al.*, 2014] and the multi-GNSS erais coming.

While numerous previous studies have focused on using a single GPS system to obtain co-seismic displacements (see, e.g., Shi et al. 2010; Colosimo et al. 2011; Li et al. 2013; Chen et al. 2015), in this paper, we tested the performance of using GPS/GLONASS for co-seismic displacements retrieving and subsequent seismic source inversion as a pioneering case study of multi-GNSS for seismic hazard application. In Section 2, mathematical model of getting co-seismic displacements based on GPS/GLONASS observations is described. In Section 3, at first, results of eight out-door experiments are shown for validation, then GPS/GLONASS data recorded during 2015 September Chile Illaple earthquake were re-processed and analyzed in details. In addition, slip distribution inversion based on co-seismic offsets derived from GPS-only and GPS/GLONASS were conducted. Finally, Section 4 summarizes main results and presents an outlook.

3.2 GPS/GLONASS model to retrieve real-time co-seismic displacements

In the context of GPS/GLONASS constellations, the combined GPS+GLONASS observation model could be written as:

$$\begin{cases} L_{r,j}^{G} = \rho_{rg}^{G} - t^{G} + t_r + \lambda_{jG}(b_{rG,j} - b_j^{G}) + \lambda_{jG}N_{r,j}^{G} - \kappa_{jG} \cdot I_{r,1}^{G} + T_r^{G} + \varepsilon_{r,j}^{G} \\ L_{r,j}^{R_k} = \rho_{rg}^{R} - t^{R} + t_r + \lambda_{jR_k}(b_{rR_k,j} - b_j^{R}) + \lambda_{jR_k}N_{r,j}^{R} - \kappa_{jR_k} \cdot I_{r,1}^{R} + T_r^{R} + \varepsilon_{r,j}^{R} \\ P_{r,j}^{G} = \rho_{rg}^{G} - t^{G} + t_r + c(d_{rG,j} - d_j^{G}) + \kappa_{jG} \cdot I_{r,1}^{G} + T_r^{G} + e_{r,j}^{G} \\ P_{r,j}^{R_k} = \rho_{rg}^{R} - t^{R} + t_r + c(d_{rR_k,j} - d_j^{R}) + \kappa_{jR_k} \cdot I_{r,1}^{R} + T_r^{R} + e_{r,j}^{R} \end{cases} \quad (1)$$

Where the indices G, R refer to the GPS, GLONASS system, respectively, and R_k indicates the GLONASS satellite with frequency factor k; r, j denote receiver, frequency; ρ_{rg} is geometric distance from satellite to receiver; t^G, t^R and t_r represent the clock biases; λ is the wavelength; b is the receiver and satellite un-calibrated phase delay while N is the integer ambiguity; c is the speed of light in vacuum; d are the code biases for receiver and satellite; I is the ionospheric delay; T means the slant tropospheric delay; ε are the sum of the measurement noise and multipath error for the carrier phase and pseudorange observations. With regard to other error budgets, e.g., tidal loading, phase center offsets and variations, phase wind-up must be corrected according to the existing models as well.

Please note, because the signal frequencies and structures are different, for each system, the code bias d_{rG}, d_{rR_k} are also different in one GPS/GLONASS receiver. Specially, for GLONASS satellites with different frequency factors, the receiver code biases d_{rR_k} are also different. In order to eliminate the singularity between receiver clock and code bias, usually the code bias for GPS satellites is set zero.

Eq.1 can be rewritten as:

$$\begin{cases} l_{r,j}^{G} = -u_r^{G} \cdot x + t_r + \lambda_{jG}(b_{rG,j} - b_j^{G}) + \lambda_{jG} N_{r,j}^{G} - \kappa_{jG} \cdot I_{r,1}^{G} + T_r^{G} + \varepsilon_{r,j}^{G} \\ l_{r,j}^{R_k} = -u_r^{R_k} \cdot x + t_r + \lambda_{jR_k}(b_{rR_k,j} - b_j^{R}) + \lambda_{jR_k} N_{r,j}^{R} - \kappa_{jR_k} \cdot I_{r,1}^{R} + T_r^{R} + \varepsilon_{r,j}^{R} \\ p_{r,j}^{G} = -u_r^{G} \cdot x + t_r + c(d_{rG,j} - d_j^{G}) + \kappa_{jG} \cdot I_{r,1}^{G} + T_r^{G} + e_{r,j}^{G} \\ p_{r,j}^{R_k} = -u_r^{G} \cdot x + t_r + c(d_{rR_k,j} - d_j^{R}) + \kappa_{jR_k} \cdot I_{r,1}^{R} + T_r^{R} + e_{r,j}^{R} \end{cases} \quad (2)$$

Where $l_{r,j}^{s}$ and $p_{r,j}^{s}$ denote "observed minus computed" phase and pseudorange observables. u_r^{s} denotes the unit vector from satellite s to receiver r; x denote the vector of position increments relative to a priori position x_0, which is used for linearization. For TPP, precise satellite orbit and clock are used and the related errors are neglected in the two equations. Taking into account that in precise positioning, pseudoranges are used mainly for initializing receiver clock bias, they are omitted in the following equations for simplicity.

Following Temporal Point Positioning (TPP) proposed by Li et al. (2013a), assuming that the position increment at the epoch t_0 (before the earthquake) is $x(t_0)$, the ambiguities N_{t0} can be estimated along with the receiver clock $t_r(t_0)$ and tropospheric delay $T(t_0)$ (fixed to a priori model) parameters at this epoch as,

$$\begin{cases} t_r(t_0) + \lambda_{jG}(b_{rG,j}(t_0) - b_j^{G}(t_0)) + \lambda_{jG} N_{r,j}^{G}(t_0) + T_r^{G}(t_0) = l_{r,j}^{G}(t_0) + u_r^{G}(t_0) \cdot x(t_0) - \varepsilon_{r,j}^{G}(t_0) \\ t_r(t_0) + \lambda_{jR_k}(b_{rR_k,j}(t_0) - b_j^{R}(t_0)) + \lambda_{jR_k} N_{r,j}^{R}(t_0) + T_r^{R}(t_0) = l_{r,j}^{R_k}(t_0) + u_r^{R}(t_0) \cdot x(t_0) - \varepsilon_{r,j}^{R}(t_0) \end{cases} \quad (3)$$

Suppose the ambiguities are unchanged over the time of interest, if epoch difference is formed between t_0 and t_n (after the earthquake breaks), then we get:

$$\begin{cases} \Delta l_{r,j}^{G}(t_0, t_n) + u_r^{G}(t_0) \cdot x(t_0) - \varepsilon_{r,j}^{G}(t_n) = u_r^{G}(t_n) \cdot x(t_n) - \Delta t_r(t_0, t_n) - \Delta T_r^{G}(t_0, t_n) \\ \Delta l_{r,j}^{R}(t_0, t_n) + u_r^{R}(t_0) \cdot x(t_0) - \varepsilon_{r,j}^{R}(t_n) = u_r^{R}(t_n) \cdot x(t_n) - \Delta t_r(t_0, t_n) - \Delta T_r^{R}(t_0, t_n) \end{cases} \quad (4)$$

Here, we can see that is cancelled out through epoch differencing, this is one special advantage should be emphasized since inter-system/inter-frequency bias does not have impact on the TPP strategy.

Usually, the station position is precisely known (mm to cm level accuracy) for epoch before earthquake breaks, that's to say, $x(t_0)$ can be treated as zero, thus Eq.6 can be rewritten as:

$$\begin{cases} \Delta I^G_{r,j}(t_0, t_n) - \varepsilon^G_{r,j}(t_n) + \Delta T^G_r(t_0, t_n) = u^G_r(t_n) \cdot x(t_n) - \Delta t_r(t_0, t_n) \\ \Delta I^R_{r,j}(t_0, t_n) - \varepsilon^R_{r,j}(t_n) + \Delta T^R_r(t_0, t_n) = u^R_r(t_n) \cdot x(t_n) - \Delta t_r(t_0, t_n) \end{cases} \tag{5}$$

As clearly shown in Eq. 5, the accuracy of the relative position change $X(t_n)$ is mainly affected by tropospheric delay variation from the epoch t_0 to t_n. Promisingly, after corrected by empirical model (e.g., Saastamoinen 1972), tropospheric delay residual is limited to several centimeters [*Schüler*, 2014]. Besides, due to the spatial and temporal correlation, tropospheric delay can be further reduced through epoch differencing, for few tens of minutes, $\Delta T(t_0, t_n)$ is expected to be at centimeter level. Consequently, estimation of $x(t_n)$ is presumed to be at centimeter level as well.

As to weighting of observations, the classical elevation dependent model is adopted:

$$P = \begin{cases} 2 \cdot \sin(E) & E \leq 30^\circ \\ 1 & E > 30^\circ \end{cases} \tag{6}$$

Lastly, with regard to real-time precise GPS/GLONASS clock and orbit determination, we follow the same procedure as described in [*Li et al.*, 2015].

3.3 Performance assessment of GPS/GLONASS for retrieving real-time co-seismic displacements

In this contribution, the application of GPS/GLONASS to get co-seismic displacements, was first analyzed based on an outdoor experimental platform and then tested by the 2015 Illaple earthquake in Chile.

3.3.1 Out-door Experiment Validation

To better validate the performance of GPS/GLONASS in retrieving co-seismic displacements, out-door experimental 1 Hz GPS/GLONASS data recorded in December 2012 by Tu and Chen (2014) were first reprocessed in real time scenario and analyzed in details. The antenna was pushed forward and backward along a straight track which was horizontally placed (see Figure 3.1). Totally, there were eight individual experiments with movements of different frequencies and amplitudes. For comparison, the antenna motion was also captured by a camera at 25 fps (frames per second) with pixel resolution of 3 mm, and here the displacements revealed from the camera were set as benchmark.

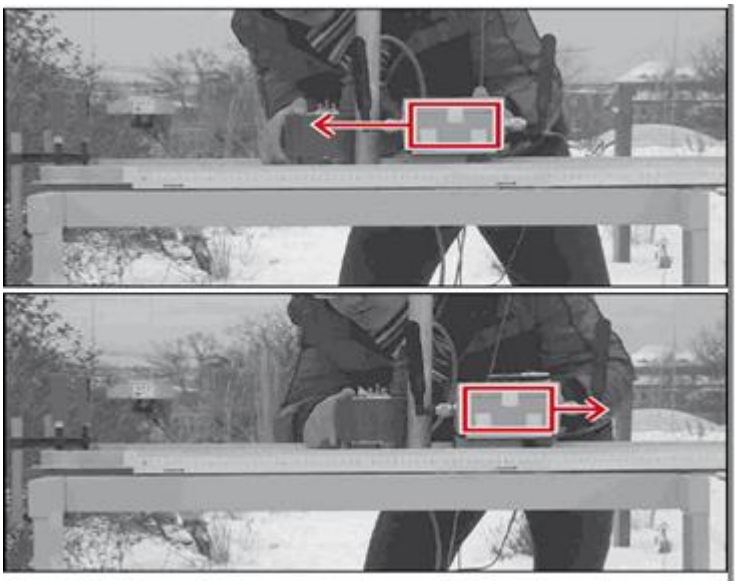

Figure 3. 1 Experimental platform and illustration of the experiment for this study

As a precise position of the station before the movement is crucial for the TPP method, three hours GPS/GLONASS data before the motion started was processed in static PPP mode to get cm level antenna position. Then GPS-only data, GPS/GLONASS data were processed using TPP, respectively. Sky view of the observed satellites during the experimental period is depicted in Figure 3.2. As clearly shown, GPS-only already shows a good geometry with evenly distributed nine GPS satellites in view. Taking into account that the camera recorded total displacements, we converted the east-west E and north-south N motion components derived from GPS, GPS/GLONASS to displacements d :

$$d = \sqrt{E^2 + N^2} \tag{7}$$

Corresponding results are shown in Figure 3.3. One can see that, the displacements from GPS/GLONASS, GPS-only and camera recordings show a high degree of consistency. Setting camera recordings as benchmarks, horizontal displacement differences are demonstrated in Figure 3.4 and Figure 3.5 presents vertical displacements. Statistical accuracies of GPS/GLONASS and GPS-only are both 0.012 m on horizontal, and 0.017 m and 0.018 m on vertical, correspondingly.

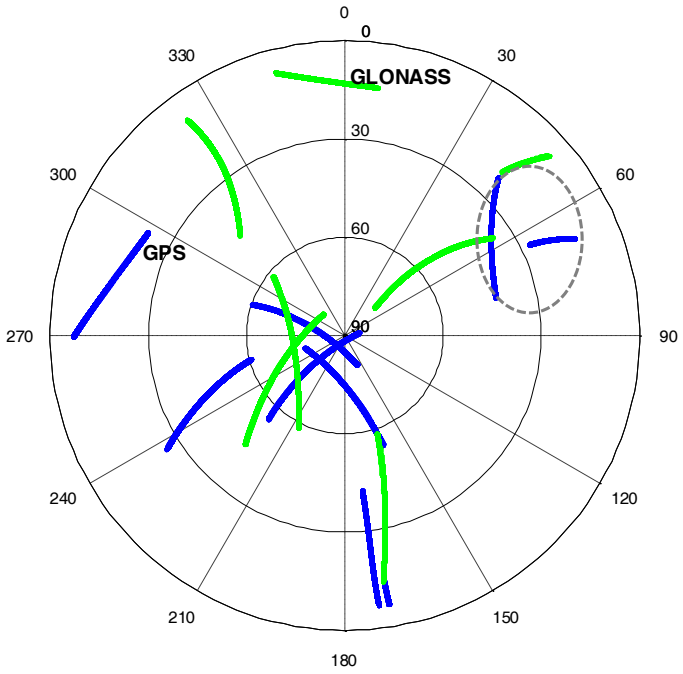

Figure 3. 2 Sky view of the GPS/GLONASS constellations during the experiment period: the blue lines denote GPS satellites and the green lines represent GLONASS satellites. The two GPS satellites in the gray ellipse are excluded for a simulation scenario.

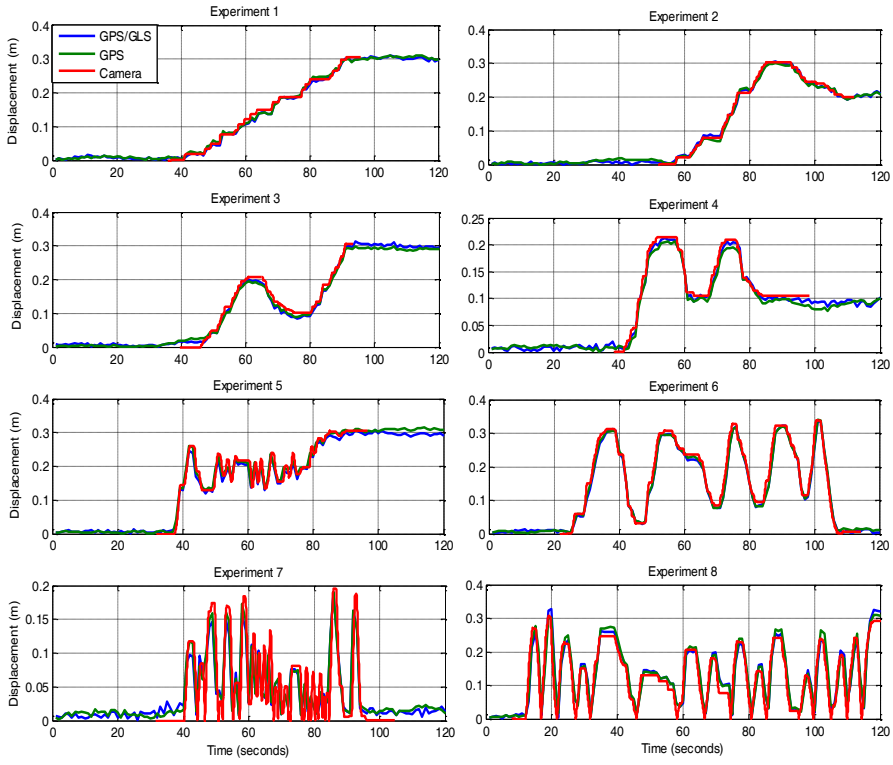

Figure 3. 3 Displacements of the eight experiments retrieved from GPS/GLONASS, GPS-only and camera recordings.

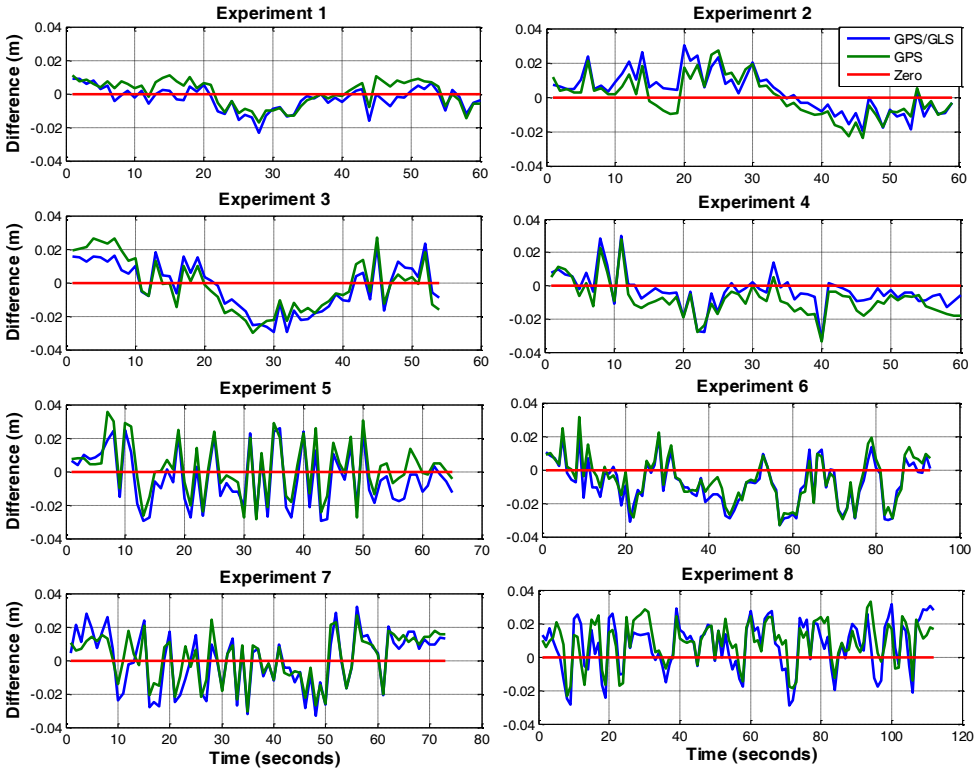

Figure 3. 4 Differences between displacements derived from GPS/GLONASS, GPS-only and camera recordings.

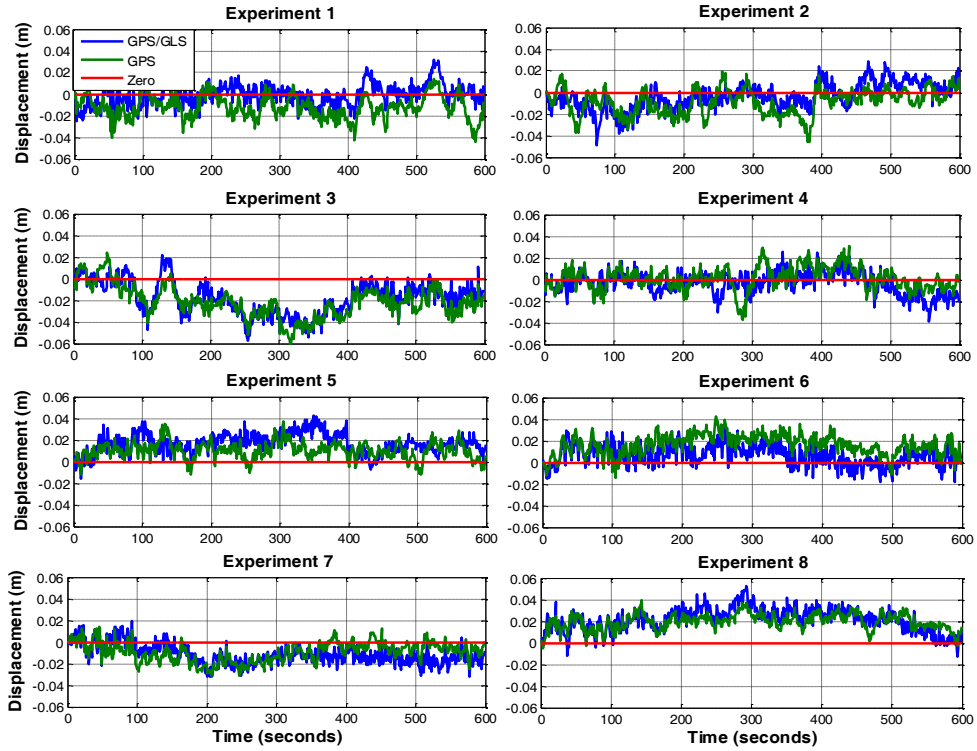

Figure 3. 5 Vertical displacements retrived from GPS/GLONASS and GPS-only. Please note, the benchmark of the vertical displacements are zero.

However, an optimal distribution of GPS satellites similar to this study could not be always guaranteed in practice. For adversary observation simulation, two GPS satellites were excluded (see in Figure 3.2), and the new TPP results from GPS/GLONASS and GPS-only are present in Figure 3.6 and Figure 3.7. Not surprisingly, displacements between GPS-only and camera have more evident differences. Nonetheless, GPS/GLONASS results are more robust and closer to the benchmark. As a matter of fact, in this scenario, accuracies of GPS/GLONASS and GPS-only are 0.013 m and 0.018 m for the horizontal components, 0.020 m and 0.029 m for the vertical components.

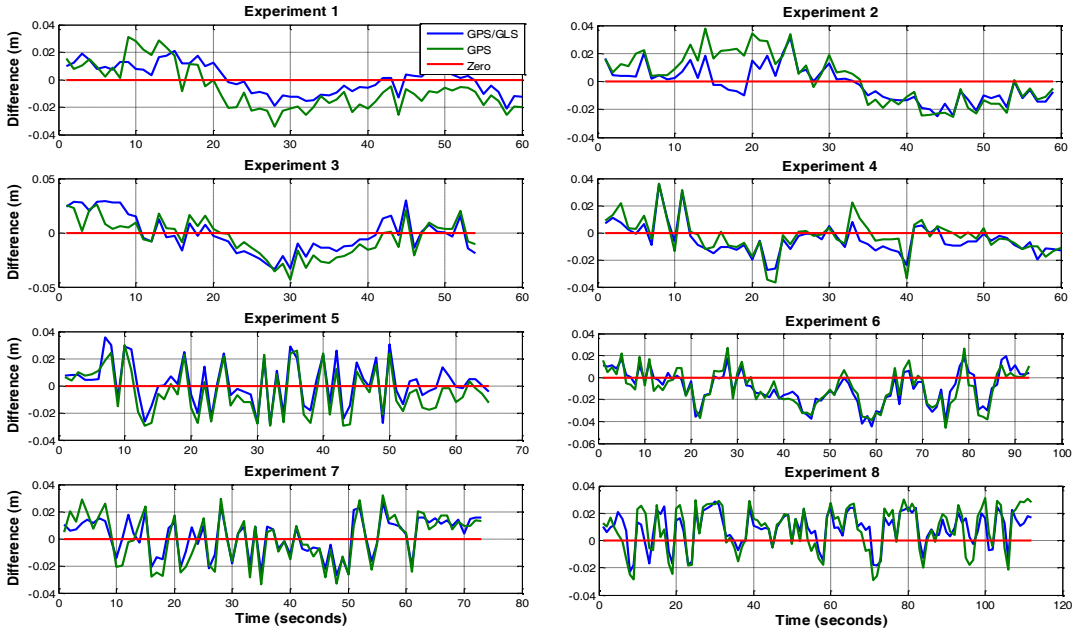

Figure 3. 6 Differences between displacements derived from GPS/GLONASS, GPS-only with two GPS satellites masked and camera recordings.

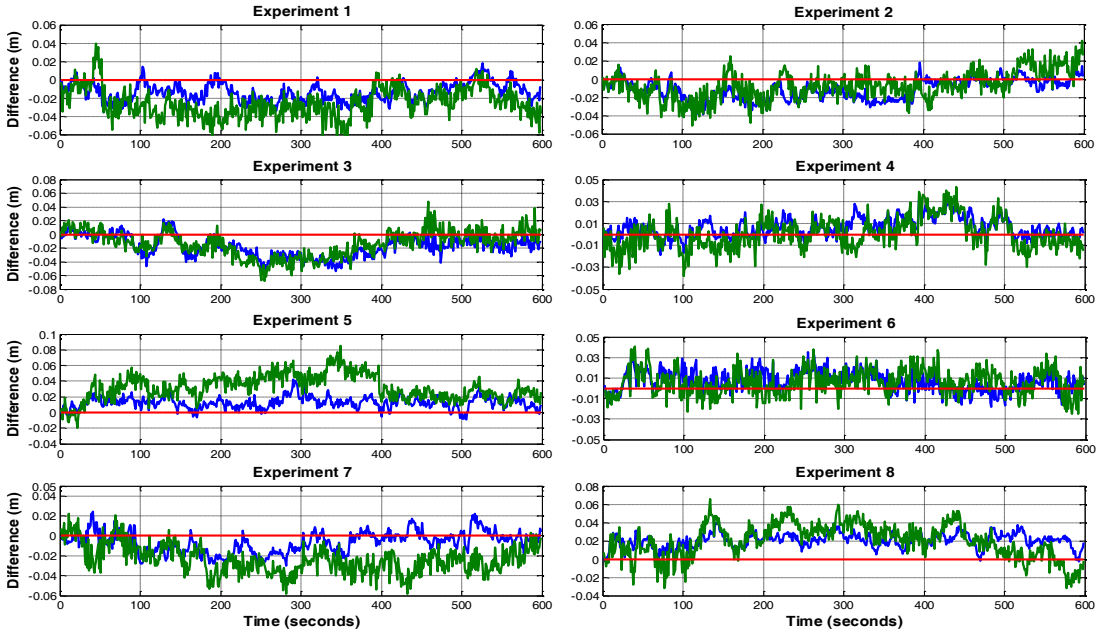

Figure 3. 7 Vertical displacements retrived from GPS, GPS/GLONASS with two GPS satellites masked. Please note, the benchmark of the vertical displacements are zero.

Through the out-door experiment, it is concluded that GLONASS contributes slightly on positioning accuracy in case of sufficient GPS satellites are tracked. However, when positioning is conducted in adversary environments with GPS signal blockages, adding a couple of GLONASS satellites can improve GPS satellite geometry, and consequently improve positioning reliability, availability and accuracy significantly.

3.3.2 A case study of September 2015 Mw8.3 Chile Illapel earthquake

While a lot of earthquakes have been recorded by real-time GPS arrays and analyzed intensively by previous studies, few ones have been recorded by GPS/GLONASS arrays, which indicate the limited data source for validation of GPS/GLONASS combination performance. Fortunately, continuous Integrated Plate boundary Observatory Chile (IPOC) stations track both GPS and GLONASS constellations. In this paper, our example is observation data from 2015 Mw=8.3 Illapel earthquake. The megathrust event occurred as the result of thrust faulting on the interface between the Nazca and South America plates in Central Chile, and notable tsunami was triggered and observed along the coast of Coquimbo and the cities of Coquimbo (http://www.ioc-sealevelmonitoring.org/).

23 continuous GPS/GLONASS stations with excellent spatial coverage near to epicenter (see Figure 3.8) were replayed using TPP in a simulated real-time mode. On average, the number of visible satellites during this period has increased from eight (GPS-only) to fourteen (GPS/GLONASS). To extract permanent deformation from the derived displacement waveforms, we applied 100 s moving average to each displacement record in each coordinate component, and the resulting static displacements from GPS/GLONASS are shown in Fig. 8. Besides, the differences between displacements obtained from GPS/GLONASS and from GPS-only are shown in Fig. 9.

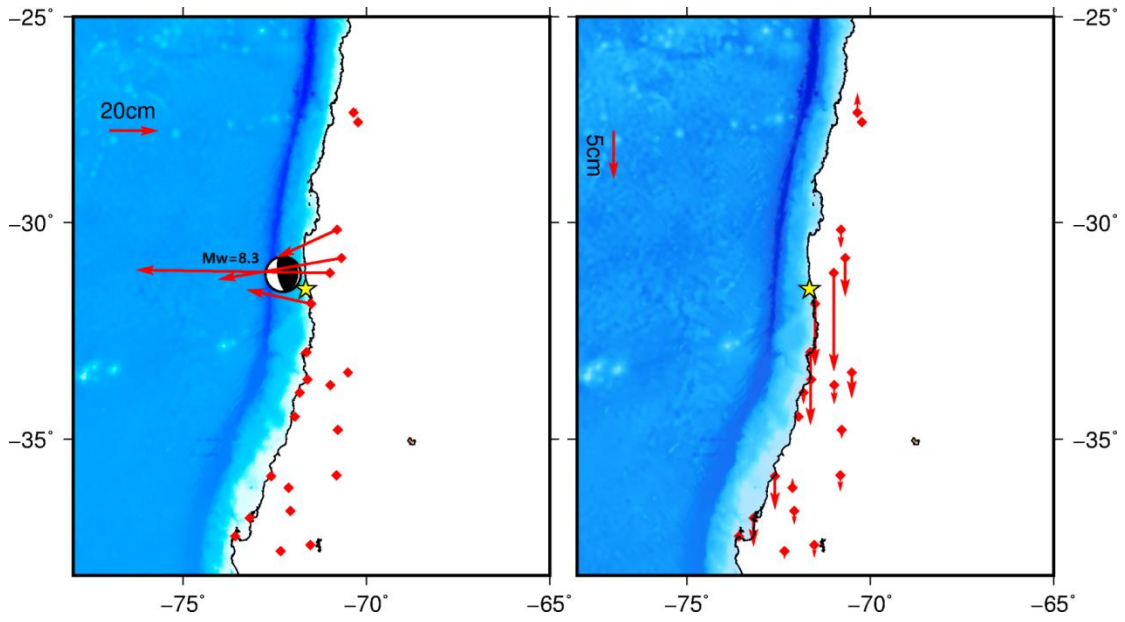

Figure 3. 8 Distribution of monitoring stations and co-seismic displacements derived from GPS/GLONASS, the left subplot is horizontal and the right one is vertical, and the yellow star and the beach-ball show the epicenter and focal mechanism provided by USGS.

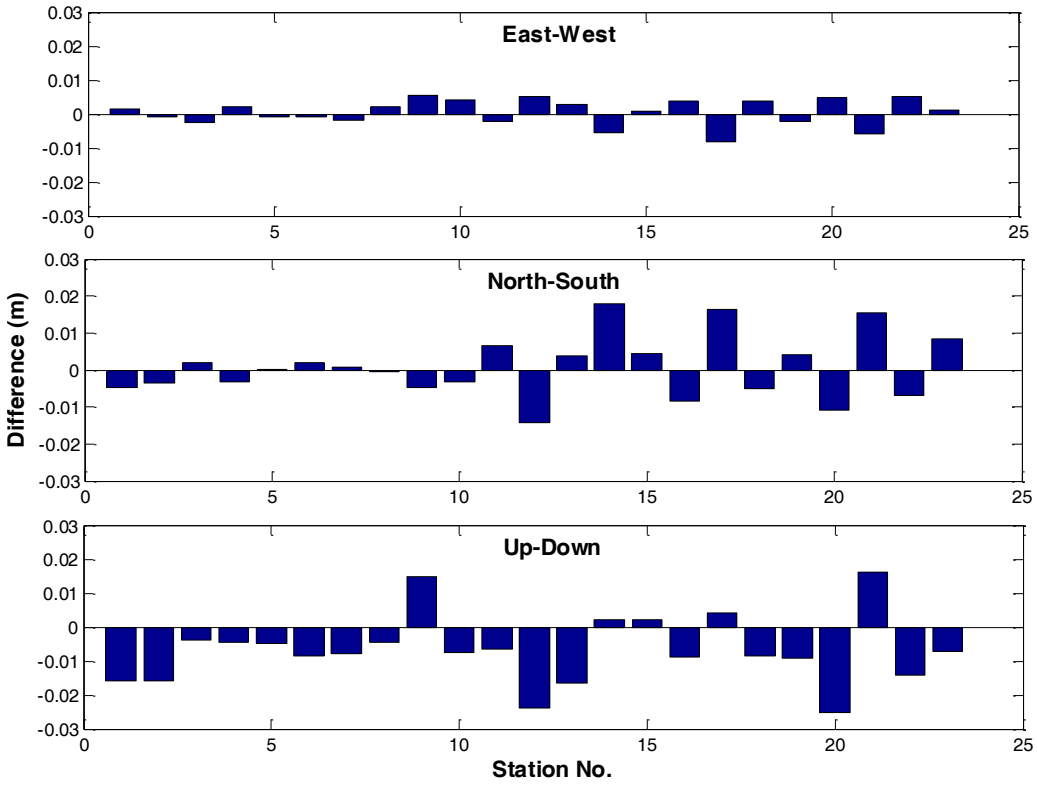

Figure 3. 9 Co-seismic static displacements differences between GPS/GLONASS and GPS-only, from top to bottom: east-west component, north-south component, up-down component.

It is clearly shown in Figure 3.8 that co-seismic offsets at most of the stations are not obvious (less than 5 cm) while four stations which are located closer to the epicenter experienced more significant shaking. Figure 3.9 indicates that the scale of co-seismic offset differences vary from station to station. At some stations, the differences are negligible. However, the biases could be up to 2 cm on horizontal direction and almost 3 cm on vertical direction at some other stations. To exploit the possible reasons, stations LNQM at which the difference is small and TAMR at which the difference is large are taken for detailed analyses. In Figure 3.10 and Figure 3.11, we show the satellite sky views at station LNQM and TAMR together with co-seismic displacement waveforms derived from GPS/GLONASS and GPS-only observations. In addition, PDOP is also present.

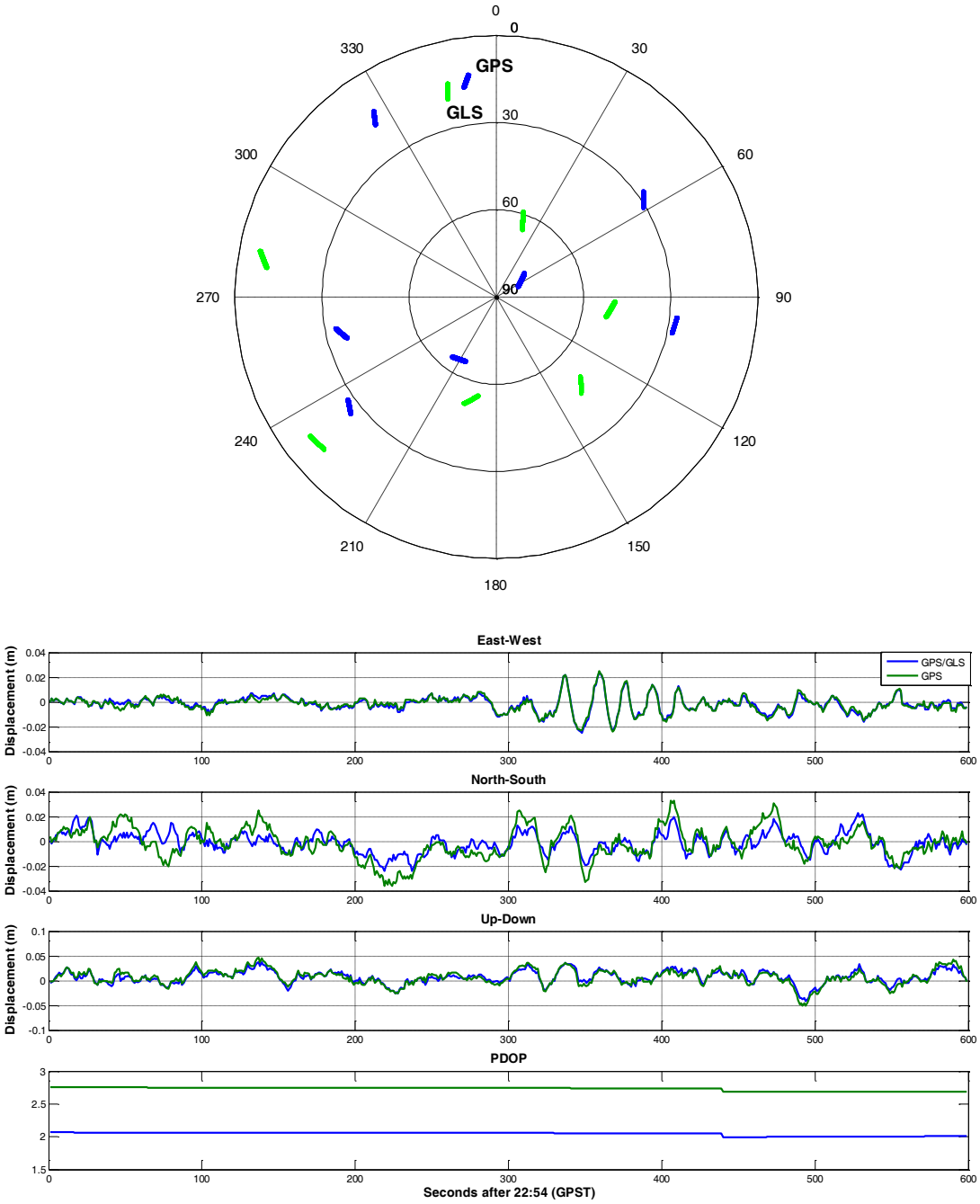

Figure 3. 10 Sky view of station LNQM and co-seismic displacements retrieved from GPS/GLONASS and GPS, together with PDOP

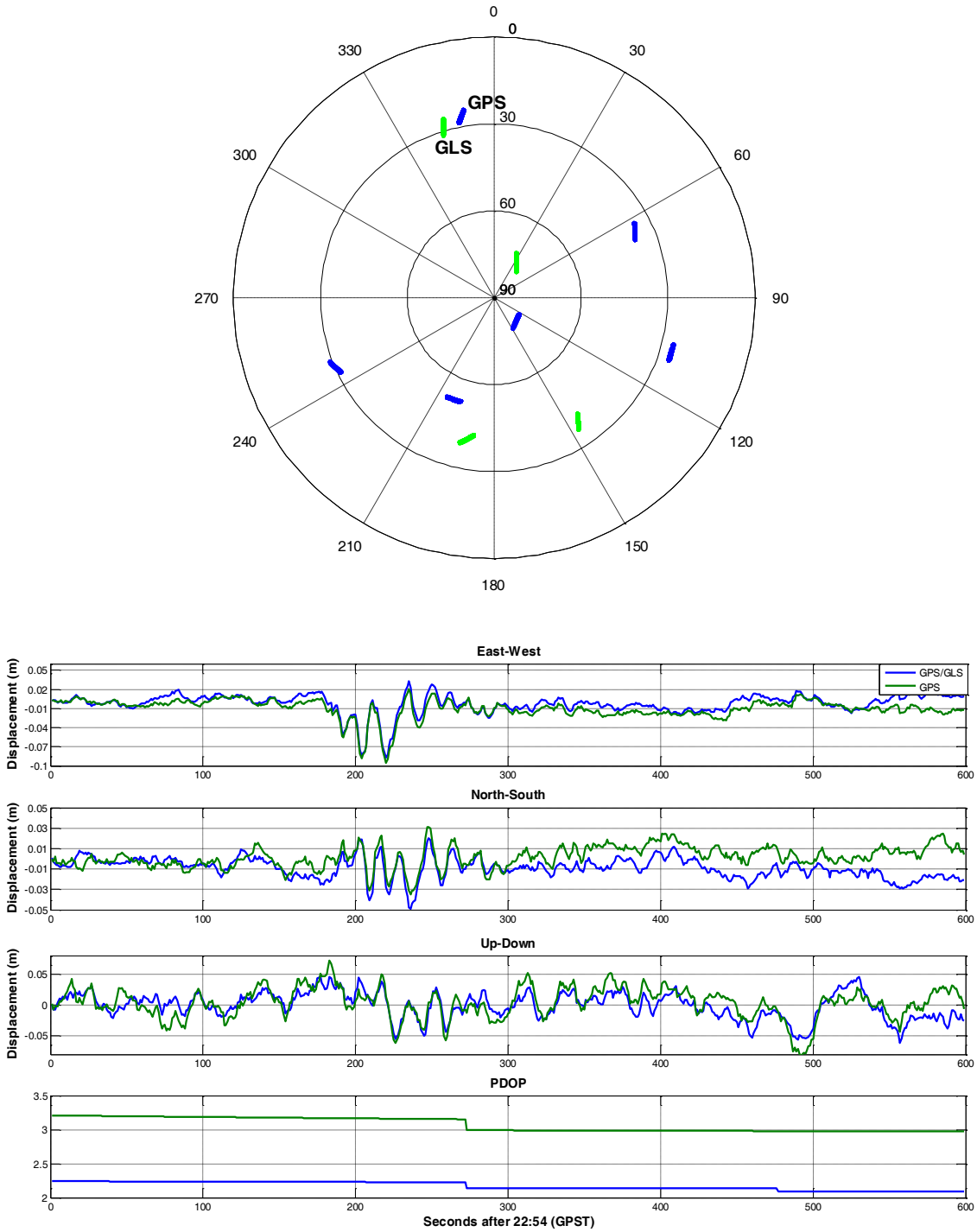

Figure 3. 11 Sky view of station TAMR and co-seismic displacements retrieved from GPS/GLONASS and GPS, together with PDOP

As Figure 3.10 and Figure 3.11 show, for station LNQM, there were eight GPS satellites observed during the earthquake time and the PDOP is 2.7 on average, which indicate an ideal observation condition. In this case, even though adding seven GLONASS satellites can reduce PDOP to 2.1 on average, there are almost no differences in co-seismic displacement waveform retrieving. By contrast, with regard to station TAMR, six GPS satellites were tracked and PDOP

is 3.2 on average, having four more GLONASS satellites in view optimizes constellation geometry greatly (PDOP is reduced to 2.2 on average), which leads to biases in co-seismic displacements retrieving.

3.3.3 Slip distribution inversions

For a geo-hazard early warning system, high-resolution slip model should be inverted once the near-field co-seismic offsets were determined, which would play an important role further for other applications, e.g., tsunami early warning and seismic hazard assessments. As the results show in Section 3.2, clear differences were observed between static offsets solved from GPS/GLOSNASS and GPS-only observations. To check how and in what extent these differences would affect the inferred slip distribution,, several inversions were performed and the results were compared. Constrained by solved co-seismic displacements, the well-developed SDM (Steepest Descent Method, Wang et al. 2009; Wang et al. 2013) inversion code was applied to invert for slip distribution on a predefined 3D plated interface.. A curved fault geometry that was inferred from the SLAB 1.0 [*Hayes et al.*, 2012] was assumed to be the rupture fault, which was then discretized into 330 rectangular fault patches. A Layered crustal model CRUST 5.1 [*Mooney et al.*, 1998] beneath the surface stations was used to compute the Green's function. We used the trade-off curve method as described in Diao et al. (2011) to fix the smoothing factor in the inversion. The final slip distributions inverted from co-seismic offsets are shown in Figure 3.12.

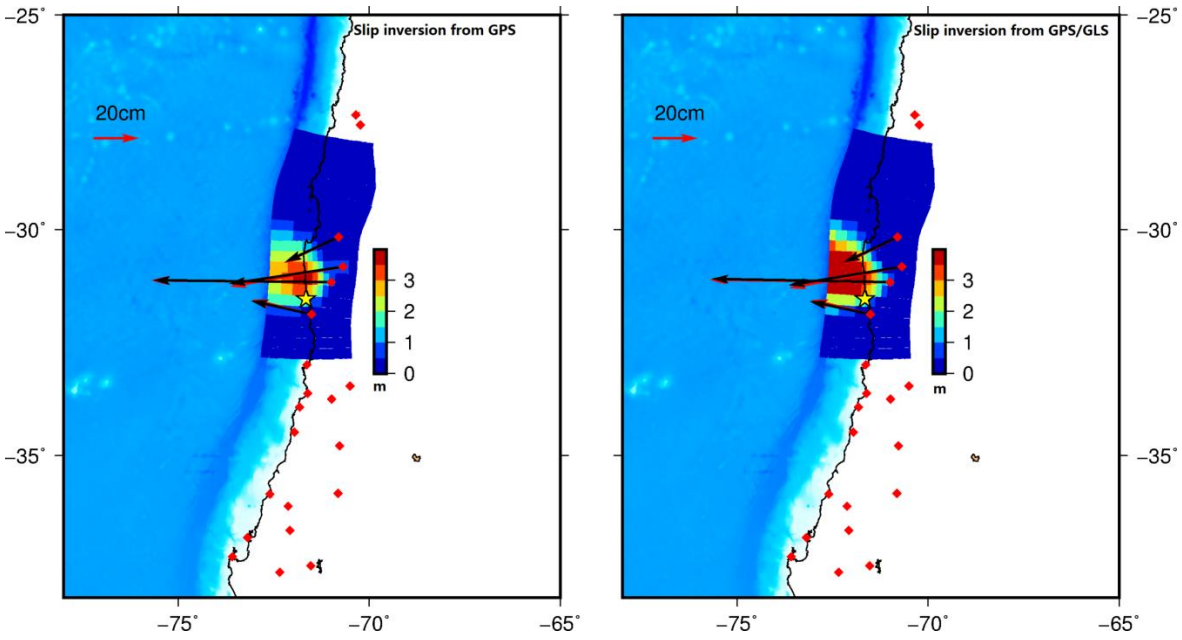

Figure 3. 12 Slip inversions based on co-seismic displacements from GPS (left) and GPS/GLONASS (right) using a curved fault with 330 individual patches, the red vectors denote observed co-seismic static offsets and the black ones represent synthetic values.

The derived slip models show general consistency in terms of moment magnitude, rupture scales and location. The moment magnitude of the earthquake inferred from GPS-only observations is 8.22, with a max slip of 3.91 m and a mean slip of 0.49 m. In comparison, inverted moment magnitude from GPS/GLONASS observations is slightly larger (8.25), with a max slip of 4.50 m and a mean slip of 0.57 m. Most importantly, the latter slip distributions tend to be shallower and toward the trench, which may produce a greater tsunami wave height in the scenario of geo-hazard early warning. .

In addition, both of the two slip models can fit the observed data pretty well. To be exact, for the GPS-only case, the root mean square (RMS) residuals in the north-south, east-west and vertical components are 0.8, 0.9 and 2.6 cm, respectively. And for the GPS/GLONASS case, the RMS residuals are 0.7, 0.8 and 1.6 cm, respectively. In general, model predictions can better explain observations from GPS/GLONASS in the vertical direction, suggesting a higher observation precision of this system.

3.4 Discussion and Conclusions

In this study, we extended TPP from GPS-only to GPS/GLONASS observations and tested the performances of GPS/GLONASS in co-seismic displacements retrieving through out-door experiments. Compared with GPS-only system, GPS/GLONASS has more satellites visible and optimizes constellation spatial geometry, and it has the advantage of providing more robust and accurate co-seismic displacements especially when GPS-only observations are not ideal enough.

The case study of 2015 September Chile Illapel earthquake reveals that the biases between co-seismic displacements derived from GPS-only and GPS/GLONASS vary from station to station and could be up to 2 cm on horizontal direction and almost 3 cm on vertical direction. Analyses show that there is an evident relationship between the bias scales and the satellites observed, for example, when only six GPS satellites were tracked and PDOP of GPS-only is relatively large, adding several GLONASS satellites can lead to significant differences in co-seismic displacement determination. Considering the results from the out-door experiments, we believe co-seismic displacements obtained from GPS/GLONASS are closer to the truth values.

Subsequent slip distribution inversion on a curved fault confirms that differences of co-seismic displacements cause variations in inversion results. Slip distributions of Illapel earthquake inferred from GPS/GLONASS observations tend to be more shallow and larger, which implies a greater tsunami impact. Nonetheless, it should be also pointed out that for slip distribution inversions, besides co-seismic displacements, there are other open options that can affect the inversion results, e.g., the inversion algorithm implemented, GPS/GLONASS array distribution, and fault geometry. However, it should mentioned that the inversion results shown in section 3.3 were derived from the same inversion frame (fault geometry, earth structure and inversion parameter). The only difference is the input co-seismic displacements that captured by GPS/GLONASS system and GPS-only system. We therefore infer that the differences between the inverted slip models are mainly induced by input observations, which highlights the importance for utilizing more precise observations. For example, in this cases study, if we use a single Okada fault and run the inversions again, then the inversion differences can be neglected safely (see Figure 3.14).

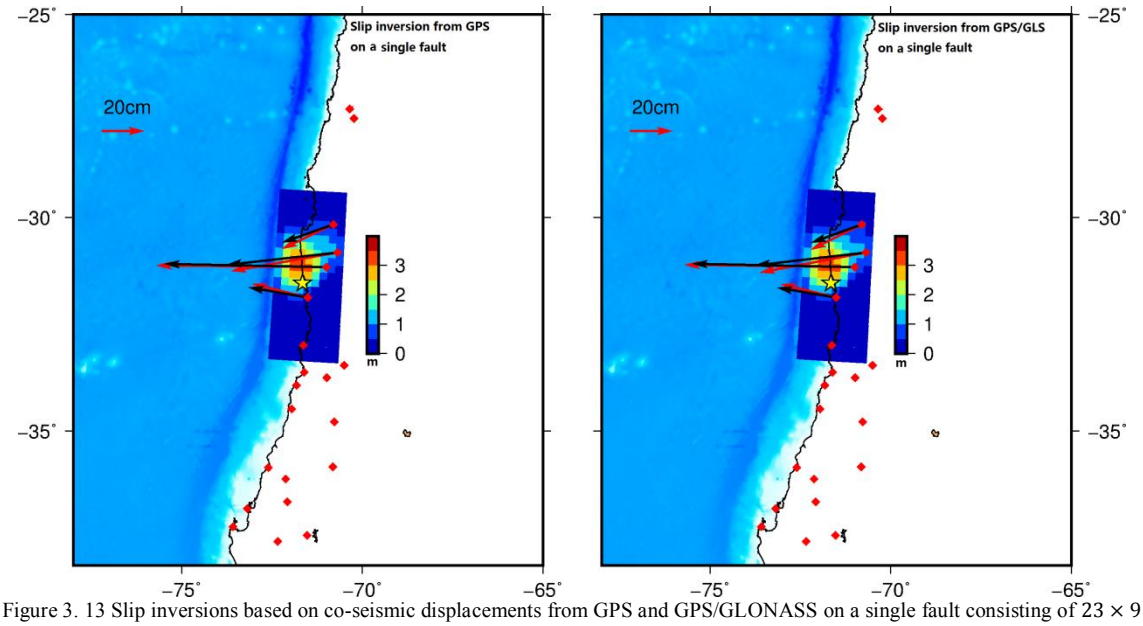

Figure 3. 13 Slip inversions based on co-seismic displacements from GPS and GPS/GLONASS on a single fault consisting of 23 × 9 uniform patches, the length and width of the fault are 450 km and 190 km, strike angle is set as 4° and dip angle is set as 19°, the red vectors denote observed co-seismic static offsets and the black ones represent synthetic values

Considering that GLONASS employs Frequency Division Multiple Access (FDMA) for signal transmission, which leads to integer ambiguity resolution difficulty, the accuracy of obtained GLONASS orbit and clock is not as good as GPS. Recently, Liu et al. (2015) have proposed new method to improve GLONASS precise orbit determination, and it is expected to help GPS/GLONASS precise positioning.

Besides GPS/GLONASS, recent studies [*Chen et al.*, 2015a; *Geng et al.*, 2015] have demonstrated the feasibility of using BeiDou for earthquake and tsunami monitoring in Asia-Pacific region. The TPP model can be extended to GPS/GLONASS/BeiDou/GALILEO systems easily, once data from four systems data recorded during earthquake time is available publicly, the application of multi-GNSS for geo-hazard monitoring could be evaluated.

3.5 Acknowledgements

Kejie Chen is financially supported by China Scholarship Council (CSC) for his PhD study at GFZ. 1 Hz GPS/GLONASS network data are provided by IPOC.

3.6 Reference

Allen, R. M., and A. Ziv (2011), Application of real-time GPS to earthquake early warning, *Geophys. Res. Lett.*, *38*(16), 1–7, doi:10.1029/2011GL047947.

An, C. (2015), Inversion of tsunami waveforms and tsunami warning.

Babeyko, A. Y., A. Hoechner, and S. V Sobolev (2010), Source modeling and inversion with near real-time GPS: a GITEWS perspective for Indonesia, *Nat. Hazards Earth Syst. Sci.*, *10*, 1617–1627, doi:10.5194/nhess-10-1617-2010.

Banerjee, P., F. Pollitz, B. Nagarajan, and R. Bürgmann (2007), Coseismic Slip Distributions of the 26 December 2004 Sumatra–Andaman and 28 March 2005 Nias Earthquakes from gps Static Offsets, *Bull. Seismol. Soc. Am.* , *97* (1A), S86–S102, doi:10.1785/0120050609.

Blaser, L., F. Kruger, M. Ohrnberger, and F. Scherbaum (2010), Scaling Relations of Earthquake Source Parameter Estimates with Special Focus on Subduction Environment, *Bull. Seismol. Soc. Am.*, *100*(6), 2914–2926, doi:10.1785/0120100111.

Blewitt, G., C. Kreemer, W. C. Hammond, H.-P. Plag, S. Stein, and E. Okal (2006), Rapid determination of earthquake magnitude using GPS for tsunami warning systems, *Geophys. Res. Lett.*, *33*(11), L11309–L11309, doi:10.1029/2006GL026145.

Blewitt, G., W. C. Hammond, C. Kreemer, H. P. Plag, S. Stein, and E. Okal (2009), GPS for real-time earthquake source determination and tsunami warning systems, *J. Geod.*, *83*, 335–343, doi:10.1007/s00190-008-0262-5.

Bock, Y., R. M. Nikolaidis, P. J. Jonge, and M. Bevis (2000), Instantaneous geodetic positioning at medium distances with the Global Positioning System, *J. Geophys. Res. Solid Earth*, *105*(B12), 28223–28253.

Bock, Y., L. Prawirodirdjo, and T. I. Melbourne (2004), Detection of arbitrarily large dynamic ground motions with a dense high‐rate GPS network, *Geophys. Res. Lett.*, *31*(6).

Bock, Y., D. Melgar, and B. W. Crowell (2011), Real-time strong-motion broadband displacements from collocated GPS and accelerometers, *Bull. Seismol. Soc. Am.*, *101*(6), 2904–2925, doi:10.1785/0120110007.

Boore, D. M., and J. J. Bommer (2005), Processing of strong-motion accelerograms: needs, options and consequences, *Soil Dyn. Earthq. Eng.*, *25*(2), 93–115.

Chen, K., N. Zamora, A. Y. Babeyko, X. Li, and M. Ge (2015a), Precise Positioning of BDS, BDS/GPS: Implications for Tsunami Early Warning in South China Sea, *Remote Sens.*, *7*(12), 15955–15968.

Chen, K., M. Ge, X. Li, A. Babeyko, M. Ramatschi, and M. Bradke (2015b), Retrieving real-time precise co-seismic displacements with a standalone single-frequency GPS receiver, *Adv. Sp. Res.*

Colosimo, G., M. Crespi, and A. Mazzoni (2011), Real-time GPS seismology with a stand-alone receiver: A preliminary feasibility demonstration, *J. Geophys. Res. Solid Earth*, *116*(B11).

Crowell, B. W., Y. Bock, and D. Melgar (2012), Real‐time inversion of GPS data for finite fault modeling and rapid hazard assessment, *Geophys. Res. Lett.*, *39*(9).

Diao, F., X. Xiong, S. Ni, Y. Zheng, and C. Ge (2011), Slip model for the 2011 M w 9.0 Sendai (Japan) earthquake and its M w 7.9 aftershock derived from GPS data, *Chinese Sci. Bull.*, *56*(27), 2941–2947.

Fang, R., C. Shi, W. Song, G. Wang, and J. Liu (2013), Determination of earthquake magnitude using GPS displacement waveforms from real-time precise point positioning, *Geophys. J. Int.* , doi:10.1093/gji/ggt378.

Ge, L. (1999), GPS seismometer and its signal extraction, in *Proc. 12th Int. Tech. Meeting of the Satellite Division of the US Inst. of Navigation GPS ION'99*.

Ge, L., S. Han, C. Rizos, Y. Ishikawa, M. Hoshiba, Y. Yoshida, M. Izawa, N. Hashimoto, and S. Himori (2000), GPS seismometers with up to 20 Hz sampling rate, *Earth, planets Sp.*, *52*(10), 881–884.

Geist, E. L. (2001), Effect of depth-dependent shear modulus on tsunami generation along subduction zones shallow depths in comparison to standard earth, , *28*(7), 1315–1318.

Geng, J., and Y. Bock (2015), GLONASS fractional-cycle bias estimation across inhomogeneous receivers for PPP ambiguity resolution, *J. Geod.*, 1–18.

Geng, T., X. Xie, R. Fang, X. Su, Q. Zhao, G. Liu, H. Li, C. Shi, and J. Liu (2015), Real‐time capture of seismic waves using high‐rate multi‐GNSS observations: Application to the 2015 Mw 7.8 Nepal earthquake, *Geophys. Res. Lett.*

Hanks, T. C., and H. Kanamori (1979), A Moment Magnitude Scale, *J. Geophys. Res.*, *84*(B5), 2348–2350.

Haskell, N. A. (1964), Total energy and energy spectral density of elastic wave radiation from propagating faults, *Bull. Seismol. Soc. Am.*, *54*(6A), 1811–1841.

Hayes, G. P., D. J. Wald, and R. L. Johnson (2012), Slab1.0: A three-dimensional model of global subduction zone geometries, *J. Geophys. Res.*, *117*(B1), B01302–B01302, doi:10.1029/2011JB008524.

Hirahara, K., T. Nakano, Y. Hoso, S. Matsuo, and K. Obana (1994), An experiment for GPS strain seismometer, in *Japanese symposium on GPS*, pp. 67–75.

Hirose, F., K. Miyaoka, N. Hayashimoto, T. Yamazaki, and M. Nakamura (2011), Outline of the 2011 off the Pacific coast of Tohoku Earthquake (M w 9.0)—Seismicity: foreshocks, mainshock, aftershocks, and induced activity—, *Earth, planets Sp.*, *63*(7), 513–518.

Hoechner, A., A. Y. Babeyko, and S. V Sobolev (2008), Enhanced GPS inversion technique applied to the 2004 Sumatra earthquake and tsunami, *Geophys. Res. Lett.*, *35*(8), L08310–L08310, doi:10.1029/2007GL033133.

Hoechner, A., M. Ge, a. Y. Babeyko, and S. V Sobolev (2013), Instant tsunami early warning based on real-time GPS – Tohoku 2011 case study, *Nat. Hazards Earth Syst. Sci.*, *13*(5), 1285–1292, doi:10.5194/nhess-13-1285-2013.

Hofmann-Wellenhof, B., H. Lichtenegger, and E. Wasle (2007), *GNSS–global navigation satellite systems: GPS, GLONASS, Galileo, and more*, Springer Science & Business Media.

Japan Meteorological Agency (JMA) (2013), Lessons learned from the tsunami disaster caused by the 2011 Great East Japan Earthquake and improvements in JMA ' s tsunami warning system October 2013 Japan Meteorological Agency, , (October), 1–13.

Jing-nan, L., and G. Mao-rong (2003), PANDA software and its preliminary result of positioning and orbit determination, *Wuhan Univ. J. Nat. Sci.*, *8*(2), 603–609.

Kanamori, H. (1983), Magnitude scale and quantification of earthquakes, *Tectonophysics*, *93*(3), 185–199.

Kanamori, H., and L. Rivera (2008), Source inversion of W phase: speeding up seismic tsunami warning, *Geophys. J. Int.* , *175* (1), 222–238, doi:10.1111/j.1365-246X.2008.03887.x.

Kennett, B. L. N., E. R. Engdahl, and R. Buland (1995), Constraints on seismic velocities in the Earth from traveltimes, *Geophys. J. Int.*, *122*(1), 108–124.

Kerr, R. A. (2005), Failure to Gauge the Quake Crippled the Warning Effort, *Sci.* , *307* (5707), 201, doi:10.1126/science.307.5707.201.

Larson, K. M. (2009), GPS seismology, *J. Geod.*, *83*(3-4), 227–233.

Larson, K. M., P. Bodin, and J. Gomberg (2003), Using 1-Hz GPS data to measure deformations caused by the Denali fault earthquake, *Science (80-.).*, *300*(5624), 1421–1424.

Li, X., M. Ge, Y. Zhang, R. Wang, B. Guo, J. Klotz, J. Wickert, and H. Schuh (2013a), High-rate coseismic displacements from tightly integrated processing of raw GPS and accelerometer data, *Geophys. J. Int.*, doi:10.1093/gji/ggt249.

Li, X., M. Ge, X. Zhang, Y. Zhang, B. Guo, R. Wang, J. Klotz, and J. Wickert (2013b), Real-time high-rate co-seismic displacement from ambiguity-fixed precise point positioning: Application to earthquake early warning, *Geophys. Res. Lett.*, *40*(2), 295–300, doi:10.1002/grl.50138.

Li, X., M. Ge, B. Guo, J. Wickert, and H. Schuh (2013c), Temporal point positioning approach for real-time GNSS seismology using a single receiver, *Geophys. Res. Lett.*, *40*(21), 5677–5682, doi:10.1002/2013GL057818.

Li, X., M. Ge, X. Dai, X. Ren, M. Fritsche, J. Wickert, and H. Schuh (2015), Accuracy and reliability of multi-GNSS real-time precise positioning: GPS, GLONASS, BeiDou, and Galileo, *J. Geod.*, *89*(6), 607–635, doi:10.1007/s00190-015-0802-8.

Liu, Y., M. Ge, C. Shi, Y. Lou, J. Wickert, and H. Schuh (2015), Improving GLONASS Precise Orbit Determination through Data Connection, *Sensors*, *15*(12), 30104–30114.

Melgar, D. (2014), Seismogeodesy and Rapid Earthquake and Tsunami Source Assessment, 247 pp., University of California San Diego,

Melgar, D., Y. Bock, and B. W. Crowell (2012), Real-time centroid moment tensor determination for large earthquakes from local and regional displacement records, *Geophys. J. Int.*, *188*(2), 703–718, doi:10.1111/j.1365-246X.2011.05297.x.

Melgar, D., Y. Bock, D. Sanchez, and B. W. Crowell (2013a), On robust and reliable automated baseline corrections for strong motion seismology, *J. Geophys. Res. Solid Earth*, *118*(3), 1177–1187.

Melgar, D., B. W. Crowell, Y. Bock, and J. S. Haase (2013b), Rapid modeling of the 2011 Mw 9.0 Tohoku-oki earthquake with seismogeodesy, *Geophys. Res. Lett.*, *40*(12), 2963–2968, doi:10.1002/grl.50590.

Menke, W., and V. Levin (2005), A strategy to rapidly determine the magnitude of great earthquakes, *Eos, Trans. Am. Geophys. Union*, *86*(19), 185–188.

Montenbruck, O., P. Steigenberger, R. Khachikyan, G. Weber, R. B. Langley, L. Mervart, and U. Hugentobler (2014), IGS-MGEX: preparing the ground for multi-constellation GNSS science, *Insid. GNSS*, *9*(1), 42–49.

Mooney, W. D., G. Laske, and T. G. Masters (1998), CRUST 5.1: A global crustal model at 5× 5, *J. Geophys. Res. Solid Earth*, *103*(B1), 727–747.

NGDC/WDS (n.d.), National Geophysical Data Center / World Data Service (NGDC/WDS): Global Historical Tsunami Database. National Geophysical Data Center, NOAA, *Access on 15.01.2015*, doi:10.7289/V5PN93H7. Available from: http://www.ngdc.noaa.gov/hazard/tsu_db.shtml

O'Toole, T. B., A. P. Valentine, and J. H. Woodhouse (2012), Centroid–moment tensor inversions using high-rate GPS waveforms, *Geophys. J. Int.*, *191*(1), 257–270.

O'Toole, T. B., A. P. Valentine, and J. H. Woodhouse (2013), Earthquake source parameters from GPS‐measured static displacements with potential for real‐time application, *Geophys. Res. Lett.*, *40*(1), 60–65.

Ohta, Y. et al. (2012), Quasi real-time fault model estimation for near-field tsunami forecasting based on RTK-GPS analysis: Application to the 2011 Tohoku-Oki earthquake (M w 9.0), *J. Geophys. Res. Solid Earth*, *117*, doi:10.1029/2011JB008750.

Okada, Y. (1985), Surface deformation due to shear and tensile faults in a half-space, *Bull. Seismol. Soc. Am.*, *75*(4), 1135–1154.

Saastamoinen, J. (1972), Atmospheric correction for the troposphere and stratosphere in radio ranging satellites, *use Artif. Satell. Geod.*, 247–251.

Schüler, T. (2014), The TropGrid2 standard tropospheric correction model, *GPS Solut.*, *18*(1), 123–131.

Shi, C., Y. Lou, H. Zhang, Q. Zhao, J. Geng, R. Wang, R. Fang, and J. Liu (2010), Seismic deformation of the M w 8.0 Wenchuan earthquake from high-rate GPS observations, *Adv. Sp. Res.*, *46*(2), 228–235.

Simons, M., Y. Fialko, and L. Rivera (2002), Coseismic Deformation from the 1999 Mw 7.1 Hector Mine, California, Earthquake as Inferred from InSAR and GPS Observations, *Bull. Seismol. Soc. Am.* , *92* (4), 1390–1402, doi:10.1785/0120000933.

Sobolev, S. V, A. Y. Babeyko, R. Wang, R. Galas, M. Rothacher, D. SEIN, J. Schröter, J. Lauterjung, and C. Subarya (2006), Towards real-time tsunami amplitude prediction, *Eos (Washington. DC).*, *87*(37).

Sobolev, S. V, A. Y. Babeyko, R. Wang, A. Hoechner, R. Galas, M. Rothacher, D. V Sein, J. Schröter, J. Lauterjung, and C. Subarya (2007), Tsunami early warning using GPS-Shield arrays, *J. Geophys. Res. Solid Earth*, *112*(B8), B08415–B08415, doi:10.1029/2006JB004640.

Song, Y. T. (2007), Detecting tsunami genesis and scales directly from coastal GPS stations, *Geophys. Res. Lett.*, *34*(19).

Tian, Y., M. Ge, and F. Neitzel (2015), Particle filter-based estimation of inter-frequency phase bias for real-time GLONASS integer ambiguity resolution, *J. Geod.*, *89*(11), 1145–1158.

Tsuji, H., Y. Hatanaka, T. Sagiya, and M. Hashimoto (1995), Coseismic crustal deformation from the 1994 Hokkaido‐Toho‐Oki earthquake monitored by a nationwide continuous GPS array in Japan, *Geophys. Res. Lett.*, *22*.

Tu, R., and K. Chen (2014), Tightly Integrated Processing of High-Rate GPS and Accelerometer Observations by Real-Time Estimation of Transient Baseline Shifts, *J. Navig.*, *67*(05), 869–880.

Vigny, C., W. J. Simons, S. Abu, R. Bamphenyu, C. Satirapod, N. Choosakul, and B. A. C. Ambrosius (2005), Insight into the 2004 Sumatra–Andaman earthquake from GPS measurements in southeast Asia, *Nature*, *436*, 201–206.

Wang, L., R. Wang, F. Roth, B. Enescu, S. Hainzl, and S. Ergintav (2009), Afterslip and viscoelastic relaxation following the 1999 M 7.4 İzmit earthquake from GPS measurements, *Geophys. J. Int.*, *178*(3), 1220–1237, doi:10.1111/j.1365-246X.2009.04228.x.

Wang, R., F. L. Mart n, and F. Roth (2003), Computation of deformation induced by earthquakes in a multi-layered elastic crust—FORTRAN programs EDGRN/EDCMP, *Comput. Geosci.*, *29*(2), 195–207.

Wang, R., F. Diao, and A. Hoechner (2013), SDM-A geodetic inversion code incorporating with layered crust structure and curved fault geometry, in *EGU General Assembly Conference Abstracts*, vol. 15, p. 2411.

Yang, Y., J. Li, A. Wang, J. Xu, H. He, H. Guo, J. Shen, and X. Dai (2014), Preliminary assessment of the navigation and positioning performance of BeiDou regional navigation satellite system, *Sci. China Earth Sci.*, *57*(1), 144–152.

Chapter 4 Comparing source inversion techniques for GPS-based local tsunami forecasting: a case study for the April 2014 M8.1 Pisagua, Chile earthquake

Kejie Chen*, Andrey Babeyko, Andreas Hoechner, Maorong Ge

German Research Centre for Geosciences(GFZ), Telegrafenberg, 14473 Potsdam, Germany;

kejie@gfz-potsdam.de

[1] Real-time GPS is nowadays considered as a valuable component of next-generation near-field tsunami early warning systems. A fast and reliable source inversion technique whose function is to convert co-seismic displacements into seismic source parameters for subsequent tsunami simulation and forecasting plays a central role in the entire warning chain. To date, there have been suggested various inversion approaches and, not surprisingly, different methods yield different inversion results even for the same input information. Differences in source parameters are then propagated to the coast by means of wave simulation and contribute to the total forecast uncertainty. The northern Chile 1st Apr. 2014 Mw8.1 Pisagua earthquake and aftermath tsunami were extensively recorded by a large number of land- and ocean-based sensors including real-time GPS. We take the opportunity and consider the 2014 Pisagua event as a case study to explore forecast uncertainty related to the GPS-based source inversion. In particular, we compare three methods: fastCMT (centroid moment tensor), distributed slip along pre-defined plate interface and unconstrained inversion into a single Okada fault. The three methods provide significantly different far-field tsunami forecast but show surprisingly similar tsunami predictions in the near-field.

4.1 Introduction

[2] In aftermath of the 2004 Sumatra tragedy and in response to the need in more reliable tsunami early warning systems (TEWS), researchers proposed continuous real-time GPS-arrays for fast and enhanced tsunami source inversion [see, e.g., *Blewitt et al.*, 2006; *Sobolev et al.*, 2006, 2007; *Song*, 2007]. The idea of using real-time GPS for TEWS is clear: for large tsunami triggering seismic events, traditional broadband instruments near the source may saturate and thus the magnitude estimation relies on teleseismic waves recorded much later at distant stations [*Kanamori and Rivera*, 2008]. To overcome this limitation, seismic stations are augmented with strong-motion recorders. The latter, however, require a double integration to convert accelerations into displacements, which may become unreliable at low frequencies because tilts of the instruments are indistinguishable from translations, and any errors are amplified in the integration [*Bock et al.*, 2011; *Li et al.*, 2013a]. Subjective correction algorithms are available but require the full waveform, and the permanent deformation that accompanies large earthquakes may be filtered out or not estimated correctly in this process [*Melgar et al.*, 2013b]. Compared with seismic approaches, GPS data directly provides arbitrary ground displacement measurements. Hence, it is considered to be a more trustworthy tool especially for near source large earthquake characteristics estimation and related tsunami early warning [*Li et al.*, 2013b].

[3] In order to be used for the tsunami early warning and forecasting, co-seismic displacements captured by a coastal GPS-network need to be inverted into source parameters (e.g., epicenter, magnitude, slip distribution) on-the-fly to initialize tsunami scenarios. Actually, numerous previous studies have been focused on inversion methodologies. Recently, *Melgar et al.* [2012] proposed an algorithm called *fastCMT* to obtain centroid moment tensor (CMT) and location for earthquakes using local and regional real-time GPS co-seismic displacements. Original *fastCMT*

algorithm assumed point source inversion, and to account for the source finiteness, it was later extended to a linear geometry by superposition of point sources [*Melgar et al.*, 2013b]. Instead of adopting residual co-seismic displacements, *O'Toole et al.* [2012] developed an algorithm to get centroid moment tensor using high-rate GPS waveforms. They also suggested an alternative to the *fastCMT* approach by simultaneously searching for the best centroid position [*O'Toole et al.*, 2013]. *Crowell et al.* [2012] inverted real-time GPS data for a finite fault slip distribution in homogeneous elastic half-space. In their method, a priori information on fault geometry can be either predefined or derived from the rapid CMT solution. Taking the 2011 Tohoku tsunami as an example, *Hoechner et al.* [2013] replayed the whole hypothetical GPS-based tsunami forecasting processing chain: starting from the real-time processing of raw GPS data down to on-the-fly tsunami simulations. The replay has demonstrated the feasibility of reliable GPS-based tsunami early warning in less than 3 minutes. Within this exercise, *Hoechner et al.* [2013] inverted co-seismic GPS-displacements into non-uniform slip distribution at a curved plate interface. *Ohta et al.* [2012] retrospectively inverted the 2011 Tohoku earthquake on a rectangular fault using uniform slip. In contrast with many other studies, their inversion algorithm does not fix the fault geometry and position a priori allowing the unconstrained inversion into Okada fault parameters.

[4] While a number of studies focused on tsunami source inversion using GPS data were published last years, no systematic study was undertaken to compare the inversion differences and, what is more important, to assess these differences in relation to the final tsunami forecasting. The north Chile, April 1, 2014, Pisagua M8.1 earthquake and tsunami were extensively recorded by a large number of land- and ocean-based instruments [e.g., *Schurr et al.,* 2014]. In particular, significant co-seismic displacements were recorded at several coastal GPS-stations. In present contribution, we take opportunity and use the 2014 Pisagua event as a case study to explore uncertainties of the GPS-based real-time tsunami forecasting related to different source inversion methods. Specifically, we compare three inversion methods: (1) *fastCMT* [Melgar et al., 2012], (2) inversion into slip distribution along the predefined curved plate interface and (3) unconstrained inversion into a single Okada fault with uniform slip. Of particular note, in contrast to mega-earthquakes like the 2011 Tohoku M9.0 event which definitely cause devastating tsunamis, earthquakes like the 2014 Pisagua event, with magnitudes ranging from M7.5 to M8.5, are especially challenging for TEWS because they belong to the „grey zone". On one hand, they do not necessarily trigger tsunamis, on another hand, GPS-fingerprints of such earthquakes may also approach the limit of real-time detect ability.

4.2 Retrieving co-seismic offsets from real-time GPS waveforms

[5] In this paper, Temporal Point Positioning (TPP) developed by *Li et al.* [2013c] was employed to retrieve real-time co-seismic offset from the GPS stations of the Integrated Plate Boundary Observatory Chile (IPOC) [*http://www.ipoc-network.org*]. To simulate data processing in a real-time mode, real-time precise satellite orbits and clock products are required. In this contribution, we generated them by PANDA (positioning and navigation data analyst) software [*Jing-nan and Mao-rong,* 2003], for detailed estimation strategy please refer to *Fang et al.* [2013]. Station distribution of the continuous GPS network is depicted in Fig.1. Among these stations, 11 ones are recorded with 1s sampling interval while the rest 15 ones are 30s. With respect to data processing, the cutoff angle is set as 7°. For troposphere, dry and wet parts were calculated using model provided by [*Saastamoinen*, 1972]. Co-seismic waveforms were retrieved through epoch solution and static offset were obtained by approach suggested by *Allen and Ziv* [2011]. Retrieved co-seismic offsets are shown in Fig.1.

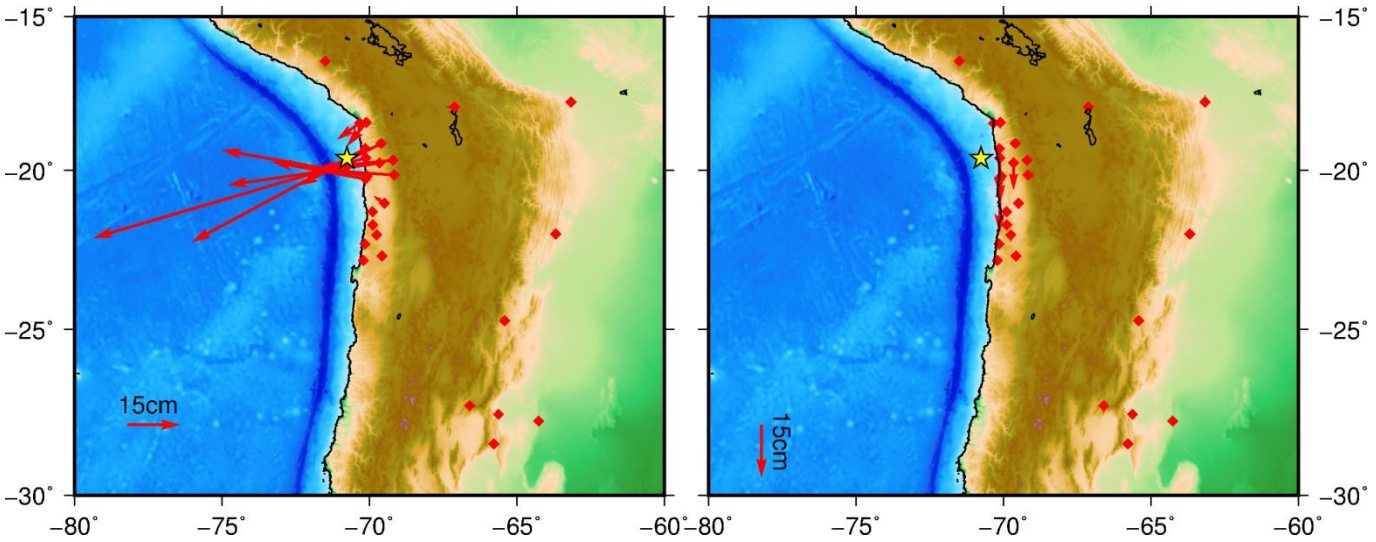

Figure 4. 1 Co-seismic offset from TPP. The left and right denote horizontal and vertical displacements while the yellow star shows the epicenter from USGS.

4.3 Inverting tsunami source by different methods

[6] Inversion of co-seismic displacements into tsunami source parameters precedes simulation of tsunami propagation and coastal forecasting. It can be done either by matching of pre-computed scenarios [*Behrens et al.,* 2010], or by on-the-fly retrieving of set of source parameters enabling initiation of tsunami propagation simulation. Sets of source parameters correspond to underlying rupture models and, hence, differ for different inversion methods. In present study we compare the three aforementioned inversion methods using co-seismic displacements from section 2. Please note, taking into account the noise level of GPS displacements, only stations with co-seismic offsets larger than 1.5 cm were included in the following inversions. In order to assess the effect of source inversion onto the final tsunami forecast, we have simulated tsunami generation and propagation for each inverted source model. *easyWave* [*Hoechner et al.*, 2013; *http://trac.gfz-potsdam.de/easywave*] code was used to calculate 4 hours of tsunami propagation. Computational algorithm closely follows the linear long-wave approximation on a staggered finite-difference grid with leap-frog explicit time stepping [*IUGG/IOC TIME Project*, 1997]. Bathymetry was GEBCO grid [*The GEBCO_08 Grid, ver. 20100927, http://www.gebco.net*] resampled to 1 arc minute, and boundary conditions include normal reflections at the coastline plus radiation b.c. at open boundaries.

4.3.1 Result from fastCMT

[7] In 2012, *Melgar et al.* [2012] proposed *fastCMT*: an effective Matlab algorithm to convert GPS residual co-seismic displacements into the central moment tensor parameters. Following Melgar‘s algorithm, we have computed moment tensor synthetic Green‘s functions using EDGRN code [*Wang et al.*, 2003] and AK135 seismic velocity model [*Kennett et al.*, 1995] with 2 km horizontal and 4 km vertical intervals. At station locations, Green‘s functions were evaluated by spline interpolation from the closest grid nodes. Since the original *fastCMT* algorithm best fits moment tensor parameters at fixed geographical location, it should be accomplished with a grid search routine to find the best-fit centroid location as well. With respect to this search, we scanned within a 3-D 2° × 2° x 40 km prism by nodes spaced 0.2° horizontal and 4 km by depth and centered on the rapid epicenter from triggering seismic message. In accord

with real-time GPS precision, horizontal components wee weighted twice as much as the vertical component.

[8] Corresponding best-fit *fastCMT* solution for the Pisagua 2014 earthquake is summarized in table 1. For reference, we compare it with the telesiesmic Global CMT (GCMT) provided by the GCMT project (http://www.globalcmt.org/CMTsearch.html).

Table 1 GPS-based *fastCMT* moment tensor solution for the April 2014, Pisagua, northern Chile M8.1 earthquake (left) as compared to the Global CMT (GCMT) teleseismic solutions. VR means variance reduction and NP stands for nodal plane

fastCMT				GCMT			
Centroid:−70.81°, −19.90°, -34.9 km				Centroid: −70.81°, −19.70°, -21.6 km			
Mw=8.2,VR=88.6				Mw=8.1			
Plane	Strike	Dip	Rake	Plane	Strike	Dip	Rake
NP1	9	38	126	NP1	355	15	106
NP2	146	60	65	NP2	159	76	86

[9] The *fastCMT* method provides source parameters in a point-source approximation. At the same time, tsunami initiation requires a finite fault model to calculate initial surface disturbance. To meet this requirement, we have extended CMT results and estimated corresponding fault length, width and slip by applying scaling relations of *Blaser et al.* [2010] to the derived magnitude. Resulting parameter set (hypocenter, strike, dip, rake, fault length, width and amount of slip) constitutes the input to the well-known *Okada* [1985] uniform slip rupture model routinely used in tsunami simulations. Of course, this procedure of transformation from point- to a finite source does not guarantee the same quality of GPS-fit by the both models. Figure 2a presents GPS-inversion results with the *fastCMT* method and the corresponding finite fault model.

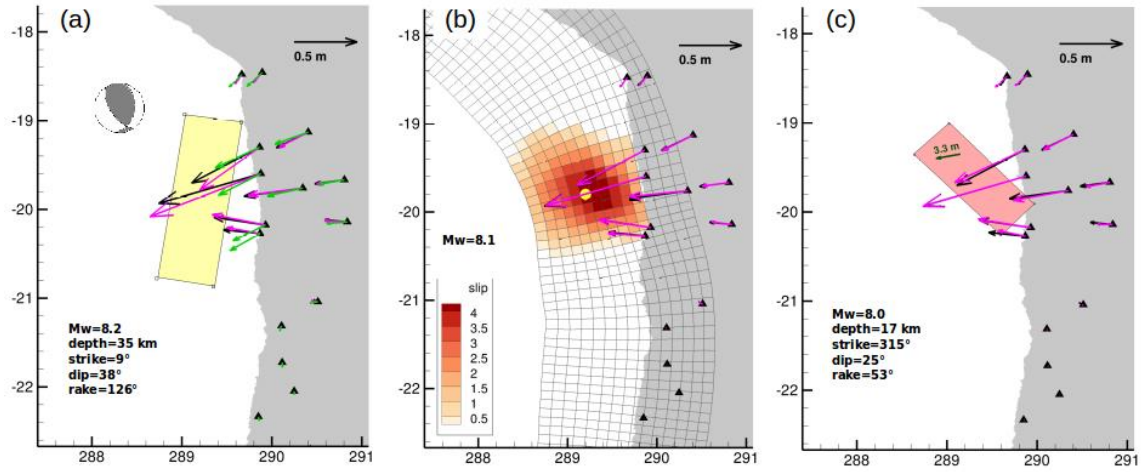

Figure 4. 2 Source models for the April 2014 Pisagua earthquake obtained by the three tested GPS-inversion methods. (A) *fastCMT* method by *Melgar et al.* [2012]. Magenta vectors correspond to the best point-source fit. Note that the finite fault model (yellow rectangle) derived from the best-fit CMT solution generates displacements (green) which fit observed GPS vectors (black) considerably worse. (B) Slip distribution along the predefined Slab1.0 curved plate interface. (B) Unconstrained inversion into single Okada plane without any a priori information. Note that strike of the plane does not follow direction of the trench.

4.3.2 Result from distributed slip inversion

[10] Slip inversion along the predefined plane or curved subduction plate interface is nowdays a common strategy for GPS-based source inversions. In this study we use the inversion algorithm described in Hoechner et al., [2008, 2013]. Slab geometry follows the Slab1.0 subduction zones model by [Hayes et al., 2012] and elastic model corresponds to layered half space. Figure 2b presents the final rupture model of the Pisagua earthquake.

4.3.3 Result from inversion into single Okada's fault

[11] Inversion into slip distribution along the predefined plate interface produces best-fit results for classical subduction zone thrust ruptures. However, and that is important to note in the context of tsunami early warning, a ‗classical' thrust rupture between the subducted and upper plate is not the only possible rupture type in the vicinity of subduction zones. Less common but still widespread are ruptures of another types originating apart of the plate interface: e.g., outer rise normal faults, inter-slab earthquakes, events in the upper plate. For a TEWS it is hence important not to treat all events as inter-slab thrusts by default (despite the latter often may be considered as worst-case scenario) but to be able to invert source without any pre-judgement on focal mechanism and orientation. To meet this requirement, we have also included into the present study unconstrained inversion into a single Okada's fault with minimal a priori information. The only constraint we used was the scaling law *Blaser et al.* [2010] linking fault size and slip to the earthquake magnitude. Independent search parameter set included: epicenter, depth, magnitude, strike, dip and rake angles. Parameter space search for the best-fit was organized as a combination of brute-force and Monte-Carlo searches. No pre-computed Green's functions were used in the inversion procedure; instead, trial displacements at GPS stations were computed each time using the *Okada* [1985] formulas. Figure 2c shows the best-fit Okada fault model. Note that due to the trade-off between the strike and rake angles, the strike of the best-fit model does not follow the actual trench direction.

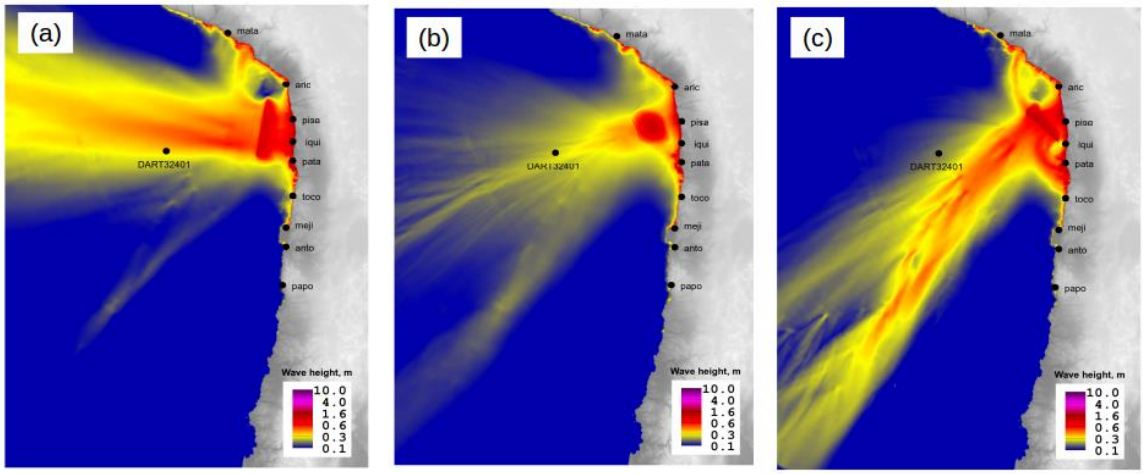

Figure 4. 3 Maximum tsunami wave heights after 4 hours of simulation for the three different source invertion models. See Fig. 2 and text for description of models a-c.

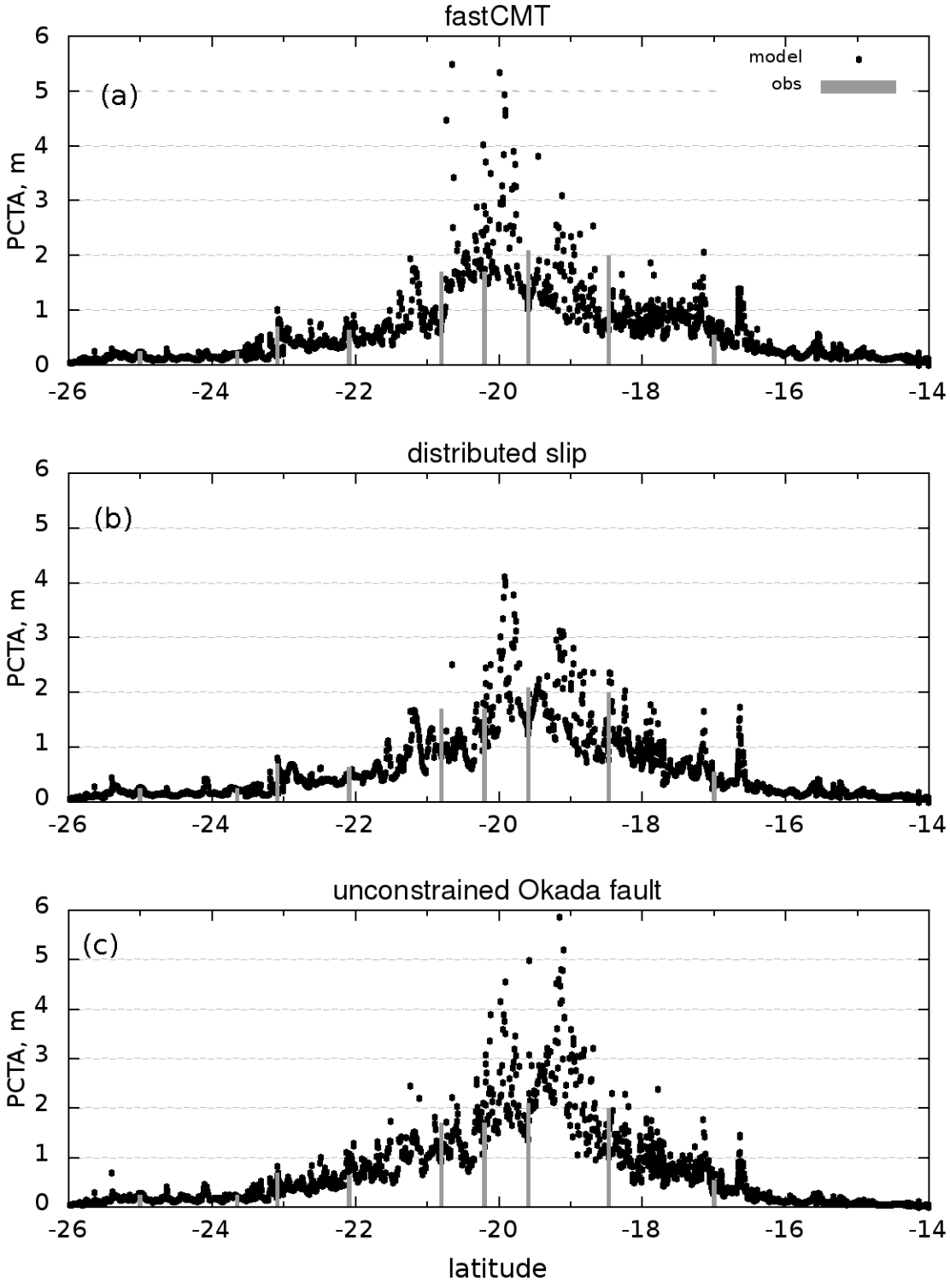

Figure 4. 4 Peak tsunami amplitudes along the Chilean coast (dots) as forecasted for the three different source inversion models (see caption of Fig. 2 for the model descriptions). Also shown are tsunami observations at the tide gauge stations (vertical bars).

4.3.4 Tsunami forecasts from different source inversions

[12] The main goal of current study is to assess the uncertainty of tsunami forecasting related to different source inversion techniques. Figures 3 and 4 display the results of tsunami propagation scenarios corresponding to the three aforementioned source inversions. Figure 3 presents distribution of maximum wave heights at a regional scale. The three different source models produce significantly different wave radiation patterns that would result in different far-field tsunami forecasting (compare Fig.3 a-c). However, closer inspection of Figure 4 showing distribution of peak tsunami amplitudes along the nearby Chilean coast reveals almost opposite result: in the context of local tsunami early warning, the three source inversions would have produced similar coastal forecasting. That is because tsunami early warning centers, operating with simulation-based forecasts, usually assign warning levels (‗advisory', ‗watch', ‗warning', ‗major warning') to wave height thresholds. For example, if we accept 0.5 meter as a ‗warning' threshold as well as some ‗uncertainty buffer', we would rise the warning alert for the Chilean coast starting from 15°S down to 24°S. Of course, predicted wave heights can exhibit significant differences at individual locations between the three source models. For example, absolute maximums of coastal tsunami amplitudes vary from 4 (Fig. 4b) to 6 meters (Fig. 4c). Also the overall amplitude pattern for the *fastCMT* source model is shifted to the north compared to another source models. But all these differences take place above the 0.5 m threshold and, therefore, become not important when a warning center evaluates its tsunami early warning forecast based on thresholds.

4.4 Concluding remarks

[13] We have used GPS data recorded by the IPOC network during the April 2014 Pisagua, northern Chile M8.1 earthquake to assess tsunami forecast uncertainty related to different GPS-based source inversion methods. Three methods were compared, all capable to work in real time with residual GPS-displacements at local stations: (1) *fastCMT* with subsequent construction of finite Okada fault, (2) inversion into slip distribution along the predefined curved plate interface and (3) unconstrained inversion into a single Okada fault with uniform slip.

[14] The three source inversion approaches give similar first-order rupture parameters including magnitude and lon-lat position of the rupture center. Other fault parameters: depth, strike, dip and rake angles show significant differences, which are later clearly manifested by different far-field tsunami propagation patterns.

[15] Despite large differences in far-field tsunami propagation, early warning tsunami forecasting along the nearby Chilean coast would be surprisingly similar for all three models. That is valid in case early warning alert is based on tsunami amplitude thresholds (e.g, 0.5 meter threshold). In this case, even remarkable differences at individual locations do not change the alert status as long as they lie above the alert threshold. Our study does not reveal any absolute favorite between the three source inversion approaches.

[16] It is important to note that the present result on robustness of the local tsunami early warning forecasting against source inversion technique should not be blindly projected to other subduction zones or to larger magnitudes. The 2014 Pisagua 2014 M8.1 rupture was rather compact (<200 km) with simple, centered slip distribution. In a hypothetical case of a longer rupture (e.g. like Sumatra 2004), local irregularities of slip distribution might strongly influence runup distribution along the nearby coast [*Geist*, 2001]. Also *Sobolev at al.* [2007] argued on extreme sensitivity of local runup against rupture position and slip distribution for the Sumatran west coast, Indonesia. In the latter case, high sensitivity to source parameters was due to specific bathymetry offshore Sumatra - the presence of irregular Mentawai island chain. Regional and national near-filed TEWS should build their own source inversion strategies based on corresponding tectonic settings.

[17] Finally, we speculate that operational tsunami forecasting deals with many sources of uncertainty; epistemic and aleatoric, related to data and related to numerical methods. It is important to assess and to rank at least major sources of uncertainties in a systematic way for a more reliable tsunami early warning.

4.5 Acknowledge

[16] Kejie Chen is supported by China Scholarship Council (CSC) for his PhD study in Germany research Centre for Geoscience. This study was also financially supported by the German Ministry of Science and Education (BMBF) research grant „Multi-Hazard System Chile". GNSS data for Pisagua earthquake was provided by IPOC (Integrated Plate Boundary Observatory Chile).

4.6 Reference

Allen, R. M., and A. Ziv (2011), Application of real-time GPS to earthquake early warning, *Geophys. Res. Lett.*, *38*(16), 1–7, doi:10.1029/2011GL047947.

An, C. (2015), Inversion of tsunami waveforms and tsunami warning.

Babeyko, A. Y., A. Hoechner, and S. V Sobolev (2010), Source modeling and inversion with near real-time GPS: a GITEWS perspective for Indonesia, *Nat. Hazards Earth Syst. Sci.*, *10*, 1617–1627, doi:10.5194/nhess-10-1617-2010.

Banerjee, P., F. Pollitz, B. Nagarajan, and R. Bürgmann (2007), Coseismic Slip Distributions of the 26 December 2004 Sumatra–Andaman and 28 March 2005 Nias Earthquakes from gps Static Offsets, *Bull. Seismol. Soc. Am.* , *97* (1A), S86–S102, doi:10.1785/0120050609.

Blaser, L., F. Kruger, M. Ohrnberger, and F. Scherbaum (2010), Scaling Relations of Earthquake Source Parameter Estimates with Special Focus on Subduction Environment, *Bull. Seismol. Soc. Am.*, *100*(6), 2914–2926, doi:10.1785/0120100111.

Blewitt, G., C. Kreemer, W. C. Hammond, H.-P. Plag, S. Stein, and E. Okal (2006), Rapid determination of earthquake magnitude using GPS for tsunami warning systems, *Geophys. Res. Lett.*, *33*(11), L11309–L11309, doi:10.1029/2006GL026145.

Blewitt, G., W. C. Hammond, C. Kreemer, H. P. Plag, S. Stein, and E. Okal (2009), GPS for real-time earthquake source determination and tsunami warning systems, *J. Geod.*, *83*, 335–343, doi:10.1007/s00190-008-0262-5.

Bock, Y., R. M. Nikolaidis, P. J. Jonge, and M. Bevis (2000), Instantaneous geodetic positioning at medium distances with the Global Positioning System, *J. Geophys. Res. Solid Earth*, *105*(B12), 28223–28253.

Bock, Y., L. Prawirodirdjo, and T. I. Melbourne (2004), Detection of arbitrarily large dynamic ground motions with a dense high‐rate GPS network, *Geophys. Res. Lett.*, *31*(6).

Bock, Y., D. Melgar, and B. W. Crowell (2011), Real-time strong-motion broadband displacements from collocated GPS and accelerometers, *Bull. Seismol. Soc. Am.*, *101*(6), 2904–2925, doi:10.1785/0120110007.

Boore, D. M., and J. J. Bommer (2005), Processing of strong-motion accelerograms: needs, options and consequences, *Soil Dyn. Earthq. Eng.*, *25*(2), 93–115.

Chen, K., N. Zamora, A. Y. Babeyko, X. Li, and M. Ge (2015a), Precise Positioning of BDS, BDS/GPS: Implications for Tsunami Early Warning in South China Sea, *Remote Sens.*, *7*(12), 15955–15968.

Chen, K., M. Ge, X. Li, A. Babeyko, M. Ramatschi, and M. Bradke (2015b), Retrieving real-time precise co-seismic displacements with a standalone single-frequency GPS receiver, *Adv. Sp. Res.*

Colosimo, G., M. Crespi, and A. Mazzoni (2011), Real-time GPS seismology with a stand-alone receiver: A preliminary feasibility demonstration, *J. Geophys. Res. Solid Earth*, *116*(B11).

Crowell, B. W., Y. Bock, and D. Melgar (2012), Real‐time inversion of GPS data for finite fault modeling and rapid hazard assessment, *Geophys. Res. Lett.*, *39*(9).

Diao, F., X. Xiong, S. Ni, Y. Zheng, and C. Ge (2011), Slip model for the 2011 M w 9.0 Sendai (Japan) earthquake and its M w 7.9 aftershock derived from GPS data, *Chinese Sci. Bull.*, *56*(27), 2941–2947.

Fang, R., C. Shi, W. Song, G. Wang, and J. Liu (2013), Determination of earthquake magnitude using GPS displacement waveforms from real-time precise point positioning, *Geophys. J. Int.* , doi:10.1093/gji/ggt378.

Ge, L. (1999), GPS seismometer and its signal extraction, in *Proc. 12th Int. Tech. Meeting of the Satellite Division of the US Inst. of Navigation GPS ION'99*.

Ge, L., S. Han, C. Rizos, Y. Ishikawa, M. Hoshiba, Y. Yoshida, M. Izawa, N. Hashimoto, and S. Himori (2000), GPS seismometers with up to 20 Hz sampling rate, *Earth, planets Sp.*, *52*(10), 881–884.

Geist, E. L. (2001), Effect of depth-dependent shear modulus on tsunami generation along subduction zones shallow depths in comparison to standard earth, , *28*(7), 1315–1318.

Geng, J., and Y. Bock (2015), GLONASS fractional-cycle bias estimation across inhomogeneous receivers for PPP ambiguity resolution, *J. Geod.*, 1–18.

Geng, T., X. Xie, R. Fang, X. Su, Q. Zhao, G. Liu, H. Li, C. Shi, and J. Liu (2015), Real‐time capture of seismic waves using high‐rate multi‐GNSS observations: Application to the 2015 Mw 7.8 Nepal earthquake, *Geophys. Res. Lett.*

Hanks, T. C., and H. Kanamori (1979), A Moment Magnitude Scale, *J. Geophys. Res.*, *84*(B5), 2348–2350.

Haskell, N. A. (1964), Total energy and energy spectral density of elastic wave radiation from propagating faults, *Bull. Seismol. Soc. Am.*, *54*(6A), 1811–1841.

Hayes, G. P., D. J. Wald, and R. L. Johnson (2012), Slab1.0: A three-dimensional model of global subduction zone geometries, *J. Geophys. Res.*, *117*(B1), B01302–B01302, doi:10.1029/2011JB008524.

Hirahara, K., T. Nakano, Y. Hoso, S. Matsuo, and K. Obana (1994), An experiment for GPS strain seismometer, in *Japanese symposium on GPS*, pp. 67–75.

Hirose, F., K. Miyaoka, N. Hayashimoto, T. Yamazaki, and M. Nakamura (2011), Outline of the 2011 off the Pacific coast of Tohoku Earthquake (M w 9.0)—Seismicity: foreshocks, mainshock, aftershocks, and induced activity—, *Earth, planets Sp.*, *63*(7), 513–518.

Hoechner, A., A. Y. Babeyko, and S. V Sobolev (2008), Enhanced GPS inversion technique applied to the 2004 Sumatra earthquake and tsunami, *Geophys. Res. Lett.*, *35*(8), L08310–L08310, doi:10.1029/2007GL033133.

Hoechner, A., M. Ge, a. Y. Babeyko, and S. V Sobolev (2013), Instant tsunami early warning based on real-time GPS – Tohoku 2011 case study, *Nat. Hazards Earth Syst. Sci.*, *13*(5), 1285–1292, doi:10.5194/nhess-13-1285-2013.

Hofmann-Wellenhof, B., H. Lichtenegger, and E. Wasle (2007), *GNSS–global navigation satellite systems: GPS, GLONASS, Galileo, and more*, Springer Science & Business Media.

Japan Meteorological Agency (JMA) (2013), Lessons learned from the tsunami disaster caused by the 2011 Great East Japan Earthquake and improvements in JMA ' s tsunami warning system October 2013 Japan Meteorological Agency, , (October), 1–13.

Jing-nan, L., and G. Mao-rong (2003), PANDA software and its preliminary result of positioning and orbit determination, *Wuhan Univ. J. Nat. Sci.*, *8*(2), 603–609.

Kanamori, H. (1983), Magnitude scale and quantification of earthquakes, *Tectonophysics*, *93*(3), 185–199.

Kanamori, H., and L. Rivera (2008), Source inversion of W phase: speeding up seismic tsunami warning, *Geophys. J. Int.* , *175* (1), 222–238, doi:10.1111/j.1365-246X.2008.03887.x.

Kennett, B. L. N., E. R. Engdahl, and R. Buland (1995), Constraints on seismic velocities in the Earth from traveltimes, *Geophys. J. Int.*, *122*(1), 108–124.

Kerr, R. A. (2005), Failure to Gauge the Quake Crippled the Warning Effort, *Sci.* , *307* (5707), 201, doi:10.1126/science.307.5707.201.

Larson, K. M. (2009), GPS seismology, *J. Geod.*, *83*(3-4), 227–233.

Larson, K. M., P. Bodin, and J. Gomberg (2003), Using 1-Hz GPS data to measure deformations caused by the Denali fault earthquake, *Science (80-.).*, *300*(5624), 1421–1424.

Li, X., M. Ge, Y. Zhang, R. Wang, B. Guo, J. Klotz, J. Wickert, and H. Schuh (2013a), High-rate coseismic displacements from tightly integrated processing of raw GPS and accelerometer data, *Geophys. J. Int.*, doi:10.1093/gji/ggt249.

Li, X., M. Ge, X. Zhang, Y. Zhang, B. Guo, R. Wang, J. Klotz, and J. Wickert (2013b), Real-time high-rate co-seismic displacement from ambiguity-fixed precise point positioning: Application to earthquake early warning, *Geophys. Res. Lett.*, *40*(2), 295–300, doi:10.1002/grl.50138.

Li, X., M. Ge, B. Guo, J. Wickert, and H. Schuh (2013c), Temporal point positioning approach for real-time GNSS seismology using a single receiver, *Geophys. Res. Lett.*, *40*(21), 5677–5682, doi:10.1002/2013GL057818.

Li, X., M. Ge, X. Dai, X. Ren, M. Fritsche, J. Wickert, and H. Schuh (2015), Accuracy and reliability of multi-GNSS real-time precise positioning: GPS, GLONASS, BeiDou, and Galileo, *J. Geod.*, *89*(6), 607–635, doi:10.1007/s00190-015-0802-8.

Liu, Y., M. Ge, C. Shi, Y. Lou, J. Wickert, and H. Schuh (2015), Improving GLONASS Precise Orbit Determination through Data Connection, *Sensors*, *15*(12), 30104–30114.

Melgar, D. (2014), Seismogeodesy and Rapid Earthquake and Tsunami Source Assessment, 247 pp., University of California San Diego,

Melgar, D., Y. Bock, and B. W. Crowell (2012), Real-time centroid moment tensor determination for large earthquakes from local and regional displacement records, *Geophys. J. Int.*, *188*(2), 703–718, doi:10.1111/j.1365-246X.2011.05297.x.

Melgar, D., Y. Bock, D. Sanchez, and B. W. Crowell (2013a), On robust and reliable automated baseline corrections for strong motion seismology, *J. Geophys. Res. Solid Earth*, *118*(3), 1177–1187.

Melgar, D., B. W. Crowell, Y. Bock, and J. S. Haase (2013b), Rapid modeling of the 2011 Mw 9.0 Tohoku-oki earthquake with seismogeodesy, *Geophys. Res. Lett.*, *40*(12), 2963–2968, doi:10.1002/grl.50590.

Menke, W., and V. Levin (2005), A strategy to rapidly determine the magnitude of great earthquakes, *Eos, Trans. Am. Geophys. Union*, *86*(19), 185–188.

Montenbruck, O., P. Steigenberger, R. Khachikyan, G. Weber, R. B. Langley, L. Mervart, and U. Hugentobler (2014), IGS-MGEX: preparing the ground for multi-constellation GNSS science, *Insid. GNSS*, *9*(1), 42–49.

Mooney, W. D., G. Laske, and T. G. Masters (1998), CRUST 5.1: A global crustal model at 5× 5, *J. Geophys. Res. Solid Earth*, *103*(B1), 727–747.

NGDC/WDS (n.d.), National Geophysical Data Center / World Data Service (NGDC/WDS): Global Historical Tsunami Database. National Geophysical Data Center, NOAA, *Access on 15.01.2015*, doi:10.7289/V5PN93H7. Available from: http://www.ngdc.noaa.gov/hazard/tsu_db.shtml

O'Toole, T. B., A. P. Valentine, and J. H. Woodhouse (2012), Centroid–moment tensor inversions using high-rate GPS waveforms, *Geophys. J. Int.*, *191*(1), 257–270.

O'Toole, T. B., A. P. Valentine, and J. H. Woodhouse (2013), Earthquake source parameters from GPS‐measured static displacements with potential for real‐time application, *Geophys. Res. Lett.*, *40*(1), 60–65.

Ohta, Y. et al. (2012), Quasi real-time fault model estimation for near-field tsunami forecasting based on RTK-GPS analysis: Application to the 2011 Tohoku-Oki earthquake (M w 9.0), *J. Geophys. Res. Solid Earth*, *117*, doi:10.1029/2011JB008750.

Okada, Y. (1985), Surface deformation due to shear and tensile faults in a half-space, *Bull. Seismol. Soc. Am.*, *75*(4), 1135–1154.

Saastamoinen, J. (1972), Atmospheric correction for the troposphere and stratosphere in radio ranging satellites, *use Artif. Satell. Geod.*, 247–251.

Schüler, T. (2014), The TropGrid2 standard tropospheric correction model, *GPS Solut.*, *18*(1), 123–131.

Shi, C., Y. Lou, H. Zhang, Q. Zhao, J. Geng, R. Wang, R. Fang, and J. Liu (2010), Seismic deformation of the M w 8.0 Wenchuan earthquake from high-rate GPS observations, *Adv. Sp. Res.*, *46*(2), 228–235.

Simons, M., Y. Fialko, and L. Rivera (2002), Coseismic Deformation from the 1999 Mw 7.1 Hector Mine, California, Earthquake as Inferred from InSAR and GPS Observations, *Bull. Seismol. Soc. Am.* , *92* (4), 1390–1402, doi:10.1785/0120000933.

Sobolev, S. V, A. Y. Babeyko, R. Wang, R. Galas, M. Rothacher, D. SEIN, J. Schröter, J. Lauterjung, and C. Subarya (2006), Towards real-time tsunami amplitude prediction, *Eos (Washington. DC).*, *87*(37).

Sobolev, S. V, A. Y. Babeyko, R. Wang, A. Hoechner, R. Galas, M. Rothacher, D. V Sein, J. Schröter, J. Lauterjung, and C. Subarya (2007), Tsunami early warning using GPS-Shield arrays, *J. Geophys. Res. Solid Earth*, *112*(B8), B08415–B08415, doi:10.1029/2006JB004640.

Song, Y. T. (2007), Detecting tsunami genesis and scales directly from coastal GPS stations, *Geophys. Res. Lett.*, *34*(19).

Tian, Y., M. Ge, and F. Neitzel (2015), Particle filter-based estimation of inter-frequency phase bias for real-time GLONASS integer ambiguity resolution, *J. Geod.*, *89*(11), 1145–1158.

Tsuji, H., Y. Hatanaka, T. Sagiya, and M. Hashimoto (1995), Coseismic crustal deformation from the 1994 Hokkaido - Toho - Oki earthquake monitored by a nationwide continuous GPS array in Japan, *Geophys. Res. Lett.*, *22*.

Tu, R., and K. Chen (2014), Tightly Integrated Processing of High-Rate GPS and Accelerometer Observations by Real-Time Estimation of Transient Baseline Shifts, *J. Navig.*, *67*(05), 869–880.

Vigny, C., W. J. Simons, S. Abu, R. Bamphenyu, C. Satirapod, N. Choosakul, and B. A. C. Ambrosius (2005), Insight into the 2004 Sumatra–Andaman earthquake from GPS measurements in southeast Asia, *Nature*, *436*, 201–206.

Wang, L., R. Wang, F. Roth, B. Enescu, S. Hainzl, and S. Ergintav (2009), Afterslip and viscoelastic relaxation following the 1999 M 7.4 İzmit earthquake from GPS measurements, *Geophys. J. Int.*, *178*(3), 1220–1237, doi:10.1111/j.1365-246X.2009.04228.x.

Wang, R., F. L. Mart n, and F. Roth (2003), Computation of deformation induced by earthquakes in a multi-layered elastic crust—FORTRAN programs EDGRN/EDCMP, *Comput. Geosci.*, *29*(2), 195–207.

Wang, R., F. Diao, and A. Hoechner (2013), SDM-A geodetic inversion code incorporating with layered crust structure and curved fault geometry, in *EGU General Assembly Conference Abstracts*, vol. 15, p. 2411.

Yang, Y., J. Li, A. Wang, J. Xu, H. He, H. Guo, J. Shen, and X. Dai (2014), Preliminary assessment of the navigation and positioning performance of BeiDou regional navigation satellite system, *Sci. China Earth Sci.*, *57*(1), 144–152.

Chapter 5 Precise Positioning of BDS, BDS/GPS: Implications for Tsunami Early Warning in South China Sea

Kejie Chen *, Natalia Zamora, Andrey Babeyko, Xingxing Li and Maorong Ge

German Research Centre for Geoscience, Telegrafenberg, 14473 Potsdam, Germany; zamora@gfz-potsdam.de (N.Z.); babeyko@gfz-potsdam.de (A.B.); lixin@gfz-potsdam.de (X.L.); maor@gfz-potsdam.de (M.G.)
Correspondence: kejie@gfz-potsdam.de; Tel.: +49-331-28828792

Abstract: Global Positioning System (GPS) has been proved to be a powerful tool for measuring co-seismic ground displacements with an application to seismic source inversion. Whereas most of the tsunamis are triggered by large earthquakes, GPS can contribute to the tsunami early warning system (TEWS) by helping to obtain tsunami source parameters in near real-time. Toward the end of 2012, the second phase of the BeiDou Navigation Satellite System (BDS) constellation was accomplished, and BDS has been providing regional positioning service since then. Numerical results indicate that precision of BDS nowadays is equivalent to that of the GPS. Compared with a single Global Satellite Navigation System (GNSS), combined BDS/GPS real-time processing can improve accuracy and especially reliability of retrieved co-seismic displacements. In the present study, we investigate the potential of BDS to serve for the early warning system of tsunamis in the South China Sea region. To facilitate early warnings of tsunamis and forecasting capabilities in this region, we propose to distribute an array of BDS-stations along the Luzon Island (Philippines). By simulating an earthquake with Mw = 8 at the Manila trench as an example, we demonstrate that such an array will be able to detect earthquake parameters in real time with a high degree of accuracy and, hence, contribute to the fast and reliable tsunami early warning system in this region.

Keywords: BDS; BDS/GPS; South China Sea; tsunami early warning system

5.1 Introduction

As one of the most devastating natural coastal disasters, tsunamis are triggered mostly by shallow earthquakes in submarine subduction zones [1] producing the most damage in the near field but also propagating basin-wide. Consequently, traditional Tsunami Early Warning Systems (TEWS) mainly rely on seismic methods in order to evaluate source parameters (magnitude, epicenter) and forecast tsunamis as soon as possible. Corresponding seismic instrumentation mainly includes broadband seismometers as well as strong-motion sensors (accelerometers). Despite the fact that these traditional techniques have proved their reliability for most historical cases over the last decades, they have failed to provide correct rapid magnitude estimation for several important events like the 2004 Mw = 9.3 Great Sumatra earthquake, the 2010 Mw = 7.8 Mentawai tsunami earthquake and the 2011 Mw = 9.0 Great Tohoku event. For example, in the latter case, the true magnitude was significantly underestimated during the fifty minutes after the earthquake [2]. Magnitude underestimation, in turn, may result in the underestimation of the tsunami forecast in the near field [2].

The reasons for magnitude underestimation during the first several minutes after large earthquakes vary for different seismic instruments as well as earthquake evaluation procedures.

Broadband seismometers saturate near the source in case of strong shaking so that the full rupture image can be analyzed only at larger epicentral distances, causing unavoidable delay due to the finite speed of seismic wave propagation. Strong motion sensors, in turn, do not saturate by amplitude and can be employed close to the source; however, the usual band-pass filtering of waveforms aimed to avoid processing unambiguity caused by co-seismic tilting [3] effectively leads to magnitude saturation due to removal of long periods which are essential for huge earthquakes [4]. See, for example, [2,5] regarding the analysis of the strong-motion magnitude saturation during the Great Tohoku earthquake.

The 2004 Great Mw = 9.3 Sumatra earthquake and tsunami boosted the development of new seismic approaches that are aimed toward the faster and more reliable characterization of tsunamigenic earthquakes. During the GITEWS Project (German-Indonesian Tsunami Early Warning System), Bormann and Saul [6] proposed a fast, non-saturating cumulative magnitude estimator based on the P-wave train. The procedure was tested at epicentral distances starting from 5° and is currently operated by the INATEWS (Indonesian Tsunami Early Warning System) [7]. Additionally, Kanamori and Rivera [8] suggested a new broadband W-phase source inversion algorithm, which is currently running in operation at PTWC (Pacific Tsunami Warning Center). During the 2011 Great Mw = 9.0 Tohoku event, this algorithm automatically detected the focal mechanism and came with magnitude estimate of Mw = 8.8 22 min after the earthquake (the true magnitude Mw = 9.0 was estimated 40 min after the earthquake) [9]. Another approach was suggested by Lomax and Michelini [10], who introduced an original duration-amplitude procedure to estimate the tsunamigenic potential of earthquakes.

Significant efforts were also undertaken to improve the quality of real-time strong-motion data processing. New studies [4,11,12] proposed fast and effective procedures for automatic base-line correction. Furthermore, the novel technique of collocation of strong-motion and GPS sensors [13,14] should help to overcome the problem of magnitude saturation since the band-pass filtering is no longer required [15].

Rapid improvement of the real-time GPS processing precision put GPS-technology at the front end of current progress in the earthquake and tsunami early warning system. Compared with seismic approaches, continuous GNSS real-time data processing provides arbitrary ground displacements that can be directly inverted into source parameters in (near-) real time. Hence, it is considered to be a more trustworthy tool, especially for the near field tsunami early warning. Several previous studies have discussed or demonstrated the potential of using GPS data for tsunami early warnings. For example, Blewitt *et al.* [16] showed that the magnitude, mechanism, and spatial extent of rupturing of the 26 December 2004 Sumatra earthquake might have been accurately determined using only 15 min of GPS data following an earthquake initiation. Simultaneously, Sobolev *et al.* [17] pointed out that the reliable prediction of tsunami waves on the Indonesian coast can be issued within less than 5 min of an earthquake by incorporating special types of near-field GPS arrays (“GPS-Shield” concept for Indonesia). They also proposed deployment of such arrays for other tsunamigenic active regions. Following this idea, GITEWS (German Indonesian Tsunami Early Warning System) became the first TEWS to implement real-time GPS for a tsunami early warning [18,19]. Recently, Hoechner *et al.* [20] replayed the Great Tohoku 2011 event in that they presented a complete processing chain starting from actual raw GPS data and fully simulated the situation as it would be in a warning center ending up with a very fast and qualified tsunami early warning. Now using real-time GPS for earthquake and tsunami early warnings is an active area of research (e.g., [18–26]).

To date, geo-hazard monitoring with GNSS is restricted to the oldest, largest and most-used GPS system. Around the end of 2012, China has completed the regional constellation of the BeiDou Navigation Satellite System (BDS), and the system has been running routinely since then. Even at its second-phase stage, numerous studies (e.g., [27–29]) have demonstrated that precise positioning performance of BDS is equal in match against that of GPS in the Asia-Pacific region. Compared with a single satellite navigation system, the fusion of GPS, GLONASS, GALILEO and BDS can significantly increase the number of observed satellites, reduce the position dilution of precision (PDOP) [29] and, thus, increase robustness and the reliability of observations. What is more, BDS, due to its similarity to GPS signal structure and frequencies, provides a much better chance for investigating the impact of multi-GNSS capacity on real-time precise positioning in terms of accuracy and reliability. In the present study, we investigate the potential of the BDS system to contribute to the tsunami early warning system in the South China Sea region. In particular, we assess the accuracy of the real-time BDS processing and corresponding source inversion due to a hypothetical tsunamigenic earthquake at the Manila trench.

As shown in previous studies (e.g., [30–33]), the Manila subduction zone (Figure 5.1) has been identified as a zone of potential tsunami hazard in the SCS region. Despite the absence of clear historical evidence on large tsunamis generated at the Manila trench, tsunami deposits found at the Xischa Islands (~1024 AD) may be attributed to a large event in this source region [34]. According to the recently compiled historical tsunami database for the northeastern South China Sea [35], annual probability of a tsunami in this region from any source is very high (~33%). However, the likelihood of a damaging tsunami per year is much smaller (1%–2%). In the absence of large historical events from the Manila Trench, damaging tsunamis in the South China Sea have been previously studied by means of numerical modeling. Simulations [30,36] suggest that an earthquake with a magnitude of Mw = 8.0 or larger at the Manila trench may cause significant tsunami damage along the whole south-eastern coast of China, Southwestern Taiwan and West Philippines. Taking the potential large-scale disaster into account, the tsunami early warning system in the SCS region was suggested by [30,37,38] based on DART-type deep ocean buoys. In fact, China has installed two buoys in SCS in 2014. In the present paper, we propose to improve the regional TEWS by installing real-time continuous BDS-network at the Luzon Island, Philippines. Being integrated with traditional seismic networks, the proposed GNSS-array will contribute to fast and reliable source inversion, which is one of the most important tasks in the early warning and forecasting of tsunamis.

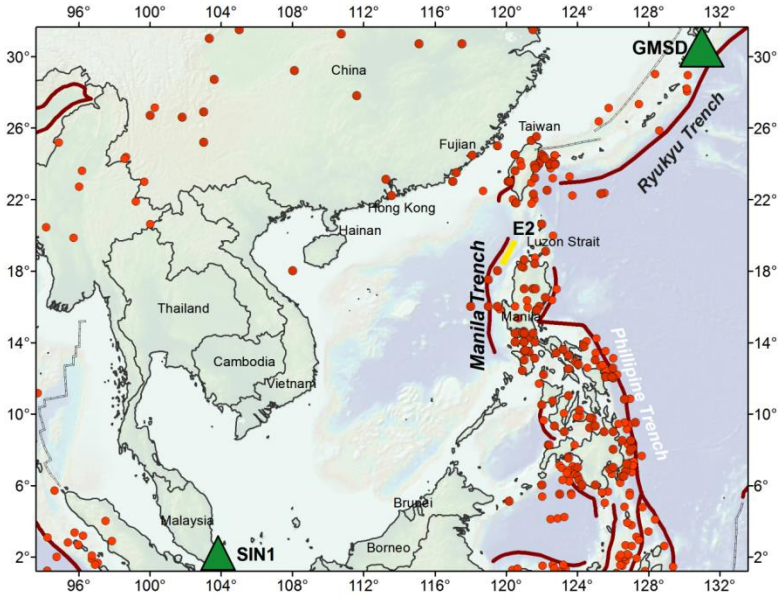

Figure 5. 1 Seismotectonic map of the Southern China Sea. The red thick line represents the Manila trench of the seismogenic Manila subduction zone. The red points show the earthquakes that have occurred from 1976–2015 with a magnitude larger than Mw = 6.5 (GCMT catalog). The yellow line E2 indicates the rupture area used in this study. The two multi-GNSS stations used in Section 2 are also shown by green triangles.

In Section 2, we test the real-time precise positioning performance of BDS and compare it with GPS and joint BDS/GPS in the SCS region. In Section 3, we simulate a test scenario of an Mw=8.0 earthquake along the Manila trench and its corresponding tsunami to demonstrate the feasibility of incorporating BDS, BDS/GPS into the regional TEWS. In Section 4, we discuss additional issues related to the performance of BDS, BDS/GPS based TEWS. Finally, Section 5 summarizes results and presents an outlook.

5.2 Real-Time Kinematic Precise Positioning Performance of BDS in South-East Asia

Generally, there are two kinds of precise positioning algorithms, *i.e.*, relative positioning and single-point positioning. With respect to relative positioning, most of the error budgets can be cancelled through double differencing between reference station and rover station; as a result, its mathematical model is relatively simple and easy to be conducted. Most importantly, double-differencing integer-cycle phase ambiguities can be resolved to their correct integer values, reliably ensuring its high precision. However, the reference station of relative positioning must be fixed, which requires that, during an earthquake, it should be located outside the zone of deformation. The latter cannot always be satisfied, especially during large tsunamigenic earthquakes [21]. By contrast, the single-point positioning approach does not need a fixed reference station to form double-difference observations and, in theory, is more desirable for the retrieval of co-seismic displacements [25]. Nonetheless, it should be pointed out that for Precise Point Positioning (PPP), ambiguity resolution needs a convergence phase that may be as long as 20 min. Fortunately, the Variometric Approach for Displacements Analysis Stand-alone Engine (VADASE) [39] and the Temporal Point Positioning (TPP) [40] are able to overcome this disadvantage. The TPP has been employed in this study.

Up to now, no BDS or BDS/GPS data recorded during an earthquake is publicly available. Considering that performances of GNSS positioning are not different between earthquake-free and earthquake-breaking periods [13], to exploit the potential of BDS and BDS/GPS in retrieving co-seismic displacements, we selected two weeks of data (from 29 December 2013 to 11 January 2014) from IGS Multi-GNSS Experiment (MGEX) stations in the Asia-Pacific region. In this case, data from a 1-Hz sampling rate MGEX stations GMSD and SIN1 were used (see station distribution in Figure 5.1). Since no earthquake happened, we take zero displacement as ground truth. In this paper, real-time precise BDS/GPS orbits and clocks were produced according to the strategies suggested by Li et al. [29]. For every station, the length of each TPP session was set to 10 min, and, in each individual hour, we employed four sessions with evenly distributed start points; in total, we have 96 sessions per day for two weeks, which ensures a more trustworthy conclusion on the precise positioning performance. Figure 5.2 presents the TPP results in modes of BDS-only, GPS-only and BDS/GPS at station GMSD which can be taken as a typical example. As clearly shown, BDS-only and GPS-only show similar positioning performances while a BDS/GPS combined solution significantly improves the accuracy. Statistical Root Mean Square (RMS) is summarized in Table 1.

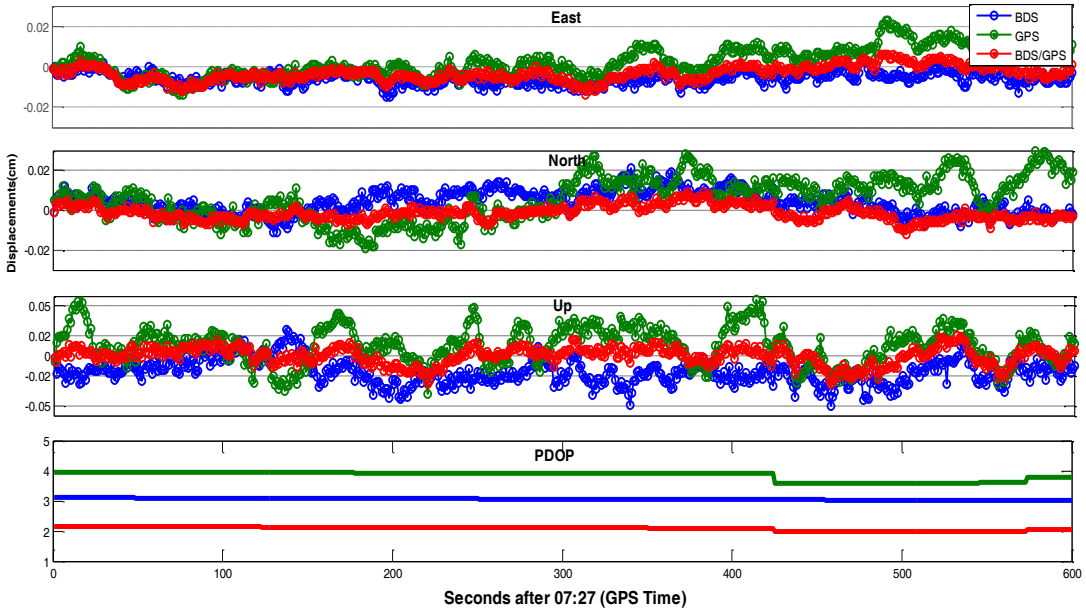

Figure 5. 2 TPP solutions of BDS, GPS and BDS/GPS at stationary station GMSD on 30 December 2013. Additionally shown is the corresponding PDOP, which specifies the effect of navigation satellite constellation geometry on positional precision. Note that, since the station did not move, the above graphs can be used to evaluate the expected uncertainty of TPP displacements.

Table 1. Expected RMS of BDS, GPS, and joint BDS/GPS real-time precise positioning using TPP in South-East Asia.

RMS (m)	BDS	GPS	BDS/GPS
East	0.0095	0.0071	0.0049
North	0.0068	0.0101	0.0048
Up	0.0203	0.0207	0.0098

5.3 Testing the Feasibility of BDS Real-Time Network at the Luzon Island for the Tsunami Early Warning in the South China Sea

In this section, we demonstrate the feasibility of BDS for the tsunami early warning in the Southern China Sea. To do that, we simulate a hypothetical tsunamigenic earthquake along the

Manila trench and try to invert resulting co-seismic displacements at a virtual BDS/GPS array distributed along the Luzon Island, northern Philippines. Previously, Kirby and Geist [41] and Liu *et al.* [30] assessed tsunamigenic potential of six rupture scenarios along the Manila trench. We follow their approach and place our fault model along the northern part of the Manila subduction zone (Figure 1). Fault parameters correspond to the rupture model E2 from Liu *et al.* (2006). This rupture scenario was selected due to its highest impact potential for the south Chinese coast. The accepted source model has a magnitude of Mw = 8.0 with the central point located at 119.8°E/18.7°N. The length is 180 km, the width 35 km, and the strike and the dip angles of the rupture plane are fixed to 35 and 20 degrees. The only difference with the original E2 rupture model is in slip distribution: we use a bell-shaped distribution rather than a uniform slip. The rupture plane consists of 75 sub-faults with a symmetry maximum at the slip center, and with the rake angles varying between 80~100 degrees.

We use code QSSP developed by Wang [42] to calculate synthetic displacement waveforms at stations of our virtual GNSS-array. With respect to the Earth model, in this study, the average global 1-D reference earth model AK135Q [43] is adopted. Figure 3 demonstrates simulated displacement waveforms at the selected station B1 (see virtual array in Figure 4a). To make our test even more realistic, we contaminate synthetic co-seismic displacements with a typical real-time BDS and BDS/GPS processing noises derived from a random segment of the GMSD (or SIN1) residual displacement time series, and the corresponding ~~"n~~oisy" displacements are also shown at Figure 5.3. These ~~"n~~oisy" displacements will be used for source inversion.

Figure 5.4a presents an overview of our forward rupture model: It shows assumed slip distribution together with the corresponding co-seismic vertical deformation as well as horizontal static offsets at the virtual BDS/GPS network.

Based on the suggested rupture, the corresponding tsunami scenario was simulated (Figure 5.5) using the *easyWave* wave propagation code [20]. *easyWave* follows the numerical algorithm by Goto et al. [45] for the simulation of linear long-wave propagation in spherical coordinates. Tsunami propagation was computed on the 1 arc minute GEBCO (General Bathymetric Chart of the Oceans) bathymetric grid [46], and the sea-level heights at offshore positions were projected to the coast using Green's amplification law [47]. As expected, due to the predominantly SW-NE orientation of the rupture, main tsunami energy is radiated towards the southeastern coast of China, between the cities of Hong Kong and Shantou (Figure 5). Expected maximum tsunami wave heights may reach up to 10 m at the west coast of the Luzon Island. At the southwest coast of Taiwan and southeastern coast of China, tsunami wave heights may reach 1–2 m.

In order to issue a reliable tsunami early warning as soon as possible, seismic parameters (e.g., epicenter, magnitude, slip distribution) should be inverted from co-seismic signal immediately after the earthquake breaks. Since the Luzon Island is located close to the northern Manila trench, our scenario rupture causes significant horizontal co-seismic displacements throughout the island. As shown in Figure 4a, stations distributed along the northwest part of the Luzon Island will experience northwest-directed surface displacements in excess of 10 cm. Taking into account the horizontal accuracy of real-time BDS and GPS processing of about 1 cm (Table 1), we conclude that co-seismic displacements due to an earthquake with a size of Mw = 8.0 should be well-detected and accurately measured with the present-day BDS/GPS observation and processing precision, which, in turn, should enable reliable source inversion and tsunami forecasting.

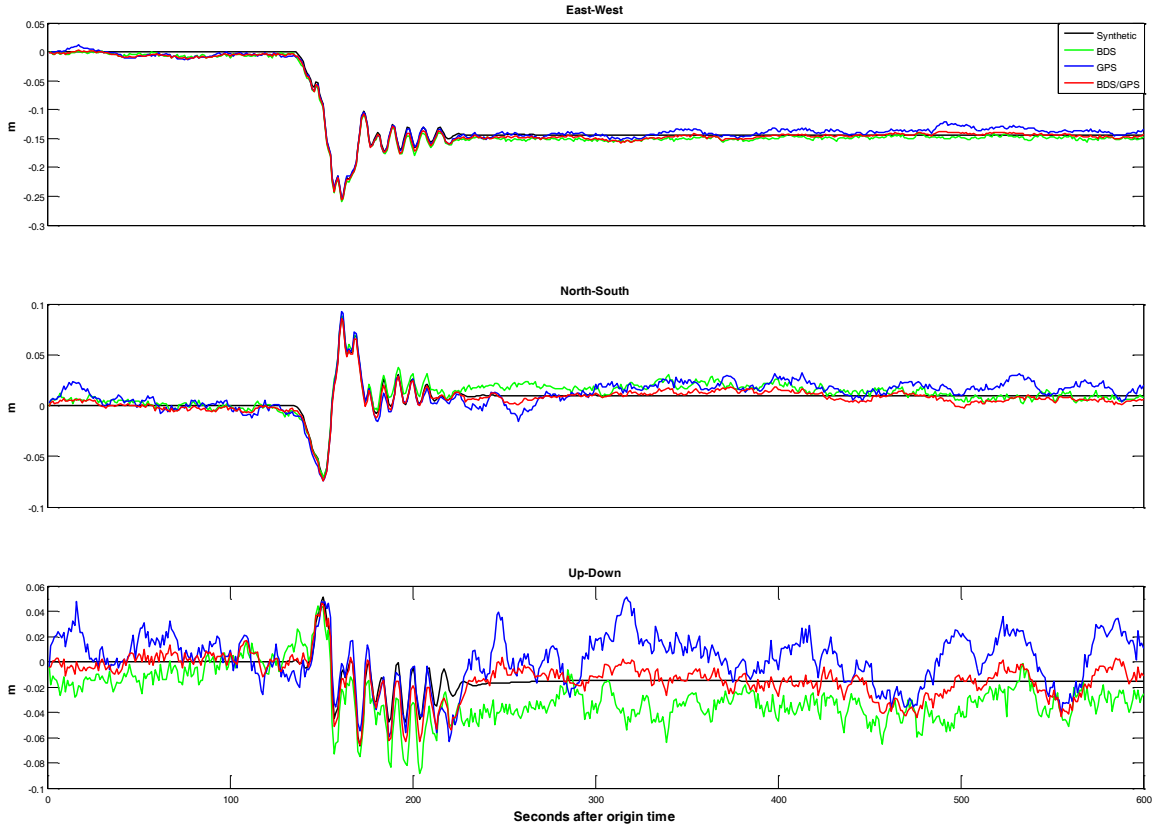

Figure 5. 3 Simulated displacement waveforms in forward-model scenario (rupture E2, see text for description). Waveforms are shown at one selected virtual GNSS-station placed at the Luzon Island (contoured triangle on Figure 4a). Black lines represent original kinematic simulations; colored lines represent the simulations after an addition of typical TPP processing noise (Secion 2). –Noisy" displacements will be used for source inversion.

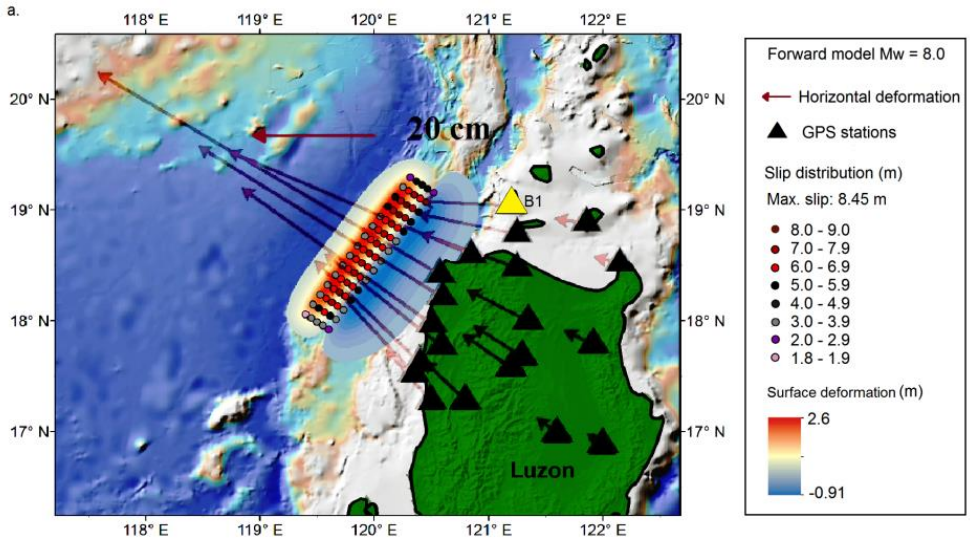

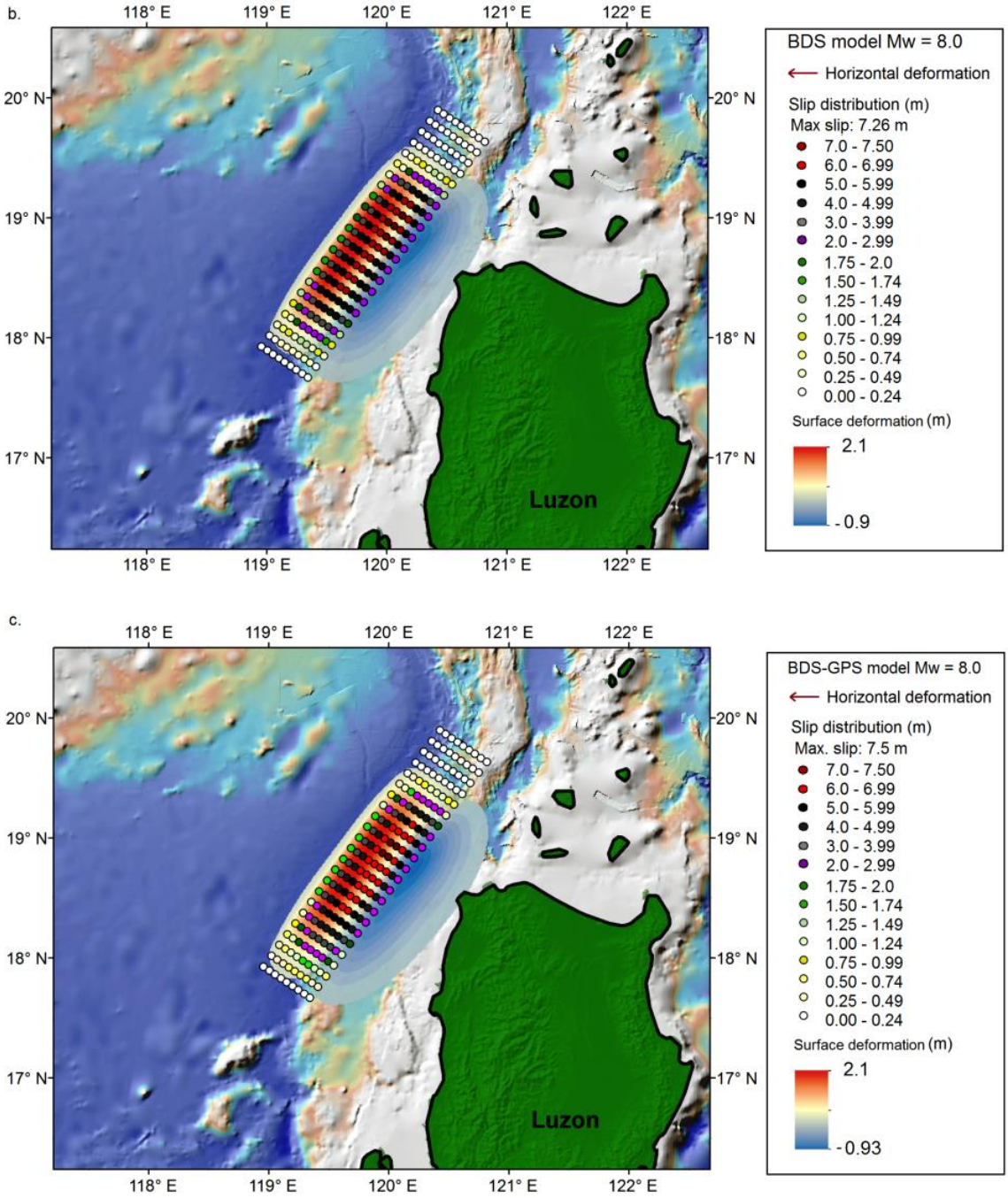

Figure 5. 4 (**a**) Assumed slip distribution (colored dots) and correspondent co-seismic surface deformation for an event with a magnitude of Mw = 8.0 rupturing along the Northern Manila mega-thrust: our forward-model scenario. Red arrows show horizontal displacements computed at the virtual BDS/GPS network (black triangles). The yellow triangle (B1) marks the station from Figure 3. (**b**) Colored dots represent slip distribution as inverted from the simulated BDS-displacements (note, synthetic BDS-displacements include real-time processing noise). Additionally shown is the resulting vertical deformation. (**c**) Same as (**b**), but for the inversion of the joint BDS/GPS displacements.

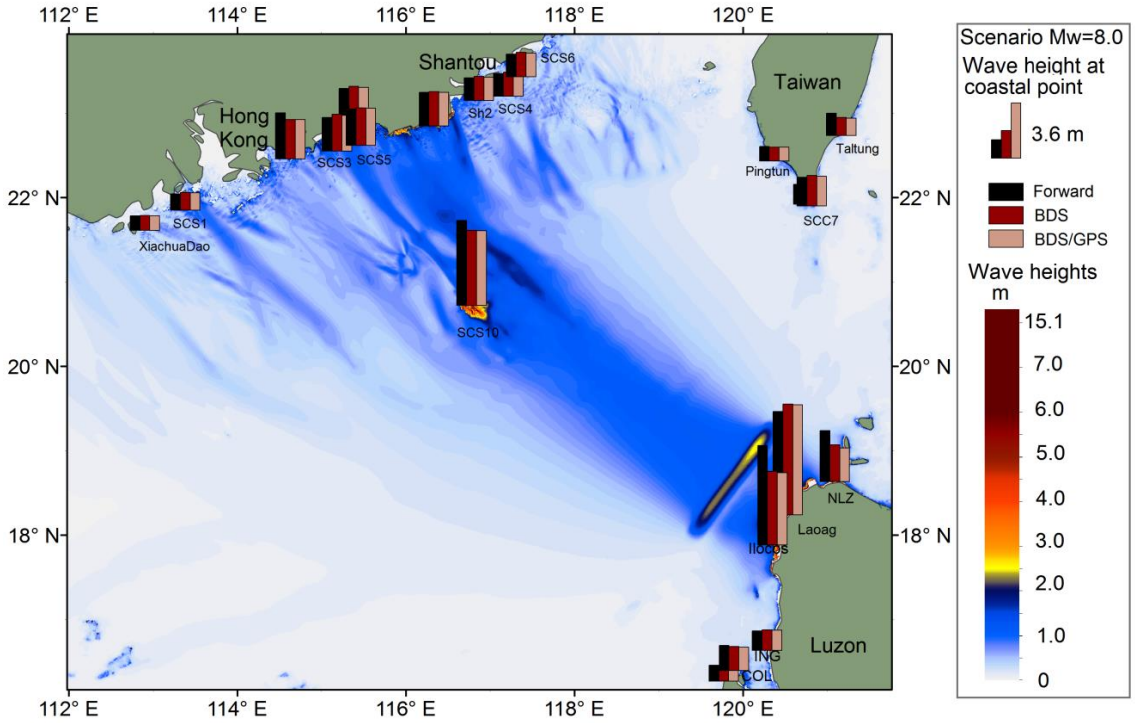

Figure 5. 5 Simulated tsunami scenarios. The color map shows the maximum wave height in the forward model (Figure 4a) after 6 h of tsunami propagation. Vertical bars are maximum wave heights as recorded at selected coastal locations for the three propagation models: forward model (black); with source as inverted from BDS-displacements (dark grey in Figure 4b); with source as inverted from joint BDS/GPS-displacements (light grey, Figure 4c).

To illustrate this, we retrieved static offsets from our simulated kinematic BDS and BDS/GPS displacements (Figure 5.3) and invert them back into the source parameters (Figure 4b,c). Finally, we compute tsunami propagations from the ~~–in~~verted sources" and compare them to the forward scenario (vertical bars on Figure 5.5). In order to get static offsets at virtual BDS/GPS stations from the contaminated displacement waveforms (Figure 5.3), we employ a method introduced by Ohta *et al.* [21]. Resulting static displacements were subsequently inverted into the slip distribution along the predefined geometry of the Manila trench using the SDM software [48]. Here, in order to make the inversion test closer to the real world scenario, we did not constrain the possible rupture geometry to the forward model area by length and width. Additionally, we employed alternative fault discretization with 23 × 9 subfaults. Since we were expecting predominantly thrust events at the Manila trench, the rake angle was allowed to vary between 70 and 100 degrees. The two horizontal components were weighted twice as much as the vertical component, and a smoothing constraint was imposed to avoid unrealistic slip patterns.

Figures 4b,c present slip distributions as inverted from the simulated real-time co-seismic BDS (Figure 4b) and joint BDS/GPS (Figure 5.4c) displacements. Inverted slip distributions from single BDS and BDS/GPS show a high degree of consistency, which is obvious since the processing accuracy is very similar in both cases (Table 1). In contrast, comparison with the forward model (Figure 5.4a) shows some bias. To be exact, inverted slip distribution covers a somewhat larger area than the original model; the maximum slip of the forward model is 8.4 m while the inverted maximum slips are 7.31 and 7.32 m, respectively, and the derived moment magnitudes are both Mw = 8.06, slightly greater than the input value of Mw = 8.0. This insignificant discrepancy is explained, first of all, by the fact that our virtual observational network is located, due to natural reasons, only on one side of the Manila trench. Nevertheless,

tsunami wave heights as predicted from the inverted source models are very similar to the forward computations (compare vertical bars on Figure 5.5 and refer to the supplementary Table S1 for more detailed information). Note that the difference in estimated wave heights is larger along the Luzon coast compared to the distant coasts of China and Taiwan. This demonstrates the known fact that, for reliable near-field tsunami early warnings, a trustworthy slip distribution is favorable.

From this synthetic inversion test, we conclude that a BDS (or a BDS/GPS) network with real-time processing, if deployed at the Luzon Island, will be able to contribute to a fast and reliable tsunami source inversion at the Manila trench.

5.4 Discussions

As we have noted before, precise real-time GNSS processing is a prerequisite for incorporation of coastal GNSS-arrays into tsunami early warnings. In this context, we assessed the potential capability of using real-time BDS to detect on-land co-seismic displacements caused by submarine rupture and addressed the special contribution from combined BDS/GPS solutions as well. According to our estimations from Section 2, horizontal accuracies of single BDS and GPS at the test site were 1.1 cm and 1.2 cm, respectively, while the joint BDS/GPS accuracy reached about 0.7 cm. For vertical component, BDS/GPS improved accuracy from about 2 cm to about 1.0 cm. In terms of current accuracy, BDS is close to GPS in the Asia-Pacific region, and the advantage of fusion of BDS and GPS is clear. Nonetheless, our simulation of the Mw = 8.0 earthquake did not show any notable difference in the case of BDS-only or BDS/GPS joint inversion (compare Figure 5.4b,c). For an earthquake with a magnitude of Mw = 8.0, near field deformation can be as large as tens of centimeters (Figure 5.4a); with respect to this scale of deformation, the signal-to-noise ratio (SNR) improvement by joint BDS/GPS processing is not clear in this case. However, joint BDS/GPS processing may show its advantage for smaller but still tsunamigenic earthquakes.

Consider a scenario of a smaller earthquake. Figure 6 presents a forward model as well as the two source inversion models for an Mw = 7.5 earthquake at the Manila trench (compare Figure 5.6 to Figure 5.4). Earthquakes of this magnitude will not pose a significant tsunami threat for the coasts of China and Taiwan but can still be dangerous in the near field (Figure 5.7). In this case, simulated co-seismic displacements are significantly smaller (Figure 6a), and the better signal-to-noise ratio of the joint BDS/GPS real-time processing results in better restoration of the original slip distribution (compare Figure 5.6b,c) and, therefore, in better tsunami forecasting for the near field (compare vertical bars on Figure 7 and refer to the supplementary Table S1 for more detailed information).

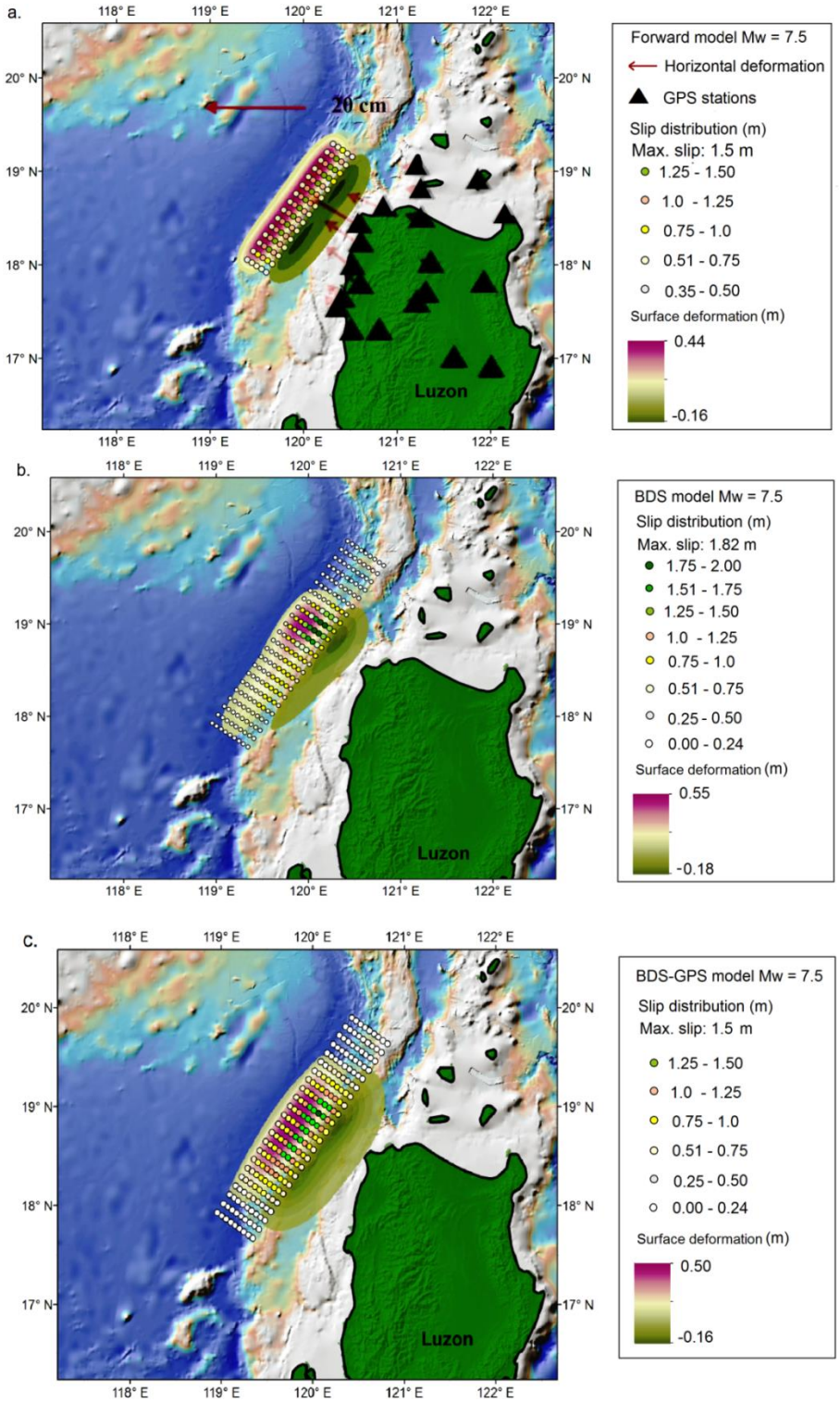

Figure 5. 6 (**a**) Assumed slip distribution (colored dots) and correspondent co-seismic surface deformation for an event with a magnitude of Mw = 7.5 rupturing along the Northern Manila mega-thrust. Red arrows show horizontal displacements computed at the virtual BDS/GPS network (black triangles); (**b**) Colored dots show slip distribution as inverted from the simulated BDS-displacements (note, synthetic BDS-displacements include real-time processing noise). Additionally shown is the resulting vertical deformation; (**c**) Same as (b), but for the inversion of the joint BDS/GPS displacements.

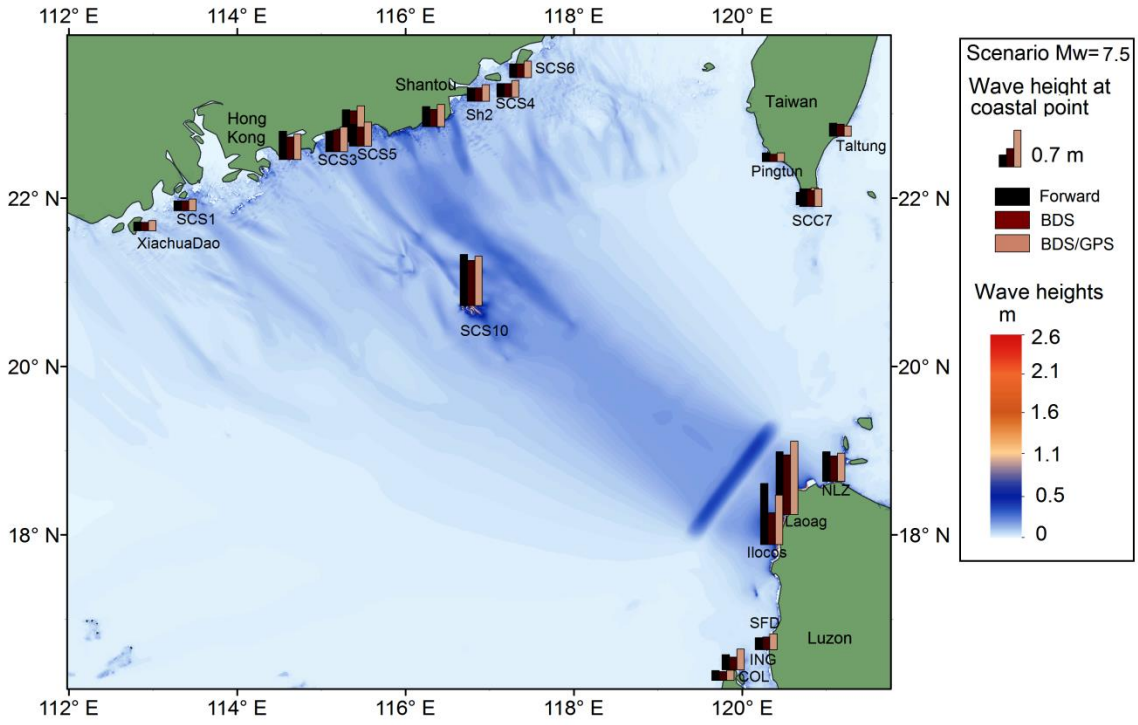

Figure 5. 7 Simulated tsunami scenarios. The color map shows the maximum wave height in the forward model (Figure 6a) after 6 h of tsunami propagation. Vertical bars are maximum wave heights as recorded at selected coastal locations for the three propagation models: the forward model (black); the model with the source as inverted from BDS-displacements (dark grey, Figure 6b); and the model with the source as inverted from joint BDS/GPS-displacements (light grey, Figure 6c).

Notice that our models are simple and generic enough to illustrate the main message of the present study: Tsunamigenic earthquakes at the Manila trench will trigger significant co-seismic deformation at the Luzon Island. Deformation amplitudes will be far above modern real-time GNSS resolution. That is why it makes sense to employ coastal GNSS-arrays for tsunami early warnings in the Southern China Sea.

At the same time, authors understand that there are many open questions regarding practical incorporation of GNSS component into any particular TEWS. For example, we opted for static inversion of final co-seismic displacements. Alternatively, some very recent studies [49,50] showed that static inversions have a tendency to over-smoothen slip distribution, which, in turn, can result in the under-prediction of tsunami heights. Kinematic (waveform) inversions demonstrate better spatial resolution and have a clear advantage when static displacements are small. On the other hand, static inversions are fast and robust, and use less data and a smaller number of control parameters.

The problem of optimal choice of methods and algorithms is not, of course, restricted to static *vs.* kinematic inversion. If the source alone is considered—the GNSS array distribution; the source forward model, which includes geometry, the elastic model, slip distribution; inversion algorithm itself—there is only a short list of issues requiring testing and optimization. It is the same for tsunami simulation and decision-making; each of them also has dozens of options. Authors believe that decisions about better methods and better practices should be taken on an individual basis, in harmonization within particular TEWS and its individual components.

5.5 Conclusions

In this study, we investigated the precise positioning performance of BDS and BDS/GPS in the Asia-Pacific region, and we specifically focused on their applications to tsunami early warnings in the SCS region. By analyzing two MGEX stationary stations, we demonstrated that BDS and GPS display similar positioning accuracy in the Asia-Pacific region. Combined BDS/GPS solution not only shows a somewhat higher degree of precision but, what is even more important for operational implementation in decision-making applications like tsunami early warnings, also improves the robustness.

By considering a scenario of a devastating tsunami in the Southern China Sea triggered by a Mw = 8.0 earthquake along the Manila trench, we propose deploying a continuous BDS/GPS-network at the western coast of the Luzon Island, Philippines. This network, if complemented with the modern real-time processing technique (here TPP), will contribute to a very fast (2–3 min) earthquake evaluation and source inversion, moving toward a higher reliability of the local and regional tsunami early warning.

Using a scenario with a smaller but still tsunamigenic earthquake (Mw = 7.5), we demonstrate that the advantage of combined BDS/GPS over single GNSS processing by source inversion grows with decreasing earthquake magnitudes. To conclude, BDS and BDS/GPS can become an important component of the future TEWS in the SCS, although numerous factors need to be optimized in future studies.

Considering that the BDS constellation is still under construction, with increasing numbers of BDS satellites and ground-tracking stations arising in the coming years, its visibility in other places in the world will improve significantly, and the orbit and clock bias products will be more accurate, which indicate that precision of BDS is expected to be equal on a global level. That is to say, the concept of BDS and BDS/GPS as a tsunami early warning component is not limited to the Asia-Pacific region, but will be able to be applied worldwide.

Acknowledgments: K.C. is supported by the China Scholarship Council (CSC) for his PhD study in the German Research Centre for Geoscience. N.Z. is supported by the Helmholtz Association through the GeoSim program. This study was also supported by the National Natural Science Foundation of China (Grant No. 41504010; 41574027; 41325015; 41231174). We appreciate valuable comments from the three reviewers which improve this manuscript greatly.

Author Contributions:

Kejie Chen initialized the idea and conception; Kejie Chen, Natalia Zamora and Andrey Babeyko wrote the manuscript; All authors reviewed the manuscript.

Conflicts of Interest:

The authors declare no conflict of interest.

5.6 References

1. NGDC/WDS National Geophysical Data Center/World Data Service (NGDC/WDS). Available online: http://www.ngdc.noaa.gov/hazard/tsu_db.shtml (accessed on 23 November 2015).
2. Japan Meteorological Agency (JMA). *Lessons Learned from the Tsunami Disaster Caused by the 2011 Great East Japan Earthquake and Improvements in JMA' s Tsunami Warning System*; Japan Meteorological Agency: Tokyo, Japan, 2013.

3. Boore, D.M.; Bommer, J.J. Processing of strong-motion accelerograms: Needs, options and consequences. *Soil Dyn. Earthq. Eng.* **2005**, *25*, 93–115.
4. Melgar, D.; Bock, Y.; Sanchez, D.; Crowell, B.W. On robust and reliable automated baseline corrections for strong motion seismology. *J. Geophys. Res. Solid Earth* **2013**, *118*, 1177–1187.
5. Hirose, F.; Miyaoka, K.; Hayashimoto, N.; Yamazaki, T.; Nakamura, M. Outline of the 2011 off the Pacific coast of Tohoku Earthquake (Mw 9.0)—Seismicity: Foreshocks, mainshock, aftershocks, and induced activity. *Earth Planets Space* **2011**, *63*, 513–518.
6. Bormann, P.; Saul, J. A fast, non-saturating magnitude estimator for great earthquakes. *Seismol. Res. Lett.* **2009**, *80*, 808–816.
7. Hanka, W.; Saul, J.; Weber, B.; Becker, J.; Harjadi, P. Real-time earthquake monitoring for tsunami warning in the Indian Ocean and beyond. *Nat. Hazards Earth Syst. Sci.* **2010**, *10*, 2611–2611.
8. Kanamori, H.; Rivera, L. Source inversion of W phase: Speeding up seismic tsunami warning. *Geophys. J. Int.* **2008**, *175*, 222–238.
9. Duputel, Z.; Rivera, L.; Kanamori, H.; Hayes, G.P.; Hirshorn, B.; Weinstein, S. Real-time W phase inversion during the 2011 off the Pacific coast of Tohoku Earthquake. *Earth Planets Space* **2011**, *63*, 535–539.
10. Lomax, A.; Michelini, A. Mwpd: A duration-amplitude procedure for rapid determination of earthquake magnitude and tsunamigenic potential from P waveforms. *Geophys. J. Int.* **2009**, *176*, 200–214.
11. Wang, R.; Schurr, B.; Milkereit, C.; Shao, Z.; Jin, M. An improved automatic scheme for empirical baseline correction of digital strong-motion records. *Bull. Seismol. Soc. Am.* **2011**, *101*, 2029–2044.
12. Tu, R.; Wang, R.; Zhang, Y.; Walter, T.R. Application of a net-based baseline correction scheme to strong-motion records of the 2011 Mw 9.0 Tohoku earthquake. *Geophys. J. Int.* **2014**, *204*, doi:10.1093/gji/ggu092.
13. Bock, Y.; Melgar, D.; Crowell, B.W. Real-time strong-motion broadband displacements from collocated GPS and accelerometers. *Bull. Seismol. Soc. Am.* **2011**, *101*, 2904–2925.
14. Li, X.; Ge, M.; Zhang, Y.; Wang, R.; Guo, B.; Klotz, J.; Wickert, J.; Schuh, H. High-rate coseismic displacements from tightly integrated processing of raw GPS and accelerometer data. *Geophys. J. Int.* **2013**, *195*, doi:10.1093/gji/ggt249.
15. Crowell, B.W.; Melgar, D.; Bock, Y.; Haase, J.S.; Geng, J. Earthquake magnitude scaling using seismogeodetic data. *Geophys. Res. Lett.* **2013**, *40*, 6089–6094.
16. Blewitt, G.; Kreemer, C.; Hammond, W.C.; Plag, H.-P.; Stein, S.; Okal, E. Rapid determination of earthquake magnitude using GPS for tsunami warning systems. *Geophys. Res. Lett.* **2006**, *33*, L11309–L11309.
17. Sobolev, S.V.; Babeyko, A.Y.; Wang, R.; Hoechner, A.; Galas, R.; Rothacher, M.; Sein, D.V.; Schröter, J.; Lauterjung, J.; Subarya, C. Tsunami early warning using GPS-Shield arrays. *J. Geophys. Res. Solid Earth* **2007**, *112*, B08415–B08415.
18. Babeyko, A.Y.; Hoechner, A.; Sobolev, S.V. Source modeling and inversion with near real-time GPS: A GITEWS perspective for Indonesia. *Nat. Hazards Earth Syst. Sci.* **2010**, *10*, 1617–1627.
19. Falck, C.; Ramatschi, M.; Subarya, C.; Bartsch, M.; Merx, A.; Hoeberechts, J.; Schmidt, G. Near real-time GPS applications for tsunami early warning systems. *Nat. Hazards Earth Syst. Sci.* **2010**, *10*, 181–189.
20. Hoechner, A.; Ge, M.; Babeyko, A.Y.; Sobolev, S.V. Instant tsunami early warning based on real-time
GPS—Tohoku 2011 case study. *Nat. Hazards Earth Syst. Sci.* **2013**, *13*, 1285–1292.

21. Ohta, Y.; Kobayashi, T.; Tsushima, H.; Miura, S.; Hino, R.; Takasu, T.; Fujimoto, H.; Iinuma, T.; Tachibana, K.; Demachi, T.; *et al*. Quasi real-time fault model estimation for near-field tsunami forecasting based on RTK-GPS analysis: Application to the 2011 Tohoku-Oki earthquake (Mw 9.0). *J. Geophys. Res. Solid Earth* **2012**, *117*, doi:10.1029/2011JB008750.
22. Wright, T.J.; Houlié, N.; Hildyard, M.; Iwabuchi, T. Real-time, reliable magnitudes for large earthquakes from 1 Hz GPS precise point positioning: The 2011 Tohoku-Oki (Japan) earthquake. *Geophys. Res. Lett.* **2012**, doi:10.1029/ 2012GL051894.
23. Melgar, D.; Bock, Y.; Crowell, B.W. Real-time centroid moment tensor determination for large earthquakes from local and regional displacement records. *Geophys. J. Int.* **2012**, *188*, 703–718.
24. Melgar, D.; Crowell, B.W.; Geng, J.; Allen, R.M.; Bock, Y.; Riquelme, S.; Hill, E.M.; Protti, M.; Ganas, A. Earthquake magnitude calculation without saturation from the scaling of peak ground displacement. *Geophys. Res. Lett.* **2015**, *42*, 5197–5205.
25. Li, X.; Ge, M.; Zhang, X.; Zhang, Y.; Guo, B.; Wang, R.; Klotz, J.; Wickert, J. Real-time high-rate co-seismic displacement from ambiguity-fixed precise point positioning: Application to earthquake early warning. *Geophys. Res. Lett.* **2013**, *40*, 295–300.
26. Fang, R.; Shi, C.; Song, W.; Wang, G.; Liu, J. Determination of earthquake magnitude using GPS displacement waveforms from real-time precise point positioning. *Geophys. J. Int.* **2013**, *196*, 461–472.
27. Zhao, Q.; Guo, J.; Li, M.; Qu, L.; Hu, Z.; Shi, C.; Liu, J. Initial results of precise orbit and clock determination for COMPASS navigation satellite system. *J. Geod.* **2013**, *87*, 475–486.
28. Li, M.; Qu, L.; Zhao, Q.; Guo, J.; Su, X.; Li, X. Precise Point Positioning with the BeiDou Navigation Satellite System. *Sensors* **2014**, *14*, 927–943.
29. Li, X.; Ge, M.; Dai, X.; Ren, X.; Fritsche, M.; Wickert, J.; Schuh, H. Accuracy and reliability of multi-GNSS real-time precise positioning: GPS, GLONASS, BeiDou, and Galileo. *J. Geod.* **2015**, *89*, 607–635.
30. Liu, P.L.-F.; Wang, X.; Salisbury, A.J. Tsunami hazard and early warning system in South China Sea. *J. Asian Earth Sci.* **2009**, *36*, 2–12.
31. Dao, M.H.; Tkalich, P.; Chan, E.S.; Megawati, K. Tsunami propagation scenarios in the South China Sea. *J. Asian Earth Sci.* **2009**, *36*, 67–73.
32. Okal, E.A.; Synolakis, C.E.; Kalligeris, N. Tsunami simulations for regional sources in the South China and adjoining seas. *Pure Appl. Geophys.* **2010**, *168*, 1153–1173.
33. Suppasri, A.; Imamura, F.; Koshimura, S. Tsunami hazard and casualty estimation in a coastal area the neighbors the Indian Ocean and South China Sea. *J. Earthq. Tsunami* **2012**, *6*, 1250010.
34. Sun,L.; Zhou, X.; Huang, W.; Liu, X.; Yan, H.; Xie, Z.; Wu, Z.; Zhao, S.; Shao, D.; Yang, W. Preliminary evidence for a 1000-year-old tsunami in the South China Sea. *Sci. Rep.* **2013**, *3*, doi:10.1038/srep01655.
35. Lau, A.Y.A.; Switzer, A.D.; Dominey-Howes, D.; Aitchison, J.C.; Zong, Y. Written records of historical tsunamis in the northeastern South China Sea—Challenges associated with developing a new integrated database. *Nat. Hazards Earth Syst. Sci.* **2010**, *10*, 1793–1806.
36. Jing, H.; Zhang, H.; Yuen, D.; Shi, Y. A revised evaluation of Tsunami Hazards along the Chinese Coast in view of the Tohoku-Oki Earthquake. *Pure Appl. Geophys.* **2013**, *170*, 129–138.
37. Ren, Z.-Y.; Liu, H.; Wang, B.-L.; Zhao, X. An investigation on Multi-Buoy Inversion Method for Tsunami Warning System in South China Sea. *J. Earthq. Tsunami* **2014**, *8*, doi:10.1142/S1793431114400041.

38. An, C. Inversion of Tsunami Waveforms and Tsunami warning. Ph.D. Thesis, The Cornell University, Ithaca, NY, USA, June 2015.
39. Colosimo, G.; Crespi, M.; Mazzoni, A. Real-time GPS seismology with a stand-alone receiver: A preliminary feasibility demonstration. *J. Geophys. Res. Solid Earth* **2011**, *116*, doi:10.1029/2010JB007941.
40. Li, X.; Ge, M.; Guo, B.; Wickert, J.; Schuh, H. Temporal point positioning approach for real-time GNSS seismology using a single receiver. *Geophys. Res. Lett.* **2013**, *40*, 5677–5682.
41. Kirby, S.; Geist, E. Great earthquake tsunami sources: Empiricism and beyond. In Proceedings of the USGS Tsunami Sources Workshop, Menlo Park, CA, USA, 21–22 April 2006.
42. Wang, R. Tidal response of the solid Earth. In *Tidal Phenomena*; Springer: Berlin Heidelberg, Germany,1997; pp. 27–57.
43. Kennett, B.L.N.; Engdahl, E.R.; Buland, R. Constraints on seismic velocities in the Earth from traveltimes. *Geophys. J. Int.* **1995**, *122*, 108–124.
44. Wang, R.; Mart n, F.L.; Roth, F. Computation of deformation induced by earthquakes in a multi-layered elastic crust—FORTRAN programs EDGRN/EDCMP. *Comput. Geosci.* **2003**, *29*, 195–207.
45. Goto, C.; Ogawa, Y.; Shuto, N.; Imamura, F. *IUGG/IOC Time Project, Numerical Method of Tsunami Simulation with the Leap-Frog Scheme*; IOC Manuals and Guides No. 35; Unesco: Paris, Frace, 1997.
46. Smith, W.H.F.; Sandwell, D. Global sea floor topography from satellite altimetry and ship depth soundings. *Science* **1997**, *277*, 1956–1962.
47. Kamigaichi, O. Tsunami Forecasting and Warning. In *Encyclopedia of Complexity and Systems Science SE—568*; Meyers, R.A., Ed.; Springer: New York, NY, USA, 2009; pp. 9592–9618.
48. Wang, L.; Wang, R.; Roth, F.; Enescu, B.; Hainzl, S.; Ergintav, S. Afterslip and viscoelastic relaxation following the 1999 M 7.4 İzmit earthquake from GPS measurements. *Geophys. J. Int.* **2009**, *178*, 1220–1237.
49. Melgar, D.; Bock, Y. Near-field tsunami models with rapid earthquake source inversions from land- and ocean-based observations: The potential for forecast and warning. *J. Geophys. Res. Solid Earth* **2013**, *118*, 5939–5955.
50. Melgar, D.; Bock, Y. Kinematic earthquake source inversion and tsunami runup prediction with regional geophysical data. *J. Geophys. Res. Solid Earth* **2015**, *120*, 3324–3349.

Chapter 6 Conclusions and future work

6.1 Conclusions

The main contributions of this thesis can be summarized as follows:

To make dense networks affordable, we presented a new approach to get precise co-seismic displacements using a standalone cost effective single-frequency GPS receiver. In this new approach, observations prior to an earthquake are used to predict ionospheric delay with high precision over a few minutes. The performance of the new approach was first validated through an outdoor experiment with a real single-frequency receiver and then by re-processing of GPS data recorded during the 2011 Tohoku Mw 9.0 earthquake in a simulated mode. As demonstrated in the experiment, the performance of single frequency receiver is almost as good as dual-frequency in the horizontal direction while the bias is limited to 5 cm in the vertical direction. In the Tohoku case, RMS against dual-frequency receivers constituted 2 cm for horizontal components and 3 cm for the vertical component, which satisfies the precision request for TEWS.

We evaluated the potential advantages of multi-GNSS over GPS-only in terms of co-seismic displacement determination. Considering that only GPS and GLONASS have global coverage and GPS/GLONASS observation data recorded during earthquake shaking are available, currently we restrict our multi-GNSS concept to GPS/GLONASS. Compared with a GPS-only system, GPS/GLONASS increases the satellite visibility and optimize the constellation spatial geometry evidently. Related out-door experiments show that GPS/GLONASS performs better when geometry of GPS satellites distribution is not ideal enough. Take the 2015 Mw 8.3 Chile Illapel event as an example, obvious biases (up to 2 cm in horizontal direction) have been found between co-seismic displacements derived from GPS-only and GPS/GLONASS at stations with only six GPS satellites tracked. We believe displacements from GPS/GLONASS are closer to the truth. Furthermore, slip inversions from GPS/GLONASS indicated a larger tsunami scenario.

We tested uncertainties related to derivation of real-time source inversion by different approaches: centroid moment tensor, single Okada fault, distributed slip in layered half space on a curved plane. Besides, we considered individual uncertainties as well as their propagation to the final tsunami forecasting. Take the 2014 Pisagua event as a case study, though the three source inversion approaches give similar first-order fault parameters including magnitude and position (longitude, latitude) of the rupture center, other fault parameters: depth, strike, dip and rake angles show significant differences, which are later clearly manifested by tsunami propagation patterns. Despite these differences, resulting tsunami forecasting along the Chilean coast is similar for all three models. Our study does not reveal any absolute favorite between the three source inversion approaches.

We assessed the precise positioning performance of BDS and BDS/GPS in the Asia-Pacific region and focused on their applications to TEWS in the SCS region. Our results reveal that positioning accuracy of BDS is equal to GPS in the Asia-Pacific region while BDS/GPS solution not only shows a somewhat higher degree of precision but also improves the robustness. A continuous BDS/GPS network at the west coast of the Luzon Island is proposed and by

simulating tsunamis triggered by Mw 8.0 and Mw 7.5 earthquakes along the Manila trench, we demonstrate the feasibility of incorporating BDS into TEWS in SCS region and addressed the advantage of combined BDS/GPS over single GNSS processing by source inversion grows with decreasing earthquake magnitudes.

6.2 Future work

In this thesis, we mainly focused on obtaining precise co-seismic displacements using real-time GNSS and inverting static seismic sources based on the derived permanent offsets. Actually, applications of GNSS for tsunami early warning are beyond our current work.

Besides monitoring ground motions, it has been verified that GNSS receivers can also track tsunamis propagations. As is well known, GNSS signals are able to measure Total Election Content (TEC) when they pass through the ionosphere from receivers to satellites, and the values of TEC may be disturbed by acoustic waves and gravity waves (tsunamis) generated by mega-thrust earthquakes. That‘s to say, each piercing point (the intersection between line of sight and this ionosphere shell) is a virtual seismograph in the upper atmosphere. Considering that GNSS receivers track satellites with lower elevation angles, they look over the horizon and can release advance warning to far field coastal communities of a coming tsunami wave.

Compared with strong motion sensors, though GNSS technology does not saturate or tilt, it has the limitation of low sampling rate and a higher noise level. In addition, it has been demonstrated that by integrating GNSS and strong motion data, advantages of both sensors can be taken, which provides a precise constrain for reliable kinematic source inversion. It is meaningful to test the performance of a kinematic seismic source for TEWS.

Appendix

Publications during Ph.D. Period

Publications online

1. Chen, Kejie, Natalia Zamora, Andrey Y. Babeyko, Xingxing Li, and Maorong Ge. "Precise Positioning of BDS, BDS/GPS: Implications for Tsunami Early Warning in South China Sea." Remote Sensing 7, no. 12 (2015): 15955-15968.
2. Chen, Kejie, Maorong Ge, Xingxing Li, Andrey Babeyko, Markus Ramatschi, and Markus Bradke. "Retrieving real-time precise co-seismic displacements with a standalone single-frequency GPS receiver." Advances in Space Research (2015).
3. Tilmann, F., Y. Zhang, M. Moreno, J. Saul, F. Eckelmann, M. Palo, Z. Deng et al. "The 2015 Illapel earthquake, central Chile, a type case for a characteristic earthquake?" Geophysical Research Letters (2015).
4. Tu, Rui, and Kejie Chen. "Tightly Integrated Processing of High-Rate GPS and Accelerometer Observations by Real-Time Estimation of Transient Baseline Shifts." Journal of Navigation 67, no. 05 (2014): 869-880.

Publications under review

1. Kejie Chen, Xingxing Li, Andrey Y. Babeyko, Maorong Ge, Faqi Diao. Retrieving real-time co-seismic displacements using GPS/GLONASS: a preliminary report from September 2015 Mw8.3 Chile Illapel earthquake. Submitted to Geophysical Journal International
2. Kejie Chen, Andrey Y. Babeyko, Maorong Ge. Comparing source inversion techniques for GNSS-based tsunami early warning: a case study 2014 Pisagua M8.1 earthquake, northern Chile. Submitted to Geophysical Research Letters

Professional experiences during this Ph.D. study

1. Poster presentation at American Geophysical Union 2015 Fall Meeting, 14-18 December, San Francisco, U.S.
2. Oral presentation at 26th IUGG General Assembly 2015, Jun.23-Jul.2, Prague, Czech
3. Oral presentation at 6th China Satellite Navigation Conference 2015, 13-15 May, Xi‘an, China
4. Poster presentation at American Geophysical Union 2014 Fall Meeting, 15-19 December, San Francisco, U.S.
5. Oral presentation at European Geosciences Union General Assembly 2014, Apr.27-May 02, 2014, Vienna, Austria
6. Oral presentation at International Association of Chinese Professionals in Global Positioning Systems,Jan.15-18, 2014, Xuzhou, China
7. Poster presentation at International Association of Geodesy Scientific Assembly, Sep.1 – 6, 2013, Potsdam, Germany
8. Presentation at 4th China Satellite Navigation Conference 2013, 15-17 May, Wuhan, China